a NASA facsimile reproduction

OF

N65 12317

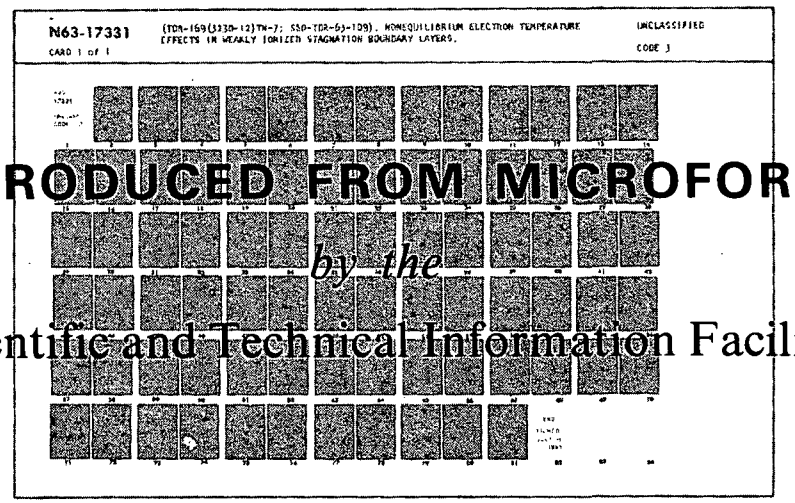

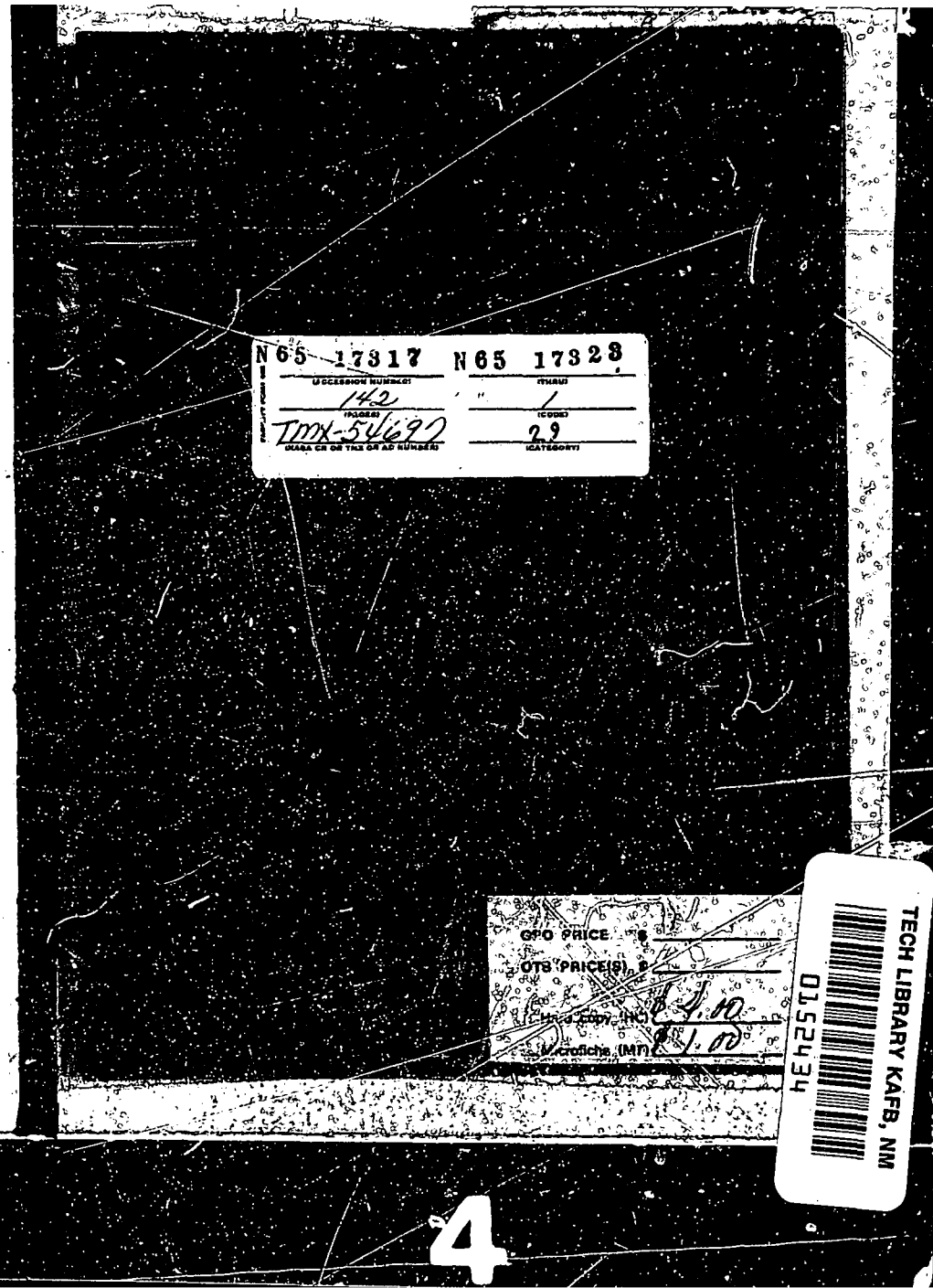

CONTENTS

SESSION IV - SPACE ENVIRONMENTAL EFFECTS

Chairman - Gerhard B. Heller, George C. Marshall Space Flight Center

17317

The proceedings will include the following additional papers under this session

[redacted]

SOME FUNDAMENTAL ASPECTS OF NUCLEAR RADIATION EFFECTS IN SPACECRAFT THERMAL CONTROL MATERIALS*

By J. E. Gilligan and R. P. Caren

The Research Laboratories
LOCKHEED MISSILES AND SPACE COMPANY
Palo Alto, California

SUMMARY

The methods and results of an investigation to determine the mechanisms by which solar reflector thermal control systems degrade under individual and combined ultraviolet and nuclear radiations are described. Appropriate optical and radiation effects theory are compared with the published results of irradiation experiments, in which transparent analogues of certain dielectric and semiconductor pigments have been studied. Conclusions have been reached regarding the equivalence of UV and nuclear radiation effects, basic causes of induced reflectance changes, and possible means of limiting the degradation due to these radiations.

INTRODUCTION

At the outset of the investigations reported in this paper, very little was known about the mechanisms responsible for the changes in thermal radiative properties of thermal control systems. While the detailed mechanisms still remain unknown for many of these systems, valuable insight has been gained in determining the fundamental causes of degradation. The paint systems dealt with in this paper are the solar reflector (white paint) class, and in what is to follow, damage (degradation) is defined as increased spectral absorptance in the solar region of the electromagnetic spectrum.

We intend to show how the reflectance spectra of irradiated paint systems can be analysed by means of theoretical relationships and to show how damage mechanisms can be deduced therefrom. Additionally, it will be shown how the deductions obtained from these analyses accord with physical observations. In order to explain the basic causes of degradation, it is necessary to understand, first, the fundamental properties of materials which govern their optical behavior; second, the interaction mechanisms of energetic radiation with matter; and, third the defects which energetic radiations produce and how these may affect optical properties. In section II a very brief sketch of these three topics will be given. Section IV will analyse the damage spectra of several typical paint systems, compare them with literature data, and speculate on the responsible damage mechanisms.

* This work was performed under Air Force Contract AF04(695)-136.

BACKGROUND THEORY

A. Optical Properties

The optical properties of solid opaque substances have been treated by many authors, Ref's 1-3. The ordinary developments of the theory seek to obtain mathematical expressions for the absorption and reflection of electromagnetic radiation as a function of basic material properties. Using Maxwell's equations, Fresnel derived the rigorous expression for reflectance, R, of a plane wave normally incident on a smooth surface of a material with index of refraction, n, and extinction coefficient, k:

$$R = \frac{(n-1)^2 + k^2}{(n+1)^2 + k^2} \tag{1}$$

The variation of the properties n and k with photon energy (or wavelength) is of immediate importance. Known as dispersion relations, these equations express the depaudence of n and k on wavelength; they have been derived on both classical and quantum mechanical theory. The expressions are:

Classical,

$$\beta = \frac{Ne^2}{4\pi m} \cdot \frac{1}{(\omega_0^2 - \omega^2) + g\omega} \tag{2a}$$

Quantum mechanical,

$$\beta = \sum_j \frac{Ne^2}{4\pi m} \cdot \frac{1}{(\omega_j^2 - \omega^2) + g_j\omega} \tag{2b}$$

where

β = volume polarizability
N = electron density
e = electronic charge
m = electronic mass
ω = circular frequency
g = damping constant
f = oscillator strength
ω_0 = circular frequency at absorption maximum

The classical and the exact quantum mechanical expressions are nearly identical, and in fact, differ only in interpretation. By rationalising eq.'s2and equating real and imaginary parts, through the relationships:

$$N = n(1 - ik),$$

and $$N^2 = 1 + 4\pi\beta$$

we finally obtain

$$n^2 - k^2 - 1 = \frac{Ne^2}{4\pi m} \cdot \frac{(\omega_0^2 - \omega^2)}{(\omega_0^2 - \omega^2)^2 + g^2\omega^2} \tag{3a}$$

$$2nk = \frac{Ne^2}{4\pi m} \cdot \frac{g\omega}{(\omega_0^2 - \omega^2)^2 + g^2\omega^2} \tag{3b}$$

In order to show how these formulae pertain to real thermal control surface coatings, we note that the optical properties of pigments and vehicles can be qualitatively described by theory if the dispersion relations and physical properties of all the components are known. In practice, however, the dispersion relations are rarely known for components of typical thermal control coating materials, and the reflectance of a given system must be predicted from empirical correlations. Among others, the parameters which determine reflectance include the ratio of indices of refraction of pigment and vehicle, pigment-vehicle ratio, and pigment particle size (s). Hence reflectance is not determined wholly by the optical properties of the components but also by geometric properties of the system, but the dispersion relations remain valid and useful in qualitatively describing R_λ, the dependence of reflectance upon wavelength.

B. Energetic Radiation Interactions

In this section we wish to very briefly sketch the important modes by which energetic radiation interacts with matter (Ref. 4, 5, and 6). In terms of the damage produced by absorption of energetic radiation, the net immediate effect is the production of free electrons. Gamma (γ) radiation, through the photoelectric effect, compton scattering, and pair production processes, releases a large number of free electrons. Neutrons (n) also produce them indirectly by displacing atoms which behave as charged particles and through their interaction create dense ionization tracks. Ultra-violet radiation also is capable of creating free electrons, by supplying the energy required to lift an electron from the valence band to the conduction band, or to the exciton band from which it may be excited to the conduction band by thermal activation, (ref's 3 & 7). Though the mechanisms involved in these processes are very different, it is important to realize the similarity of their end results, the production of free electrons, the fate of which is of prime interest in examining the observed degradation of thermal control materials.

C. Defect Absorption

For the sake of simplicity, we refer to any radiation-caused condition in a material as a "defect." Since a real material always contains a certain density of "natural" defects, it is of importance to determine the effects of changing their concentrations, as by radiation damage. A large number of

different types of defects are known, but it will be of interest to identify only those which can possibly influence solar absorptance. As will become clear later, this is not a simple task; each material differs in the identities of defects responsible for changes in spectral reflectance, R_λ. The defects almost always involve electron deficiencies or excesses, vacancies, interstitials, and the combinations of these. The F-center for example, is an electron trapped at an anion vacancy, but this defect is known as an "F'-center" when two electrons are so trapped. The important point is that optical properties, especially in the near infrared, visible, and uv regions, are sensitive to the local electronic structure and physical state of the crystal. An extensive literature exists describing the investigations of the effects of radiation on the optical properties of transparent materials. Alkali halides have been studied in the greatest detail. Silicas also have received considerable attention. In contrast, very little work has been conducted on other materials with the exception of certain of the semiconductors. Along with the experimental phases of these studies, much theoretical work has been accomplished to obtain semi-quantitative estimates of the effects of defects on optical properties. Unfortunately, most of the theoretical work has dealt principally with simple substances such as the halides. Many of the theoretical works (Ref.'s 8-15), nevertheless, provide insight into the effects of radiation on the optical properties of more complex materials.

An important theoretical and experimental result of work with alkali halides is the correlation of positions of absorption band maximum with crystal lattice parameters. Known as Mollwo relationships, these expressions are usually given in the form

$$\nu_m \cdot d^n = c \qquad (4)$$

ν_m = frequency at absorption band maximum
d = crystal interatomic distance
n = constant depending upon the type of defect producing the absorption
c = constant

Ivey (Ref. 16) has improved Mollwo's original correlations and gives both calculated and experimental values for ν_m for most of the alkali halides. Still another important expression is the well-known Smakula's formula, (Ref. 2 & 8), which relates optical absorption to the density of defects producing it.

$$N_i = 8.21 \times 10^{16} \frac{n}{(n^2+2)^2} \cdot \frac{W_i}{f_i} \qquad (5)$$

Here f_i = oscillator strength of I^{th} type defects
N_i = density of defects of I^{th} type, cm^{-3}
n = index of refraction of host medium
W_i = area under absorption curve due to I^{th} type defect

The above statements apply mainly to transparent materials and particularly to the alkali halides. To make use of the theory touched upon here in interpreting radiation effects in solid opaque materials, Fresnel's Equation (eq. 1) and the dispersion equations (eq.'s 3) must be applied. As k increases, we see that the index of refraction, n, goes through a minimum in the neighborhood of an absorption band, and the reflectance passes through a minimum. The extension of the above theoretical results to opaque systems thus depends upon how Fresnel's law follows the dispersion relations, and how the parameters in the latter depend upon defect structure.

D. Related Experimental Results

Before examining data we will discuss the general results of many investigators, principally those pertaining to alkali halides and silica structures. Because of the immensity of the data and the large number of important contributors, we have not in the following discussions credited specific authors but have compiled under appropriate headings a representative bibliography from which we have obtained the bulk of the information presented. In the silicas (we use this term broadly to designate any system which contains the basic silica structure; quartz, fused silica, silicate glasses, etc.), it was found that several bands develop under irradiation which are specific to the SiO_2 system, and others which are attributable to impurity atoms. Each band produced has been identified with (assigned to) a particular type of defect. Because of interactions between defects, the assignments are made in many cases by noting how the destruction of one band leads to the formation or enhancement of another. This latter analysis is an extremely important one in explaining the dependence of damage upon the wavelength of damaging and/or bleaching ultraviolet radiation.

With transparent materials a number of common results are obtained. First, the concentration of defects to produce measurable absorption is of the order of 10^{17} cm^{-3} (ref. 19) and to produce maximum absorption (saturation) is of the order of 10^{18} cm^{-3}. (Note that Smakula's formula Eq. 5 predicts the same range.) Second, defects comprised of single electron deficiences or excesses produce bands at shorter wavelengths (are more energetic) than do those comprised of multiple type defects, (compare, for example, the location of absorption bands in alkali halides due to F- and M- centers (ref. 16). Third, illumination of x- or γ-irradiated materials with light of wavelength(s) in the energy region of the induced absorption band will decrease the band intensity; the "holes" or electrons liberated in the process may become trapped at other defect sites to produce or enhance other bands. Fourth, there exists for each material or system of materials a wavelength above which the incident radiation will cause no damage; this wavelength always

lies in the uv region of the electromagnetic spectrum for dielectric materials and is in the infrared region for many semiconductor materials. Fifth, the rate at which damage is produced under irradiation diminishes exponentially with increasing dose; this behavior eventually manifests itself as an asymptotic approach to an equilibrium concentration of defects and thus to an equilibrium optical damage level.

EXPERIMENTAL RESULTS

A. Introductory Remarks

In order that the objectives of this section can be better understood, we will first list the immediate results of the studies and then show how these were obtained by examining the reflectance spectra of irradiated materials.

1. In paint systems containing semi-conductor pigments, TiO_2, ZnO, and ZnS (band gaps ~ 3.2 eV.), the pigment alone determines the observed damage; the vehicle influences the amount of damage but does not influence the character of the damage spectra.

2. In paint systems containing dielectric pigments, the same conclusion can be reached as above, except in the case of inorganic silicate vehicles, where there are effects definitely attributable to vehicle damage.

3. Degradation of semi-conductor pigments is due mainly to photo-reduction (oxidation of the volatile anion), and to a lesser extent the formation of color centers.

4. Degradation of dielectric pigments (and silicate vehicles) is principally due to the formation of color centers.

Conclusions 3 & 4 have been reached principally on the basis of the results of experiments reported in the literature, but have been verified by work at IMSC and to a lesser extent by the comparative studies described below. Conclusion 3 is not difficult to understand when it is realized that the fundamental absorption edges of TiO_2, etc. lie at wavelengths easily obtained in many types of solar simulating uv sources; in the case where a radiation of wavelength shorter than the edge wavelength is absorbed, an electron is raised from the valence to the conduction band; when this occurs with the anion, the anion is reduced and has a high probability for escaping the lattice structure (under the influence of thermal energy). As the anion is removed, the cations are reduced eventually to free metal atoms; the effect during this process is to induce free carrier absorption.

The differences in degradation mechanisms between semi-conductor pigments and dielectric pigments now become more clear. With dielectrics, damage occurs principally in the short wavelengths and is due to band absorption. Degradation in the semiconductor pigments stems principally from free carrier

absorption, and results in decreased near infrared reflectance.

B. Data Analysis

The data presented here are spectral absorptance data, taken from spectral reflectance curves in the wavelength region 0.275 to 1.8μ by subtracting the latter from unity. Reflectances were measured using a Cary Model 14 doublebeam spectro-photometer with an integrating sphere attachment. Absorptance as used here is the ratio of energy absorbed to that incident. This must be carefully distinguished from absorption coefficient, and extinction coefficient, all of which have specific meanings.

The data presented in this section, unless otherwise noted, pertain to samples which have received a nuclear radiation dose of approximately 10^8R of gamma and 5×10^{14} neutrons ($\phi \geq 2.9$ mev) /cm^2, and approximately 200 sun hours of UV irradiation. The UV and nuclear doses were achieved non currently. Some data will be given which pertain to samples irradiated simultaneously by nuclear and UV; in these cases the nuclear doses were the same as above, but the UV doses exceed 500 sun hours. This information is given for the sake of completeness, but bears little on the qualitative aspects of damage analysis. Except as noted, all data pertain to irradiations conducted in vacuo.

1. Silicate Pigments

In Fig. 1 is shown the spectral absorptance of the system Lithafrax/Sodium Silicate. (The notation used here is: pigment/vehicle). Lithafrax has the approximate stoichiometric formula $Li_2O{\cdot}Al_2O_3{\cdot}6SiO_2$. In this figure are shown the pre-irradiation (control), n-y and UV irradiated spectra. Fig. 2 shows the spectra for the system Ultrox/Potassium Silicate. An experimental system comprised of Lithium Fluoride (LiF)/Sodium Silicate is shown in Fig. 3. By intercomparing these three figures one can immediately see the close similarity of UV and nuclear damage spectra in silicate systems. Of particular importance is Fig. 3 which shows silicate vehicle damage; we assume that the LiF does not chemically react with the vehicle. The peak in the n-y spectrum at 0.45μ corresponds almost exactly with that reported by Ivey at the M-center absorption band peak (Ref. 16 and Refs. therein). Further indication of vehicle damage may be seen in Fig. 4 which shows the spectra for CaF_2/Sodium Silicate. The peak at 0.575μ in the nuclear curve does not show up in the UV curve. This effect is not well understood. It is apparent from Fig.'s 3 and 4 that the alkali halide damage, which is well known from the literature, can not account for the total damage observed and that the vehicle must also be damaged. Other data, not included, lead to the two conclusions that the spectral damage is not qualitatively a function of pigment-vehicle ratio, and that damage to silicate pigments (Lithafrax, ultrox, etc.) can not be qualitatively distinguished from silicate vehicle damage. Fig. 5 also presents data for the system Ultrox/Aluminum Phosphate. Here again silicate damage is evidenced in the location of the absorptance peaks, but the differences in the

damage spectra between the silicate and phosphate vehicles are equally apparent in both the UV and nuclear curves.

Our analyses have been made on the basis of the following considerations. First, the spectra shown have been compared with respect to the position of absorptance peaks, since the various radiation sources employed will differ in their respective abilities to induce damage in any given band. Since the bandwidth, and to a minor extent the peak wavelength of the band, will also vary depending upon irradiation conditions. Second, the wavelength for minimum absorption (extinction) will differ from that for minimum reflectance (Ref. 3). Silica systems in general develop, under irradiation, absorption bands at 2.3, 4.1, and 5.5 ev. The latter peak will not significantly influence solar absorptance. The 2.3 ev. and 4.6 ev. peaks are actually observed as absorptance peaks at 2.0 and 3.1 ev., the displacements agreeing rather well with the theoretical shift of $g/2$, where g is the width of the absorption band (in ev.) at half maximum height. Third, all silicate systems, with the exception of Lithafrax, in a nuclear environment, show the same relative development of the 2.0 and 3.1 ev. absorptance bands. The very large thermal neutron cross-section of lithium may account for the disproportionate (increased) development of the 2.0 ev. absorptance band. Fig. 5 illustrates the latter point; the positions of reflectance minima are the same for each curve and, with the exception of nuclear irradiated Lithafrax, the damage spectra are quite similar.

Several systematic studies have been reported in which sodium silicate glasses containing varying levels and identities of impurities have been irradiated (ref's. 17, 18, 19 and 20). (A bibliography of radiation effects in silicas is given at the end of the references). As a result, the nature of the defect which gives rise to the 2.3 ev. band has been well established as substitutional Aluminum (Al) impurity (i.e., Al atoms occupying normal silicon sites). Some speculation, however, does persist in describing the electronic nature of this defect - whether the neighboring oxygen captures a hole or whether the atom exists in the vacancy together with an alkali atom. The latter explanation seems to be favored, particularly in view of the fact that silicate glasses containing aluminum will not develop 2.3 ev. bands under irradiation without a certain amount of alkali atoms present, (Ref. 17). Irrespective of the electronic nature of this defect, the import of these finding lies in the possibility of purifying the silicate systems to remove as much Al impurity as possible, and thus achieving much more stable silicate paint systems. The nature of the 4.1ev band defect still remains obscure, although it apparently also involves an Al impurity (probably interstitial) in association with an F-center or with an alkali atom. Further increases in silicate paint system stability are unlikely until the defect(s) responsible for the 4.1 ev. band are better identified.

The curves of damage spectra shown in Fig's 1 - 5 display the fact that UV and nuclear produce the same defects. The differences in optical effects lie chiefly in the relative intensities of the bands produced. The same effects have been found in UV, X-, gamma and electron irradiation of transparent silicate glasses (see bibliography-silicas), that is, the same relative development of the absorption bands. In the present work

this is not necessarily to be anticipated - for two reasons; first, the neutron induced damage may be expected to augment the development of one or more bands but with a different "efficiency" for each; second, the changes in reflectance are complex functions of all the bands (see eq. 3).

Other investigators (Ref. 21, 22 and 23) have studied the kinetics of radiation induced color centers. The results of their analyses can be expressed functionally by the equation

$$\frac{dN_i}{dt} = A - BN_i$$

where
N_i = Number of centers/unit volume
t = time
A = constant, depending upon irradiation rate and temperature
B = constant, depending upon temperature

The actual expressions for the growth rate of absorption bands involve much more complicated terms than those given in Eq. 6. The important results of these studies include the qualitative prediction of rate-and temperature-dependence of optical damage, and the further elucidation of band defect in interactions. In the case of inorganic solar reflectors, rate-dependance rarely occurs (the reciprocity law), while considerable temperature dependence has been observed. Fig. 6 shows damage spectra of materials irradiated at 77°K. The explanation for the greatly increased absorptance in these samples is that defects normally unstable or easily bleached at room temperature are not thermally activated at 77°K. The defects normally present in a crystal are greatly increased in number by neutron radiation, and at 77°K these are "frozen in", thus increasing by one or more orders of magnitude the number of defect sites available for electron or hole capture. The Varley multiple ionization mechanism (Ref. 24) would quite likely serve to intensify this effect.

From the spectra so far shown plus those referred to, it is evident that UV and nuclear irradiations produce the same defects, and, as we have shown, UV irradiations cause absorption bands at 2.3 and 4.1 ev., the latter being much more broad and intense. Experiments have shown that when UV radiation of wavelength longer than 3500 Å is used, the damage spectrum differs markedly from that observed when radiation of wavelengths shorter than about 3000 Å is used. A simple way of understanding this is to note that defects are always formed in pairs; for example, when a vacancy is created and the displaced atom goes into an interstitial site, or when an electron, raised to the conduction band, is captured by a vacancy - in the latter case, a positive hole is created at the atom which lost the electron and an F-center at an anion vacancy which captured it. When pairs of defect sites are created, each will behave optically according to the new electronic environment in which it exists. Thus, each will tend to capture whatever type(s) of particle will re-establish local electro-neutrality. Wavelength dependence will arise as a result of the different rates at which these defects will capture electrons, holes, excitons, or displaced atoms and the different rates at which they will

absorb incident radiation, - in this case, solar radiation. Bleaching experiments (see Bibliography: silicas), in which x- or gamma-irradiated materials are subsequently exposed to UV and/or visible radiation, in demonstrating the inter-relationships between band defects, have also pointed up the sensitivity of equilibrium band intensity to wavelength and intensity of bleaching radiation. Fig. 7 compares the spectra for the system Lithafrax/Sodium Silicate irradiated by concurrent and non-concurrent UV & nuclear radiations. These curves show a strong inter-dependence of UV and nuclear radiations and, more importantly, they show that the degradation sustained in non-concurrent radiations cannot be used to predict degradation when these two environments are concurrent.

2. Semiconductor Pigments

In this section we will discuss the damage spectra of paint systems comprised of semiconductor pigments in both silicate and silicone vehicles. In either case the damage spectra, allowing for such vehicle effects as silicate damage and characteristic silicone absorption, will be ascribed to induced free carrier absorption. The lack of any band structure in the damage spectra of these paint systems may be regarded as an indication of free carrier absorption. The fact that the b and gaps of these pigments (TiO_2, ZnO, and ZnS) lie at approximately 3.2 ev. strongly suggests that these pigments may indeed undergo photo-reduction when illuminated by UV light of corresponding or greater photon energy. Experiments conducted at LMSC and by other investigators have clearly shown the differences between vacuum and air irradiations of paint systems containing these pigments. In general these experiments have established the dependence of many electronic properties of TiO_2, ZnO, and ZnS upon the environment during UV illumination. The observations of photoconductivity in these materials, when irradiated with UV photons with energies equal to or exceeding band gap energies, and of the dependence of photoconductive current upon the nature and pressure of the environment, adds further credibility to the arguments for induced free carrier absorption. Theory predicts that free carrier absorption will follow the dispersion equations in which ω_j is set equal to zero. The optical constants would then be obtained from the formulae

$$n^2 - k^2 - \epsilon = \sum_j \frac{Ne^2}{4\pi^2 m_j \epsilon_0} \cdot \frac{1}{\omega^2 + g_j^2} \qquad (7a)$$

$$2nk\omega = \sum_j \frac{Ne^2}{4\pi^2 m_j \epsilon_0} \cdot \frac{g_j}{\omega^2 + g_j^2} \qquad (7b)$$

where,

ϵ = dielectric constant
ϵ_0 = electric permittivity of free space
m_j = effective mass of the j^{th} type carrier

These equations predict decreasing reflectance with increasing frequency. In a real paint system, however, the optical properties will be given by a combination of eq's 3 and 7, that is, by an expression of the form

$$n^2 - k^2 - \epsilon = \sum_j \frac{Ne^2}{4\pi^2 m_j \epsilon_0} \cdot \frac{\omega_j^2 - \omega^2}{(\omega_j^2 - \omega^2)^2 + g_j^2 \omega^2} + \sum_k \frac{Ne^2}{4\pi^2 m_k \epsilon_0} \cdot \frac{1}{q_k^2 + \omega^2} \qquad (8)$$

Since there are a number of unknowns in these equations, it is extremely difficult to obtain other than a qualitative notion of how reflectance will vary with wavelength. This difficulty is compounded by the fact that the "N" and "g" values in eq. 8 will be dependent, for a given paint system, upon the product of intensity and time, and perhaps on each independently. Therefore, it should not be surprising to find that the reflectance of a semiconductor paint system with induced free carriers will not in general display damage spectra typical of free carrier (metallic) absorption. Indeed, as can be seen from Fig.'s 8 - 10, reflectance decreases with decreasing wavelength. This can be explained by pigment-vehicle interactions, such as those due to geometrical effects, chemical reaction, etc. Nevertheless, the absence of any induced band structure in the damage spectra is obvious. In the case of the silicone vehicles, we note that the damage spectra contain the original absorptance bands characteristic of the polymethyl-siloxane polymers, thus showing that silicone vehicle damage, if any, does not affect solar absorptance. On the other hand, the systems with silicate vehicles exhibit damage in the 3.0 ev. region. A tentative explanation of these findings is that vehicles with loosely bound oxygen atoms will give them up to the pigment rather easily under irradiation, thus offering the pigment some degree of stability.

Other evidence suggesting induced free carrier absorption is the fact that semiconductor paint systems when irradiated in air by nuclear radiation often exhibit increased, rather than decreased, reflectance. This can be explained on the basis of an increased competition of the 2nd term in eq. 8 to dominate the spectral character of the irradiated material, and/or by noting that the pigment may, initially, have been slightly reduced and is oxidized in the presence of air during irradiation.

The similarity of the UV and nuclear spectra of the semiconductor paint systems, as shown in fig's 8 - 10, indicates that the damage mechanisms are identical. The explanation follows the same arguments offered previously regarding the formation of defects in pairs. In the semiconductor systems, however, only one of these defects is important in effecting changes in solar absorptance. From these discussions it seems clear that the semiconductor paint systems could be improved in stability by providing more loosely bound anions or by making their escape less probable, or both.

CONCLUSIONS

The important results of this investigation follow directly from the statements made in Section IV A. and from several other observations made in the body of this paper. We can summarize these in this way. Paint systems comprised of dielectric pigments will in general sustain reflectance changes due to induced absorption bands, but since the development of these bands depends upon the initial concentration of defects, degradation may be minimized by reducing the number of initial defects. Thus, in the case of silicate pigments, damage would be lessened by minimizing initial aluminum impurity. Semiconductor paint systems degrade chiefly because of the photo reduction of the pigment and consequent generation of free carriers. The latter effect could be minimized by reducing the effective loss of volatile anion from the pigment. From theory and from the data given in the figures, we can speculate about the temperature dependence of radiation induced damage. In the case of UV radiation, damage would be directly dependent upon temperature; in other words, damage would be small at cryogenic temperatures and would be severe at high temperatures. Damage due to gamma radiation alone would produce roughly the same temperature dependence, except that at cryogenic temperatures, the damage would be slightly greater relative to UV. A neutron-gamma radiation environment would produce severe damage at both cryogenic and elevated temperatures.

REFERENCES

1. F. Seitz, "Modern Theory of Solids," McGraw - Hill Book Co., N. Y., 1940.
2. D. L. Dexter, "Theory of the Optical Properties of Imperfections in Nonmetals," Solid State Physics, Advances in Research and Applications, 6, pp. 353 - 411, Academic Press, Inc., N. Y., 1958.
3. T. S. Moss, "Optical Properties of Semi-Conductors," (Semi-conductor monographs), Butterworth's Scientific Publications, London, 1959.
4. F. Seitz, "On the Disordering of Solids by Action of Fast Massive Particles," Disc. Far. Soc. 5 pp. 271-82, 1949.
5. W. S. Snyder and J. Neufeld, "Disordering of Solids by Neutron Radiation," Phys. Rev., 97, (6), pp. 1636-46.
6. R. D. Evans, "The Atomic Nucleus," McGraw - Hill Book Co., N. Y., 1955.
7. N. F. Mott and R. W. Gurney, "Electronic Processes in Ionic Crystals," Oxford Univ. Press, 2nd Ed., 1946.
8. D. L. Dexter, "Absorption of Light by Atoms in Solids," Phys. Rev. 101, (1), pp. 48-55, Jan. 1956.
9. K. Huang and A. Rhys, "Theory of Light Absorption and Non-radiative Transitions in F-centers," Proc. Roy. Soc. (London). A204, pp. 406-23, 1951.
10. F. Seitz, "Color Centers in Alkali Halide Crystals"
    Part I, Rev. Mod. Phys. 18, pp. 384-408, 1946.
    Part II, Rev. Mod. Phys. 26, (1), pp. 7-94, Jan. 1954.
11. E. W. J. Mitchell, "The Effect of Radiation Damage on the Electronic Properties of Solids," Brit. Jour. Appl. Phys. 8, pp. 179-89, May, 1957.
12. R. E. Peierls, "Quantum Theory of Solids," Oxford, Clarendon Press, 1955.
13. R. W. Montroll & R. B. Potts, "Effects of Defects on Lattice Vibrations," Phys. Rev. 100, (2), 525-43, 1955.
14. K. Lehovec, "Energy of Trapped Electrons in Ionic Solids," Phys. Rev., 92, (2), pp. 253-58, 1953.
15. J. C. Slater, "Interactions of Waves in Crystals," Rev. Mod. Phys., 30, (1), pp. 197-222, 1958.
16. H. F. Ivey, "Spectral Location of the Absorption due to Color Centers in Alkali Halide Crystals," Phys. Rev. 72, (4), 341-43, 1947.

17. J. R. Hensler, N. J. Kreidl, and E. Lell, "Irradiation Damage to Glass," TID-21034, Bausch and Lomb, Inc., Nov., 1960.

18. E. Lell, "Synthesized Impurity Centers in Fused Silica," J. Am. Ceram. Soc., 43, (8) pp. 422-29, Aug. 1960.

19. A. J. Cohen, "Substitutional and Interstitial Aluminum Impurity in Quartz, Structure and Color Center Interrelationships," J. Phys. Chem. Solids, 13, pp. 321-25, 1960.

20. A. Kats and J. M. Stevels, "The Effects of U. V. and X-Ray Radiation on Silicate Glasses, Fused Silica, and Quartz Crystals," Philips Research Reports, 11, pp. 115-156, 1956.

21. P. W. Levy, "Reactor and Gamma-Ray Induced Coloring of Corning Fused Silica," J. Phys, Chem. Solids, 13, pp. 287-95, 1960.

22. M. Levy and J.H.O. Varley, "Radiation Induced Color Centers in Fused Quartz," Proc. Phys. Soc. (London), B 68, pp. 223-33, 1955.

23. P. W. Levy, "The Kinetics of Gamma-Ray Induced Coloring of Glass," J. Am. Ceram. Soc., 43, (8), pp. 389-95, Aug. 1960.

24. J. H. O. Varley, "Radiation Damage in Ionic Solids," Jour. Inst. of Metals, 84, pp. 103-105 (1955-56); "A New Interpretation of Irradiation Induced Phenomena in Alkali Halides," J. Nuclear Energy, 1, pp. 130-143, 1954.

BIBLIOGRAPHY

A. Theory

. M. Born and K. Huang, "Dynamical Theory of Crystal Lattices," Oxford, Clarendon Press, 1954.

. G. Joos, "Theoretical Physics," 2nd. Ed. Hafner Publ. Co. N. Y., 1950.

. L. D. Landau and E. M. Lifshitz, "Electrodynamics of Continuous Media," Pergammon Press, 1960.

. C. Kittel, "Introduction to Solid State Physics," 2nd Ed. Wiley and Sons, Inc., N. Y., 1957.

. F. S. Kroger and H. J. Vink, "Relations Between the Concentrations of Imperfections in Solids," Solid State Physics - Advances in Research and Applications, 3, pp. 307-435, 1956.

. D. S. McClure, "Electronic Spectra of Molecules and Ions in Crystals, Pt. II - Spectra of Ions in Crystals," Solid State Physics - Advances in Research and Applications", 9, pp. 399-525, 1959.

. C. Cuan-in', "Possible Shapes of the Reflection Band, and their Variation as a Function of the Angle of Incidence and State of Polarization, the Dispersion Effect of Reflection Bands," Optics and Spectroscopy, 13, pp. 299-302, 1962.

. R. C. Gex, "Optical Absorption and Reflection of Solids, An Annotated Bibliography," LMSC 3-34-61-4, Feb., 1962.

B. Silicas

. C. M. Nelson and J. H. Crawford, Jr., "Optical Absorption in Irradiated Quartz and Fused Silica," J. Phys. Chem. Solids, 13, pp. 296-305, 1960.

. K. Kubo, "Radiation Induced Optical Absorptions in Crystalline Quartz and Fused Silica," J. Phys. Soc. (Japan), 16, (1), pp. 108-13, 1961.

. G. V. Byurganovskaya and N. P. Orlov, "Formation of Color Centers in Sodium Silicate and Quartz Glasses under the action of Gamma Radiation," Optics and Spectroscopy, 12, pp. 151-54, 1962.

. E. W. J. Mitchell and E. G. S. Paige, "The Optical Effects of Radiation Induced Atomic Damage in Quartz," Phil. Mag. Ser. 8, 1, pp. 1085-1115, Dec., 1956.

C. Semiconductors

. R. E. Dietz, J. J. Hopfield, and D. G. Thomas, "Excitons and the Absorption Edge of ZnO," J. Appl. Phys., Suppl. to Vol. 32, (10), pp. 2282-86, Oct., 1961.

. V. N. Filiminov, "Electronic Absorption Bands of ZnO and TiO_2 in the Infrared Region of the Spectrum," Optics and Spectroscopy, 5, (6), pp. 709-11, 1958.

. W. A. Weyl and T. Forland, "Photochemistry of Rutile," Ind. Eng. Chem., 42, (2), pp. 257-63, 1950.

. R. A. Soffer, "Studies of the Optical and Infrared Absorption Spectra of Rutile Single Crystals," J. Chem. Phys., 35, (3), pp. 940-45, Sept. 1961.

. W. W. Piper, "Some Electrical and Optical Properties of Synthetic Single Crystals of Zinc Sulfide," Phys. Rev., 92, (1) pp. 23-27, Oct. 1953.

. G. Heiland, "Photo conductivity of Zinc Oxide as a Surface Phenomenon," J. Phys. Chem. Solids, 22, pp. 227-34, 1961.

. F. A. Grant, "Properties of Rutile (Titanium Dioxide)," Rev. Mod. Phys., 31, (3), pp. 646-74, July, 1959.

. D. B. Medved, "Photodesorption in Zinc Oxide Semiconductor," J. Chem. Phys., pp. 870-73, 1958.

. D. A. Melnick, "Zinc Oxide Photoconduction, An Oxygen Adsorption process," J. Chem. Phys., 26, 1136-46, 1957.

. W. W. Piper, P. D. Johnston, and D. T. F. Marple, "Optical Properties of Hexagonal ZnS Single Crystals," Phys. Rev., 110, (2), pp. 323-26, 1958.

. N. A. Vlasenko, "Study of the Absorption Spectra of Zinc Sulfide," Optics and Spectroscopy, 7, pp. 320-24, 1960.

D. General and Miscellaneous

. J. J. Markham, "Interaction of Normal Modes with Electron Traps," Rev. Mod. Phys., 31, (4), pp. 956-89, Oct., 1959.

. E. Rabinowitch, "Electron Transfer Spectra and Their Photochemical Effects," Rev. Mod. Phys., 14, pp. 112-31, 1942.

. B. S. Gourary and A. A. Maradudin, "Absorption and Emission Spectra of an Electron in a One-dimensional Deep Trap," J. Phys. Chem. Solids, 13, pp. 88-104, 1960.

. P. D. Johnson, "Optical Absorption from Diffuse Reflectance," J. Opt. Soc. Am., 42, pp. 978-81, 1952.

. R. C. O'Rourke, "Absorption of Light by Trapped Electrons," Phys. Rev., 91, (2), pp. 265-70, 1953.

. O. R. Evans and W. E. Price, "The Effects of High Energy Radiation on Infrared Optical Materials, An Annotated Bibliography," LMSC 3-77-61-2, May, 1961.

. R. C. Cox, "Ultraviolet and Vacuum Effects on Inorganic Materials, An Annotated Bibliography," LMSC-SB-61-19, Apr. 1961.

. R. C. Cox, "Effects of Nuclear Radiation on the Optical, Electrical and Thermophysical Properties of Solids, An Annotated Bibliography," LMSC 3-34-61-8, August, 1961.

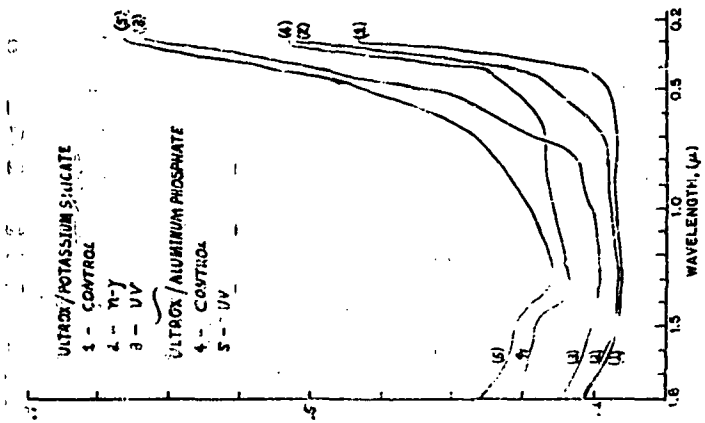

Figure 2

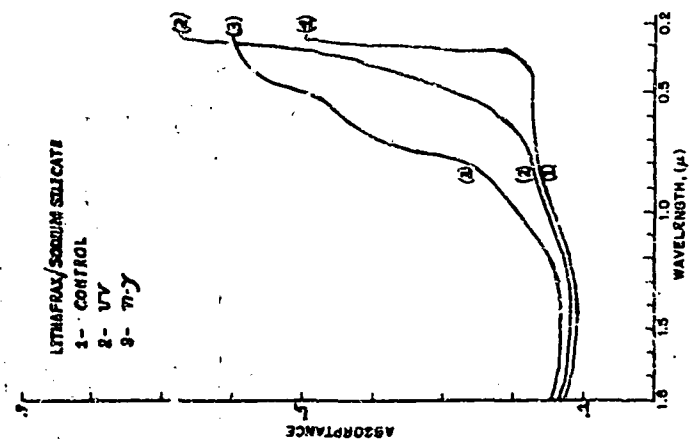

Figure 1

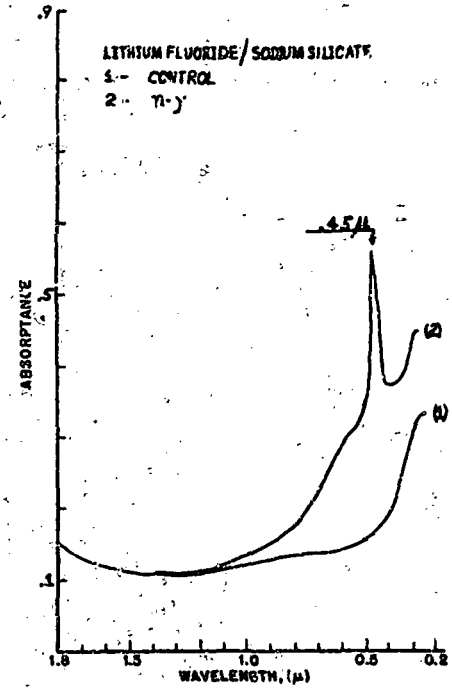

Figure 3

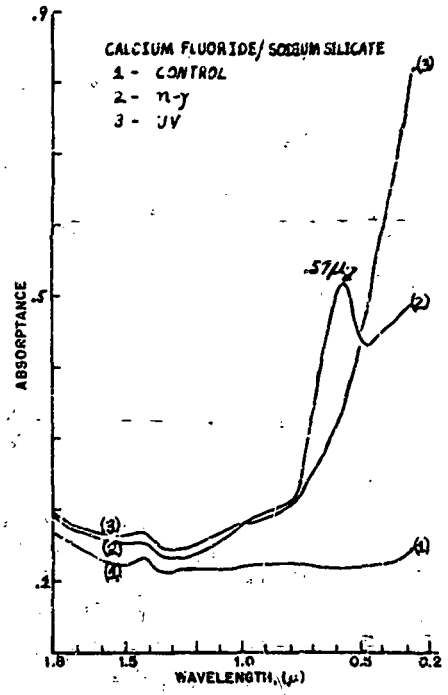

Figure 4

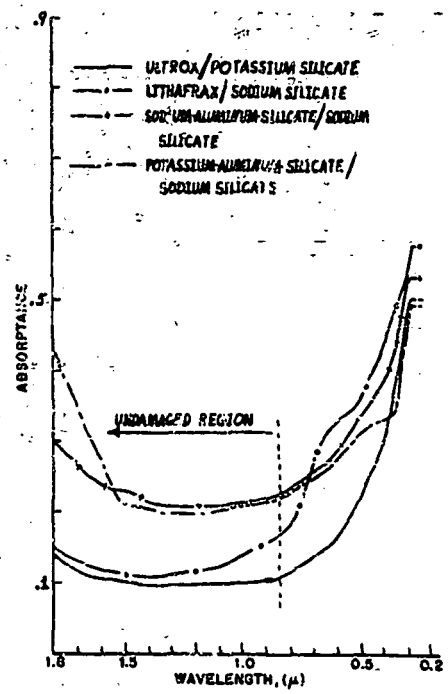

Figure 5

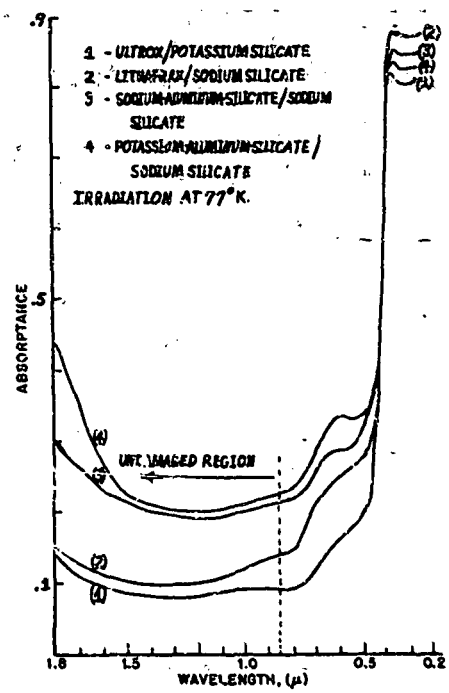

Figure 6

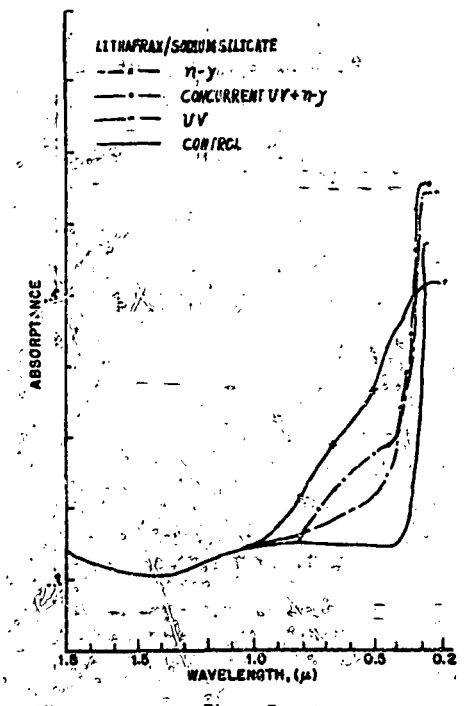

Figure 7

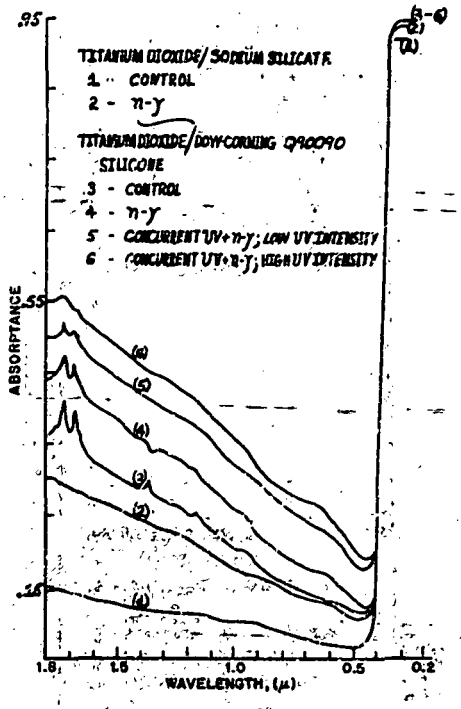

Figure 8

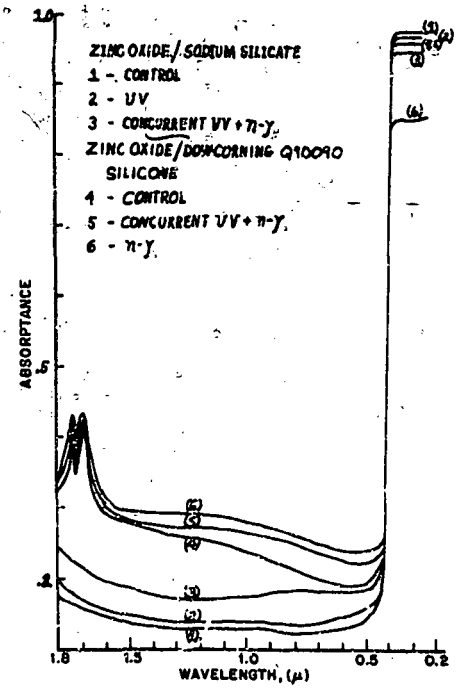

Figure 9

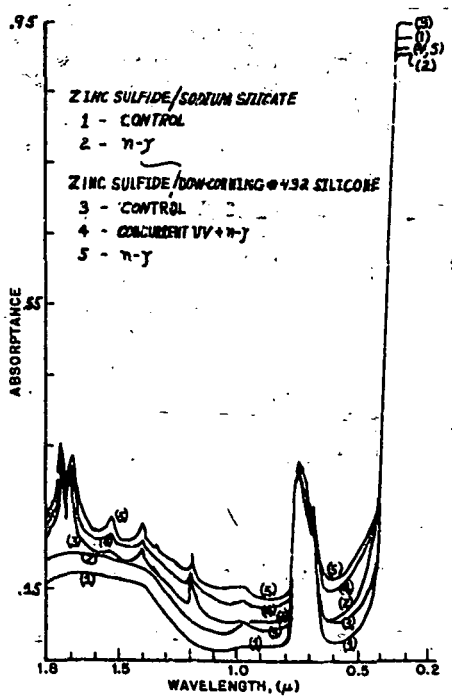

Figure 10

N	Micrometeoroid flux (number of incident particles per square meter per second)
m	Mass of a micrometeoroid
m_o	Cut off mass (minimum mass of a micrometeoroid)
V	Volume
v	Velocity of the micrometeoroid

MICROMETEOROIDS IN SPACE

Flashes across the night sky have long proclaimed the existence of meteoroids in space. In fact, an estimate of the number of meteoroids in space was first deduced by counting the number of meteor streaks of a certain intensity in a certain section in the sky and thereby calculating the number that would pass through a square meter per second. This number is called the meteoroid flux and actually is an accumulative number because it is the total number of meteoroids which have a meteor intensity greater than a given intensity.

The efficiency of changing mass to the energy noted in the meteor trails has been calculated by several investigators [1, 2] . As a result of these studies, it is possible to plot the flux of meteoroids greater than a given mass. This plot results in a straight line when using a log-log coordinate system, and can be extended into the region where meteor trails would not be observable here on the earth. These supposed particles are called micrometeoroids, and from the extrapolated line they are expected to be much more numerous than observable meteorites because of the negative slope of the plot.

Observations of the zodiacal light and the scattering of the F-corona of the sun give additional evidence that a comparatively large number of micrometeoroids exist [3] . A measure of the amount of mass accretion of deep-sea sediments has also given an indication that a large number of meteoroids has settled to the earth's surface. Recent satellite data have given additional information.

Essentially two types of satellite experiments exist. One measures the sound produced when a particle strikes a sounding board attached to a piezo-electric crystal. The amplitude of the sound generated can be related to the momentum of the particle through a ground-based calibration over a limited particle velocity range. The other type of measurement either involves perforating, or piercing, a material and releasing a gas or shorting a capacitor. A calibration of a device of this sort indicates that the thickness of the perforated material is almost a linear function of the energy of the particle. Unfortunately, these two types of measurements sometimes disagree by four orders of magnitude where the microphone data are high and the perforation data are low. This discrepancy can be explained by various difficulties in calibration or perhaps by the fact that different types of phenomena are being measured. Even the basic assumptions may not be correct. For example, one speed is usually assumed in all calculations in the reduction of data, depending upon the investigator. Thus, velocities of 15 to 30 kilometers have been assumed as the

average [3] . An average density of the particle is also used and if the guess is wrong, i.e., if the micrometeoroid is underdense, then the perforation data would be expected to be lower than the microphone data. In Fig. 1 a plot of the most authoritative flux laws is given.

In the following discussion, a parameter study will be stressed more than any one flux law because there still exists a large uncertainty of the micrometeoroid environment in space.

THE EFFECTS OF MICROMETEOROID IMPACTS ON SURFACES

Micrometeoroid damage to a surface may be classified into three types: (1) the case in which the micrometeoroid penetrates all the way through the material and is designated as perforation, (2) the case, related to the above, in which the micrometeoroid does not penetrate all the way through the material but forms a crater, and (3) the case distinguished by a surface removal accomplished by cratering, and perhaps exposing a substrate surface. Emphasis is placed on the cratering phenomena because perforation is relatively rare for any incident particle and real thickness. Likewise, surface removal would be extremely small even for an extreme amount of time, and, hence, it will also be excluded.

The cratering of materials for large particles has been studied extensively. At first, a great deal of confusion existed in trying, even empirically, to describe what was happening, but now a few ideas are generally accepted. The penetration of a particle of relatively slow velocities is almost a linear function of momentum and at very high velocities is a function of energy. This idea is depicted in Fig. 2 and is dependent on the material of the particle and of the target. At some point greater than the transition point, the craters broaden into a hemispherical shape. This transition region occurs around 2-5 km/sec for soft metals, 7 km/sec for aluminum, and higher for the more brittle materials, but generally under 11 km/sec. Usually the average speed assumed for micrometeoroids in space is equal to, or greater than, 15 km/sec and would produce hemispherical craters characteristic of the hypervelocity region for most metals. Brittle materials have a tendency to shatter around the crater.

The cratering efficiency in the hypervelocity region is measured experimentally, although there are some attempts to write a descriptive equation. The empirical data can be given as a constant K where

$$V = KE$$

relating V (the volume of a crater) and E (the energy of the impacting particle). Table I lists several values for K in the hypervelocity region.

One would expect that the inside surface of the craters would be different from the original surface. Figure 3 shows a copper plate which was bombarded, cut, and etched, indicating that there is a considerable amount of "mechanical working" near the surface, demonstrated by the lack of large crystalets as one approaches the crater surface. This mechanical working is very similar to buffing and actually does not have to extend too far beneath the surface to affect the emissivity, since, for a metal, most of the electromagnetic energy is emitted at a depth of less than 100 Å. For low velocities, fragments of the impacting particle may be partially buried in the crater wall. These fragments may still exist at higher velocities although probably at a much smaller size. In the hypervelocity region, the surface is not contaminated by fragments of the impacting particle because at these velocities the crater continues to grow even after the particle has been consumed.

ANALYTICAL DERIVATION OF THE CHANGE IN EMITTANCE DUE TO CRATERING

The emittance of a surface is defined as the ratio of the amount of energy radiated per second by a unit area of surface at a particular temperature to the amount of energy that is radiated by a perfect radiator (black body) of the same area and at the same temperature. Mathematically this can be written as:

$$e = W/W_b \tag{1}$$

Thus the change in emittance is given by:

$$\Delta e = e_n - e_o = (W_n/W_b) - (W_o/W_b) \tag{2}$$

where:

e = the emittance

Δe = the change in emittance

e_n = the emittance of the surface after cratering

e_c = the emittance inside a crater

e_o = initial emittance

W = radiative energy flux = energy radiated per second and unit of area

W_b = radiative energy flux for a black body

W_n = radiative energy flux for the cratered surface

W_o = initial radiative energy flux

The amount of energy emitted by the cratered sample is given by the sum of the energy emitted by the cratered and uncratered portion.

$$W_n = \frac{(A_T - A_c)\, e_o W_b + A_c F W_b}{A_T} \tag{3}$$

where

A_T = total area of the surface of interest

A_c = cratered area

$A_T - A_c$ = area not cratered

$F = W_c/W_b$ = configuration factor

The quantity F is the ratio of the radiative energy flux of a hemispherical surface to that of a black body and may be considered as a function of geometry and the emittance of the crater. The name "configuration" will be used for this term.

Substituting this expression into Eq. (2), the change in emittance can be written as:

$$\Delta e = \frac{A_c}{A_T}(F - e_o) \tag{4}$$

The configuration factor for a diffuse ellipsoidal crater can be calculated in almost the same manner as the hemisphere although not as easily. Remember that the configuration factor is defined as the ratio of the energy emitted by the crater to the energy emitted by a black body with the same size opening. Thus:

$$F = \frac{\text{energy emitted and reflected from the crater}}{\text{energy emitted by a black body with the same size opening}}$$

The energy emitted directly from an element of area dA_1 on the crater wall would be:

$$\text{Energy emitted directly} \quad dA_1 = e_c W_b \frac{\cos \beta_1 \cos \beta_0}{\pi R_{10}^2} \, dA_0$$

$$= e_c W_b \, G(1,0) \tag{5}$$

where the quantitites are defined in the Fig. 4 and where $G(1,0)$ is the fraction of the energy from dA_1 passing through A_0.

The amount of energy reflected once from the element of area dA_1 would be:

$$\text{(Energy reflected once)} \quad dA_1 = e_c (1 - e_c) W_b \left(1 - G(1,0)\right) G(1,0)$$

$$\text{(Energy reflected twice)} \quad dA_1 = e_c (1 - e_c)^2 W_b (1 - G(1,0))$$

$$\left\{ 1 - \left(\frac{\int \left\{ \frac{G(2,0) \cos \beta_2 \cos \beta_1}{\pi R_{12}^2} \right\} dA_2}{1 - G(1,0)} \right) \right\} G(1,0) \tag{6}$$

From the first mean value integral theorem, the integral can be expressed by:

$$\int \left\{ \frac{G(2,0) \cos \beta_2 \cos \beta_1}{\pi R_{12}^2} \right\} dA_2 = G(\xi, 0) \int \frac{\cos \beta_2 \cos \beta_1 \, dA_2}{\pi R_{12}^2}$$

$$\frac{}{(1 - G(1,0))} \qquad \frac{}{(1 - G(1,0))}$$

$$= G(\xi, 0) \, , \tag{7}$$

where $G(\xi, 0)$ is a function of a constant ξ where $0 \leq \xi \leq P$. For the hemisphere case $\xi = z_1$ and the energy reflected twice from dA_1 is equal to

$$e_c (1 - e_c)^2 W_b (1 - G(1,0))^2 G(1,0) \, .$$

The exact expression for a general ellipsoidal case could easily be computed, but since the approximation will occur only after the first reflection, it will obviously be minor when the surface has a fair-sized emittance and/or when the crater is nearly hemispherical.

For three reflections, or more, the energy reflected from dA_1 would be approximately equal to $e_c(1-e_c)^n W_b (1-G(1,0))^n G(1,0)$ where "n" is the number of reflections that occur.

Thus, the amount of energy emitted and reflected from the crater would be equal to

$$\int e_c W_b \, G(1,0) \sum_{n=0}^{\infty} (1 - e_c)^n (1 - G(1,0))^n \, dA_1$$

$$= \int \frac{e_c W_b \, G(1,0)}{1 - (1 - e_c)(1 - G(1,0))} \, dA_1 = \int \frac{(W_b \, G(1,0)) \, dA_1}{1 + \frac{(1-e_c)}{e_c} G(1,0)}$$

and the configuration factor then is given by:

$$F = \frac{1}{A_0} \int \left\{ \frac{G(1,0)}{1 + \frac{1 - e_c}{e_c} G(1,0)} \right\} dA_1 \, . \tag{8}$$

If $e_c = 0$, then $F = 0$ which means that no amount of energy emitted would be equal to zero. If all the emitted energy from the crater were reflected, then from Eq. (8), $F = e_c A_1 / A_0$ which is valid. If $e_c = 1$, then

$$F = \int \frac{G(1,0)}{A_0} \, dA_1 = 1 \, .$$

and must be equal to one because the structure of any perfectly radiating surface does not change its effective emittance.

The percentage of energy emitted through the opening of the crater, A_o, is usually called the geometry factor and can be represented by the function $G(1,0)$. There are several methods of finding an expression for $G(1,0)$, but the simplest seems to be a method described by Sparrow [4]. Here $G(1,0)$ is defined by:

$$G(1,0) = \oint \frac{\cos\beta_1 \cos\beta_c \, dA_o}{\pi R_{10}^2}$$

$$= \ell_1 \oint_{\text{opening}} \frac{(z_o - z_1)\, dy_o - (y_o - y_1)\, dz_o}{2\pi R_{10}^2}$$

$$+ m_1 \oint_{\text{opening}} \frac{(x_o - x_1)\, dz_o - (z_o - z_1)\, dx_o}{2\pi R_{10}^2}$$

$$+ n_1 \oint_{\text{opening}} \frac{(y_o - y_1)\, dx_o - (x_o - x_1)\, dy_o}{2\pi R_{10}^2} \qquad (9)$$

where ℓ_1, m_1, and n_1 are the direction cosines of the normal to the elemental area dA_1. The direction cosines can easily be figured and are given by:

$$\ell_1 = \frac{x_1}{q} \quad q = \sqrt{r_1^2 + \frac{r_o^2}{q^2}(r_o^2 - r_1^2)}$$

$$m_1 = \frac{y_1}{q} \qquad (10)$$

$$n_1 = \frac{z_1 - a}{q} = \frac{r_o^2}{pq}\sqrt{1 - \left(\frac{r_1}{r_o}\right)^2}$$

where the constants and variables are defined in Fig. 5 and where, in a cylindrical coordinate system,

$$x_o = r_o \cos\theta_o$$
$$y_o = r_o \sin\theta_o$$
$$z_o = z_o$$

and r_1, z_1, θ_1, a, ℓ_1, m_1 are constants when integrating over dA_o. Since only a line integral is being considered, $r_o = b$, $z_o = 0$, and θ_o is the variable.

Thus, using these considerations and several steps later

$$G(1,0) = \frac{1}{2\pi} \oint_{\text{opening}} \frac{b}{R^2} \left[(A+C)\cos(\theta_1 - \theta_o) + B\right] d\theta_o , \qquad (11)$$

or substituting in for R^2,

$$G(1,0) = \frac{1}{2\pi} \oint_{\text{opening}} b\left[\left(\frac{A+C}{E}\right) + \frac{BE - D(A+C)}{E(D + E\cos(\theta_1 - \theta_o))}\right] d\theta_o \qquad (12)$$

where A, B, C, D, and E are constants given by:

$$A = \frac{-r_1 z_1 p}{\sqrt{p^2 r_1^2 + b^2(b^2 - r_1^2)}}$$

$$B = \frac{-b^2\sqrt{b^2 - r_1^2}}{\sqrt{p^2 r_1^2 + b^2(b^2 - r_1^2)}}$$

$$C = \frac{b r_1 \sqrt{b^2 - r_1^2}}{\sqrt{p^2 r_1^2 + b^2(b^2 - r_1^2)}} \qquad (13)$$

$$D = (z_1^2 + r_1^2 + b^2)$$

$$E = -2 r_1 b$$

$$R^2 = D + E\cos(\theta_1 - \theta_o)$$

In order that this contour integral be positive, it must be integrated clockwise around the opening. A function of arctan is evaluated with a similar argument, but since it is a many valued function, the evaluated solution of the integral equations is:

$$G(1,0) = -b\left[\frac{A+C}{E} + \frac{BE - D(A+C)}{E\sqrt{D^2 - E^2}}\right] \qquad (14)$$

Substituting in values of A, B, C, D, and E in terms of z_1, p, and b, Eq. (14) reduces to:

$$G(1,0) = \frac{z_1}{2b\sqrt{p^4 + (b^2 - p^2)\, z_1^2}} \left[(b^2 - p^2) + \frac{2p^4 b^2 + (p^2 - b^2)^2 z_1}{\sqrt{4p^4 b^2 + (p^2 - b^2)^2 z_1^2}} \right] \quad (15)$$

Earlier the integral $1/A_0 \int G(1,0)\, dA_1$ was shown that it must be equal to one. After involved but straightforward manipulation, this was shown to be true for all z_1, b, and p .

The change per percent area cratered can then be written as:

$$\frac{\frac{\Delta e}{A_C}}{\left|\frac{A_C}{A_T}\right|} = (e_c F - e_o) \quad (16)$$

where F is given by Eq. (8) and G(1,0) by Eq. (15).

A parameter study was performed for several values of the depth of the crater to the radius (Figs. 6-19). When this ratio is equal to one, the case is for a hemisphere where F reduces to the simple expression

$$F = \frac{2 e_c}{1 + e_c} \quad (17)$$

One can also derive the expression for F for the specular reflecting case for a hemisphere such that

$$F = e_c \left[1 + \sum_{i=1}^{\infty} (1 - e_c)^i \cos \alpha_i \right] , \quad (18)$$

where $\alpha_i = \pi/2\,(i+1)$. The dotted curve in Fig. 20 is for the specular reflecting case and is near the solid line, or the diffuse reflecting case.

COMPARISON OF THE MATHEMATICAL MODEL TO LABORATORY DATA

The mathematical model derived in the preceding sections was compared with experimental data obtained by bombarding surfaces with particles. A full description of these data is found elsewhere [6] . Table II shows a comparison of the computed values for a change in emittance and the actual measured values. The speed of the particles is less than a hypervelocity so that one would expect that perhaps small fragments of the particle may still be embedded in the sample. Obtaining data for higher velocities with an electrostatic accelerator is under consideration at the present time.

As was shown earlier, the total number of micrometeoroid particles passing through a square meter per second is given by

$$N = \alpha m_0^{\beta} \quad ; \quad (19)$$

this equation is usually referred to as the micrometeoroid flux law. Since α and β are constants, the positive number of particles with masses between m and m + Δm passing through a square meter per second is given by

$$\Delta N = -\alpha\beta\, m^{\beta - 1}\, \Delta m \quad (20)$$

and where β is a negative constant. Each particle (in the hypervelocity regime) if it happens to strike any surface, will crater a volume given by:

$$V = C(\tfrac{1}{2} m v^2) , \quad (21)$$

where C is a constant empirically determined for every material and v is the velocity. Thus, the cratered surface area for one incident particle would be:

$$A_c = \pi \left(\frac{3c}{4\pi}\, m v^2\right) . \quad (22)$$

The total cratered area by Δn particles would be

$$A = (A_c)(n) = -A_c(\Delta N)(t)(A) =$$

$$= (t)(A)\,\pi\alpha\beta\left(\frac{3c}{4\pi}v^2\right)^{\frac{\beta}{3}} m^{\beta-\frac{1}{3}}\Delta m \quad (23)$$

Or the total crater area in time t, where A = area available to be cratered, will be the integral of Eq. (23) from the cut-off mass m_o to extremely large masses.

$$A_c = -(t)\frac{(A)\pi\alpha\beta}{(\beta+\frac{2}{3})}\left(\frac{3c}{4\pi}v^2\right)^{\frac{\beta}{3}} m^{\beta+\frac{2}{3}}\Big|_{m_o}^{\infty} \quad (24)$$

or

$$A_c = +t\frac{(A)\pi\alpha\beta}{(\beta+\frac{2}{3})}\left(\frac{3c}{4\pi}v^2\right)^{\frac{\beta}{3}} m_o^{\beta+\frac{2}{3}} \quad (25)$$

Now, A is the total available area that can be cratered and would be given by:

$$A = \frac{(A_T - A_c)}{A_T} \text{ where } A_T \text{ is the total area.} \quad (26)$$

Solving for the amount of time to crater a certain percent of the area A_c/AT:

$$t = \left(\frac{A_c}{AT - A_c}\right)\frac{(\beta+\frac{2}{3})}{\pi\alpha\beta\left(\frac{3c}{4\pi}v^2\right)^{\frac{\beta}{3}} m_o^{\beta+\frac{2}{3}}} \quad (27)$$

A value for t versus the percent area cratered was computed for a number of representative materials and plotted in Fig. 21 where the flux law is shown at the side. The time scale can be contracted or expanded, depending upon the flux law that was used.

CONCLUSIONS

The analytical model developed to predict the change in emittance compares favorably with experimental values. When applied to the space environment, one would expect detectable changes in temperatures in a month when using micrometeorite data contrary to what is observed. For lower flux laws, such as those predicted from penetration measurements or Watson's flux law [3], the time scale would be contracted by 10^4, and indeed there would be not detectable change in temperature for years. When information is available from certain space emissivity experiments then, in effect, thermal micrometeoroid flux could be calculated and used to predict the change of emittance of any material in space.

REFERENCES

1. Jacchia, L. G., "Havard Coll. Observatory Reprint Series II," No. 26, 1945.

2. Whipple, F. L., and Hawkins, G. S., "Meteors," Handbuch der Physics," 52, 519-564, 1959.

3. Vedder, J. F., "Micrometeorites" (F. S. Johnson, ed., Stanford University Press, Stanford, California, 1961), p. 91.

4. Sparrow, E. M., "A New and Simpler Formulation for Radiative Angle Factors," Transactions of the ASME, Sept. 10, 1962, paper No. 62-HT-17.

5. Eichelberger, R. J., and Gehring, J. W., "Effects of Meteoroid Impacts on Space Vehicles," ARS 32, October 1962, p. 1583.

6. Schocken, K., "Emissivity of Metals After Damage by Particle Impact," NASA TN-D-1645, (To be published).

TABLE I

Material	K in m^3 /joule x 10^{-8}
Aluminum, 250	13
2014	4.5
17ST	3.0
75ST	2.5
Cadmium	15
Copper, soft	10
bar	4
-	3
Brass	2.5
Lead	35
Steel 1020	2.7
4140	1.8
-	1.1
Titanium	1.5

TABLE II

Comparison $\overline{\Delta e_\lambda} = \frac{\int \Delta^e(\lambda)^d \lambda}{\int d_\lambda}$

Metal	Depth/Radius at 5 to 600 fps ~2km	% Area $\frac{Ac}{A_T}$	Measured change $\left(\frac{\overline{\Delta e_\lambda}}{Ac/A_T}\right)$	Calculated change $\overline{\Delta e_\lambda}$
Gold	1.4	10.05	.0062	.0025
Aluminum 2S	1.8	3.36	.0057	.0050
Stainless Steel 304	1.2	1.47	.014	.0070
Stainless Steel 316	.6	6.43	.0053	.0030
Chromium	1.0	4.09	.0090	.0070
Tungsten	.4	2.33	.013	
Silver	1.4	7.43	.013	.0025

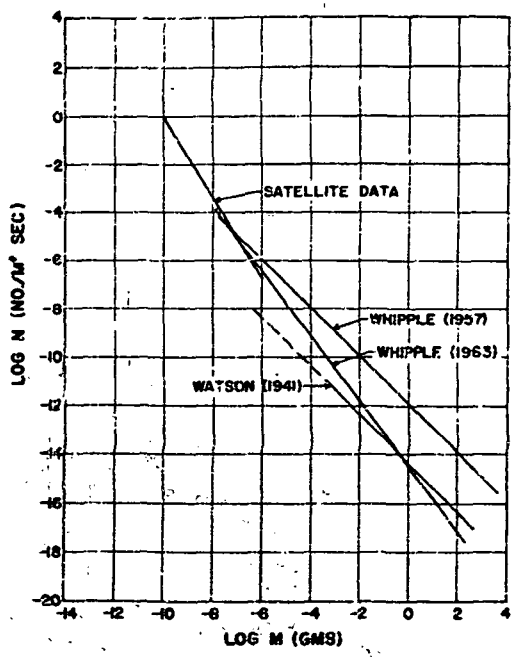

Figure 1.- Flux versus mass.

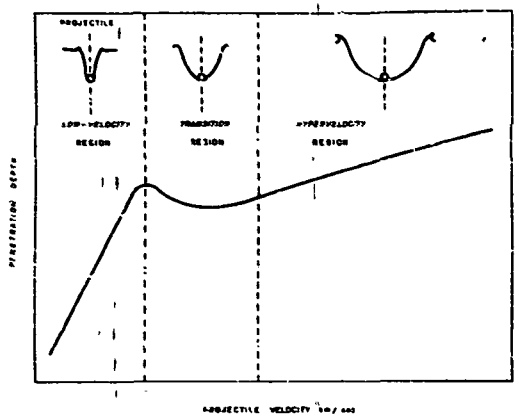

Figure 2.- Penetration versus velocity for metal-to-metal impacts with associated crater shapes.

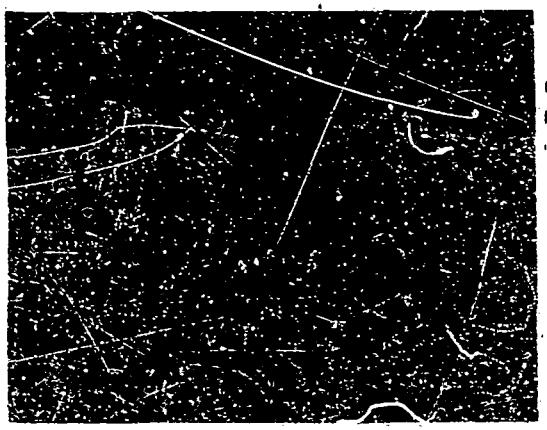

Figure 3.- Hemispherical micrometeoroid crater.

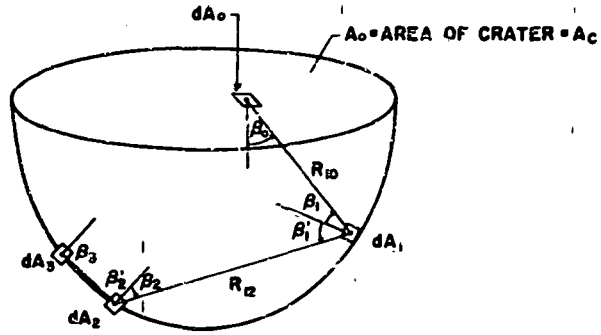

Figure 4

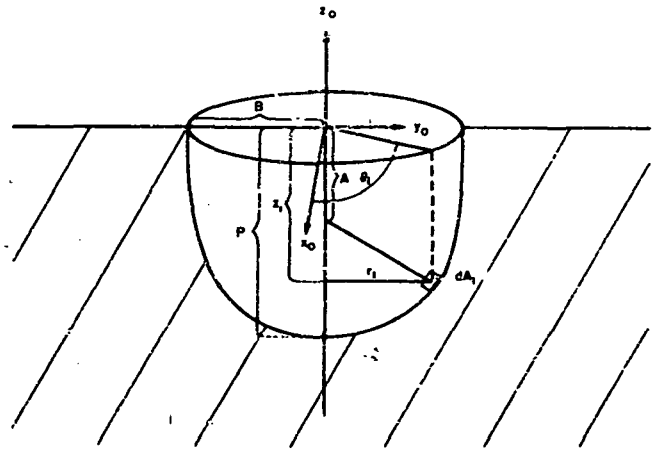

Figure 5

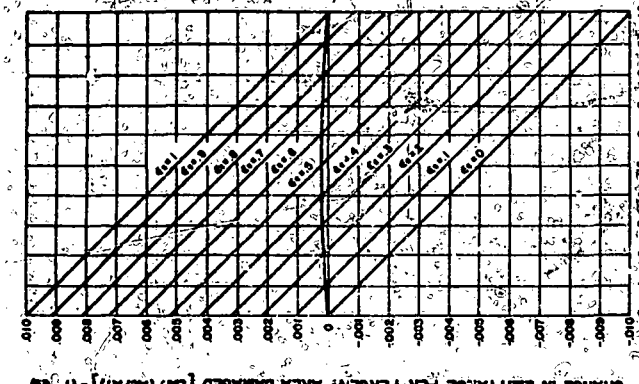

Figure 7.- Change in emittance for radius to penetration ratio of .2.

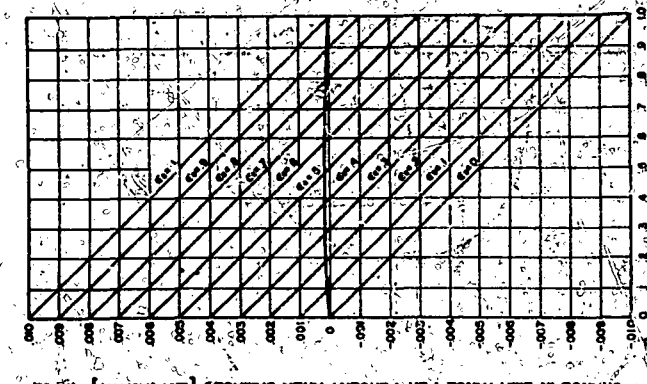

Figure 6.- Change in emittance for radius to penetration ratio of .1.

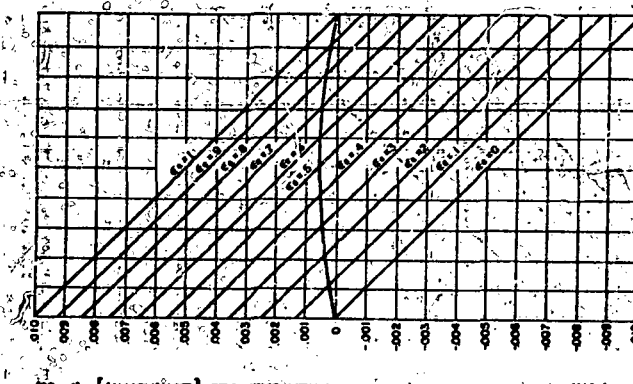

Figure 9.- Change in emittance for radius to penetration ratio of .4.

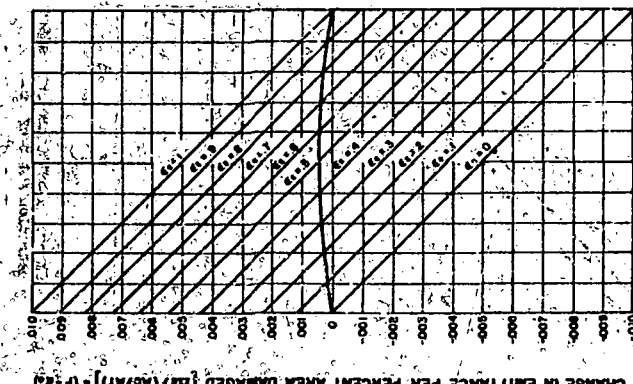

Figure 8.- Change in emittance for radius to penetration ratio of .3.

Figure 10.- Change in emittance for radius to penetration ratio of .6.

Figure 11.- Change in emittance for radius to penetration ratio of .8.

Figure 12.- Change in emittance for radius to penetration ratio of 1.0.

Figure 13.- Change in emittance for radius to penetration ratio of 1.2.

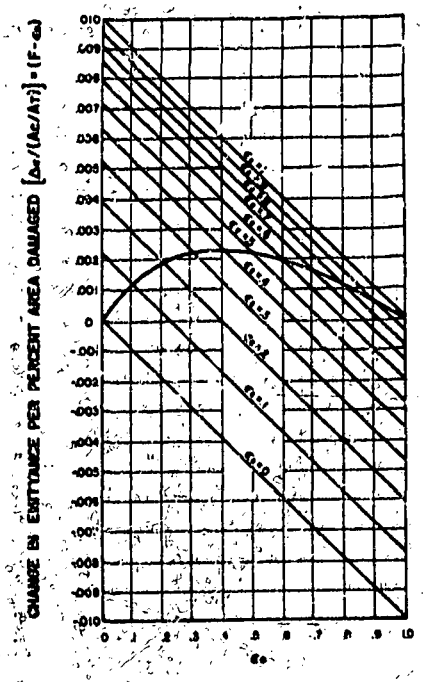

Figure 14.- Change in emittance for radius to penetration ratio of 1.6.

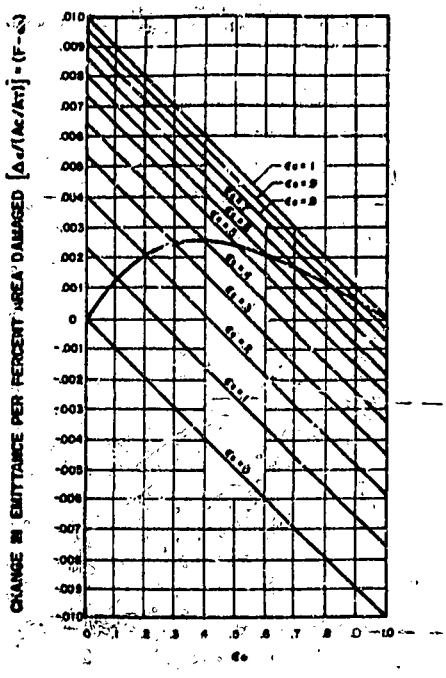

Figure 15.- Change in emittance for radius to penetration ratio of 1.6.

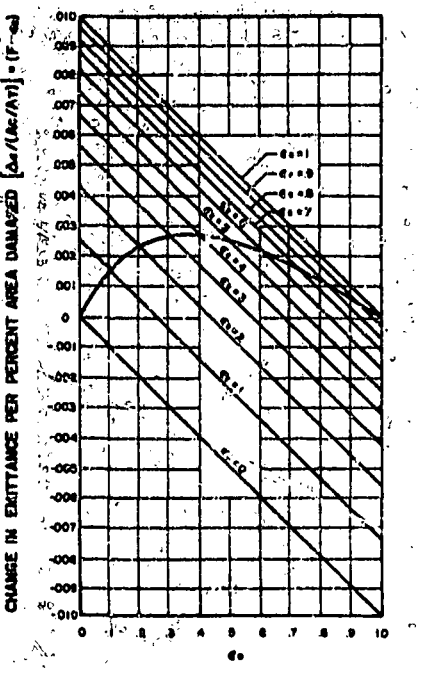

Figure 16.- Change in emittance for radius to penetration ratio of 1.8.

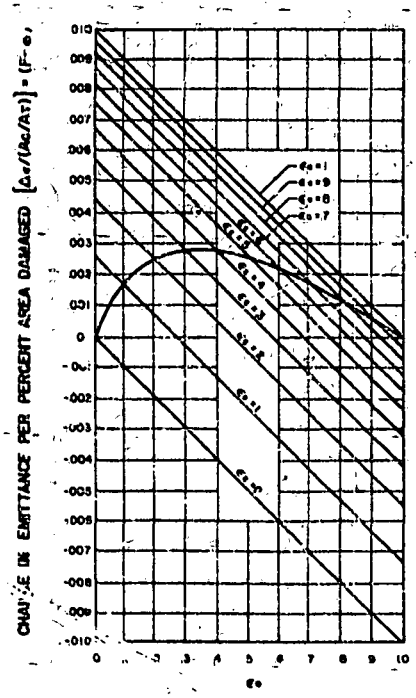

Figure 17.- Change in emittance for radius to penetration ratio of 2.0.

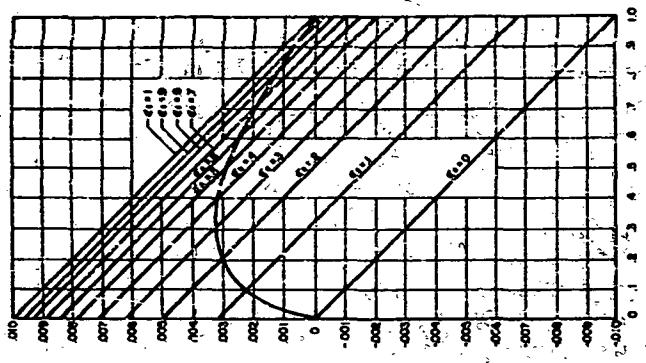

Figure 19.- Change in emittance for radius to penetration ratio of 3.0.

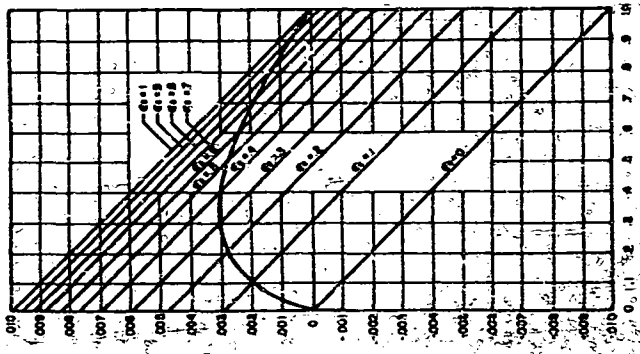

Figure 18.- Change in emittance for radius to penetration ratio of 2.5.

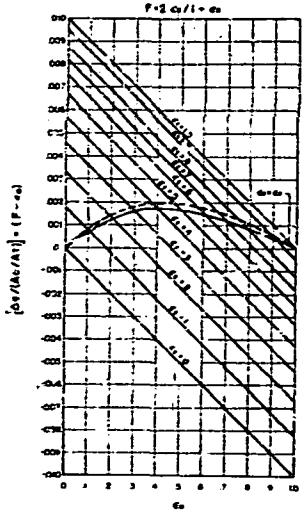

Figure 20.- Parametric study - percent crater area with different ε_c and ε_0.

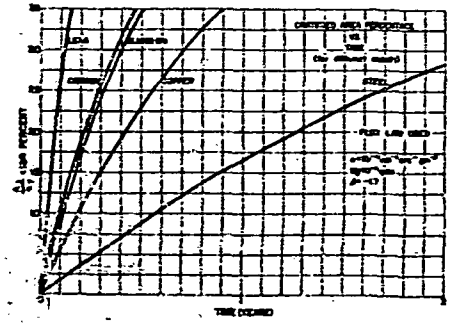

Figure 21.- Result of micrometeroid erosion.

Solar-Wind Bombardment of a Surface in Space*

by
G. K. Wehner
General Mills, Inc., Electronics Division
2003 East Hennepin Avenue
Minneapolis 13, Minnesota

ABSTRACT

The surface of any body in space, when unprotected by a shielding atmosphere, is under bombardment by high- and low-energy, elementary particles. The question discussed here concerns what effects will arise on a surface under solar-wind bombardment, i.e., by low-energy protons and α-particles. From astrophysical observations and measurements with Explorer X, Lunik II, and Mariner II, data for flux density, composition, and energies of the solar wind are now fairly well established. Under a quiet Sun there is a flux of 2×10^8 protons/cm^2 sec with 600 km/sec average velocity in earth orbit distance from the Sun. The protons are accompanied by 15% α-particles with the same velocity. Under solar-storm conditions, the flux and the particle velocity increase to much higher values. The bombarding energies correspond to 1850 ev for protons and 7.4 kev for α-particles under solar-wind conditions and 5 kev for protons and 20 kev for α-particles under solar-storm conditions.

One can simulate these solar-wind bombardment conditions on a much accelerated scale in the laboratory and, with much higher flux

*This work is supported under a contract with the National Aeronautics and Space Administration (NASw-751).
NASA

densities for ... bombardment times, obtain measurable results on sputtering effects and on damage to a surface. With the goal of studying possible modifications of the lunar surface, measurements were performed with mass separated H^+, H_2^+, and H_3^+ beams and in low-pressure, noble gas plasmas. One has to distinguish between purely physical effects such as crystal damage, sputtering, etc., (such as with α-particles or noble metals) and superimposed chemical reactions between hydrogen and compounds such as oxides. The sputtering rates are rather small and amount to ~1 Å/year for Cu and ~0.5 Å/year for Fe, with many oxides roughly in the same range as that of Fe. Thus the Moon should have lost a layer of 17 cm thickness in 4.5×10^9 years or a 1-cm thick Cu plate would be sputtered away in approximately 10^8 years. Physical sputtering will therefore hardly present any erosion problems in space missions. These results have been reported in detail in a recent paper.[1] However, more serious attention is required of secondary effects which arise for instance from the cementing together of powder particles by sputtered atoms or from chemical reactions or the bombardment-induced breakup of molecules. Experiments with metal targets and metal-, oxide-, and rock-powder samples demonstrate the leveling and smoothing of macroscopic surface features, the etching of polished surfaces (because differently oriented grains have different sputtering rates) and the cementing together of loose particles into a porous, brittle, fibrous crust. We have observed

1. G. K. Wehner, C. E. KenKnight, and D. L. Rosenberg, Planetary and Space Science 11, 885 (1963).

that many compounds, such as white oxides, acquire a yellowish tint or darken under the bombardment because oxygen is more likely to escape in the breakup process resulting in a metal enrichment at the surface. Black CuO is first converted into red Cu_2O and finally becomes covered with a very porous Cu layer under noble gas ion bombardment. Under hydrogen ion bombardment we observed an immediate conversion to a metallic Cu. The x-ray diffraction analysis shows that the red Fe_2O_3 converts into Fe_3O_4, FeO, and Fe under the ion bombardment. Compact $BaTiO_3$ becomes covered with a layer of Ti fairly rapidly. Very pronounced chemical effects were observed in the case of Sn bombarded by hydrogen ions. Here the hydrogen combines with Sn and forms the volatile SnH_4 which leads to much higher apparent sputtering rates. The controlled ion bombardment of insulator surfaces in a plasma was made possible with a recently developed technique, in which a high frequency voltage provides the necessary neutralization of surface charges at the target.[2] Many of the experimental results are discussed in a forthcoming paper where we studied the modification of the lunar surface by the solar-wind bombardment.[3]

It is not expected that the thermal radiation properties of metals or fairly stable solids such as SiO, ZnO, or TiO_2 will

2. G. S. Anderson, W. N. Mayer, and G. K. Wehner, Journal of Applied Physics 33, 2991 (1962).
3. G. K. Wehner, C. E. KenKnight, and D. L. Rosenberg, "Modification of the Lunar Surface by the Solar-Wind Bombardment". To be published in Planetary and Space Science.
4. G. L. Anderson and George J. Rothwang. NASA Tech. Note D-1646, Ames Research Center, Moffet Field, California.

undergo catastrophic changes from the slight bombardment of the solar wind, which corresponds to only ~ 50 monolayers per year. But, one cannot exclude the possibility that in violent solar storms, in missions closer to the Sun and of long duration, and with certain materials, or in ion engine environments the problem can be more serious and warrants further study.

THE EFFECTS OF MICROMETEOROIDS ON THE EMITTANCE OF SOLIDS

By Ronald B. Merrill

Research Projects Laboratory
George C. Marshall Space Flight Center, Huntsville, Ala.
National Aeronautics and Space Administration

SUMMARY

An analytical model is developed to predict the change in the emittance of a surface caused by particle impact. This model is applied in a representative fashion to determine the change in the emittance due to the space environment.

INTRODUCTION

Before artificial satellites were placed into orbit, it was uncertain what effects various parameters of the space environment would have on them. Satellites have been designed which have successfully operated for more than one year in the space environment. Indeed, to some it is surprising that the space environment is so mild. One such mild space environment parameter is the presence of a relatively large number of solid particles in space. One usually neglects the effect of the impingement of these particles on the thermal radiative characteristics of surfaces partly because even erosion- and cratering-sensitive surfaces have not changed enough to significantly affect the satellite's temperature. However, the question of "what is the effect" has really never been answered. In the future this answer will become more important because of the postulated increase in particle flux near the lunar surface and the anticipated use of more critical surfaces such as lenses and windows.

This paper will be restricted to the change in emittance of a surface due to particle impact as applied to the space environment. Hence, several topics are discussed only in general terms mainly for a background and for particular information needed in the development of an analytical model which will be used to predict the change in emittance in the space environment.

LIST OF SYMBOLS

e	The emittance
Δe	Change in the emittance
e_n	The emittance of the surface after cratering
e_c	The emittance inside a crater
e_o	The initial emittance of a surface
W	The radiative energy flux (energy radiated per second and per unit of area)
W_b	The radiative energy flux for a black body
W_n	The radiative energy flux for a cratered surface
W_o	The initial radiative flux of a surface
A_T	The total area of the surface of interest
A_c	Area of the openings of a crater
A_l	Area of an ellipse
F	Configuration factor
dA_o	Elemental area on the area of the opening of the crater
dA_i	Elemental area on an ellipsoidal crater where i can equal 1, 2, 3. . .
βi	The angle with the perpendicular of the ray from elemental area dA_i to dA_{i-1}
β_i	The angle with the perpendicular of the ray from dA_i to dA_{i+1}
R_{ij}	Distance between elemental area dA_i and dA_j
$G_{(i,j)}$	The fraction of energy from dA_i to dA_j

N65 17321

CR NASA. Ames Research Center, Moffett Field, Calif.

EXPERIMENTAL DEVELOPMENT OF A TECHNIQUE FOR THE CORRELATION OF FLIGHT- AND GROUND-BASED STUDIES OF THE ULTRAVIOLET DEGRADATION OF POLYMER FILMS

By John A. Parker,[1] Carr B. Neel,[1] and Morton A. Golub[2] (Stanford Res. Inst.)

In NASA, Washington ... 15p refs (See ...)

N65 17321

1 - 14

SUMMARY

The surface temperatures and the environmental stabilities of thermal control surfaces have been observed to change measurably in a near-earth orbit on the S-16 Orbiting Solar Observatory (OSO). The changes in surface temperatures caused by in-space ultraviolet degradation do not correlate with predictions from ground-based simulation of environmental conditions. The general behavior of these surfaces has suggested a possible technique of evaluating the accuracy of ground-based simulation experiments, namely, the measurement of surface temperature of a film consisting of a well-behaved polymer system. Films of both polymers and copolymers of vinyl chloride were exposed to ultraviolet radiation in vacuum and were found to exhibit a regular and quantitatively measurable change in solar absorptance with time. The major changes produced by this exposure occurred in the ultraviolet and visible regions. Virtually no change has been observed in the infrared absorption spectra of these films, even after exposure to the equivalent of 72 hours of space solar radiation. In the exposures to simulated conditions of vacuum and ultraviolet radiation, a linear change with time in the ratio of solar absorptance to emittance has been observed to occur after an initial transient period. The regular behavior of these films indicates that a reasonable prediction of the temperature changes which would occur in the real space environment can be made.

17321

To obtain the desired mechanical properties for a flight test, a surface consisting of a pure polyvinyl chloride terpolymer film (VMCH) was cast on a polished aluminum substrate. This material is found experimentally to behave almost identically to the pure polyvinyl chloride. Predicted temperature changes of such a surface will be compared with the actual results obtained by orbiting the surface on the S-57 OSO. The amount of gamma radiation required to produce a given change in the absorptance equivalent to that produced by a specific amount of ultraviolet radiation has also been determined experimentally. The gamma radiation which would produce the same effect as

[1]NASA-Ames Research Center, Moffett Field, California
[2]Stanford Research Institute, Menlo Park, California

a 9-hour exposure to the solar ultraviolet would require a period of 3 or 4 years exposure in space; and, hence, would not influence the results of the correlation of the ultraviolet exposure.

INTRODUCTION

Reflective white paints, consisting of inorganic pigments and organic polymeric binders, have been employed as thermal control surfaces for space vehicles. A variety of polymeric types of binders have been investigated for this purpose. Paints based on acrylics, silicones, phenolics, and epoxy resins have been used (ref. 1). None of these materials are unstable in a vacuum in the range of operating temperatures encountered on a spacecraft. The inorganic pigments, for example, titanium dioxide, are relatively stable to the action of the incident electromagnetic radiation encountered in these applications. All available evidence obtained to date points to an alteration of the molecular structure of the polymeric components produced by the incident ultraviolet radiation as the principal cause of change in the thermal control characteristics of these coatings. Nine percent of the total energy of incident solar radiation in near-earth orbit lies in the region from 2200 to 4000 Å and only 0.02 percent below 2200 Å (ref. 2). The energy of photons in the wave-length region from 2200 to 4000 Å ranges from 5.6 to 3.1 electron volts. These photons have sufficient energy to break carbon-carbon bonds characteristic of organic polymers, the strength of which is of the order of 3 electron volts (72 kcal per mole), and this can initiate molecular damage processes. The specific chemical structure of the polymeric binder determines both the specific wave lengths and the degree of absorption of the incident ultraviolet radiation. The basic chemical constitution of the polymer also determines the course of the ensuing degradation reaction.

The degradation reaction may produce scissions, cross-linking, or functional group alteration. Only when the damage process leads to the production of highly absorbing groups may one expect a significant change in the optical properties of coatings formulated from these polymers.

To correlate quantitatively the effects of a simulated environment with those of an actual orbital flight on the rate of change of temperature of a polymeric film, a basic polymer with the following properties is required:

(1) It absorbs photons in the range from 2200 to at least 3000 Å and these photons should be effective in generating color-producing groups.

(2) Its principal damage reaction is chromophore production so that absorptivity changes in a regular manner with time of exposure. (Under the conditions of exposure there should be no significant autocatalysis; that is, this reaction should be zero order with respect to the chromophoric reaction.)

(3) It undergoes the required chromophoric reaction without significant alteration in the basic mechanical properties of the film; that is, its physical properties should not be affected either by cross-linking or by scission so that the film can endure a reasonable orbital flight and experience the expected temperature changes while still retaining its mechanical integrity.

(4) Its specific color-producing reactions are free from the the effects of differences in spectral distribution. The quantum efficiency and both the number and kinds of groups formed should be independent of the wave length of ultraviolet radiation absorbed.

(5) It is sufficiently stable at the operating temperature of the film that thermal degradation does not occur, and thus complicate the interpretation of the ultraviolet damage process.

Information on the photochemical degradation reactions of polyvinyl chloride and copolymers containing a substantial portion of polyvinyl chloride monomer suggests that such polymers could possibly meet the foregoing requirements (ref. 3).

97321 cont.

The specific research to be described is concerned with the evaluation of thin films of polymers and copolymers of vinyl chloride as indicator coatings, as well as with approaches to ground-based simulation which, if successful, could be used ultimately to predict both the expected temperatures and temperature changes with time of exposure to solar radiation. This paper discusses the research to date on the ground-based phase of this program. The results obtained herein will be correlated ultimately with an in-flight test on the S-57 Orbiting Solar Observatory which should provide an evaluation of the simulation technique.

Author

EXPERIMENTAL RESULTS

TiO_2-Epoxy and TiO_2-Silicone Coatings Used as Thermal Control Surfaces on the S-16 OSO Satellite

The surface temperatures attained by TiO_2-epoxy and TiO_2-silicone coatings during the first orbit of the S-16 OSO are shown in figure 1. It can be seen that the maximum temperature reached by the TiO_2-epoxy

coating is about 15° F, whereas that of the white silicone coating is about 30° F. These temperatures agree with those calculated by the relation given in reference 3 with initial values for α_s/ϵ for these coatings of 0.27 and 0.36.

The increase in solar absorptance of these coatings calculated from the observed increase in surface temperature in the space environment is shown in figure 2. Here the increase in solar absorptance is given as a function of exposure in equivalent sun hours in a near-earth orbit. A nonlinear change in solar absorptance with time indicates the presence of an autocatalytic effect. At the beginning of the exposure, the rate of change in the epoxy is greater than in the silicone coating, but after 10^3 equivalent sun hours, the rate of change of the silicone solar absorptance is essentially the same as that for the epoxy coating. These differences in environmental aging characteristics are apparently due to basic differences in the photochemistry of the two polymer binders concerned.

These specific changes in the solar absorptance obtained from in-flight measurements of the temperature have been compared with the changes predicted by ground-based simulation experiments by two different groups of investigators. Unfortunately, the ground-based experiments cannot perfectly reproduce the conditions of space. Specifically, the temperature of the films during ultraviolet irradiation and the intensity and spectral distribution match of the simulation lamps were not the same as the space exposure in any of these experiments. In the test run with a BH-6 lamp, the average film temperature was 185° F at 7 solar constants of ultraviolet flux. With an AH-6 lamp, on the other hand, the temperature was 75° F at 1 to 10 solar constants. The results are compared in figures [illegible]4 with the flight results with an average in-flight temperature of 0 F at one solar constant. For the time interval of exposure considered, there is apparently better agreement between the actual and the predicted values of absorptance change with the flight test in the case of the silicone (fig. 4) than in the case of the epoxy (fig. 3). The tests suggest that the rate of change of solar absorptance is dependent on changes in the [illegible] mentioned test parameters for the polymeric systems in question. These results cannot be interpreted more precisely until the relationships among the rate of chromophore production, temperature, intensity, and wave length are established.

Some of the difficulties involved in obtaining a simulation match between an ultraviolet mercury vapor lamp and the actual solar radiation are shown in figure 5. In this particular case, the distance from the lamp source to the detector (or sample) has been adjusted to provide an average of one solar constant of ultraviolet radiation in the wave length from 2200 to 4000 Å. It can be seen that in the case of the G.E. UA-2 lamp shown here, as with all mercury vapor lamps, there are numerous band emissions present in the spectral distribution. If the total energy flux is matched over the region from 2200 to 4000 Å, this matching produces, at certain wave lengths, about a fivefold difference in flux compared to

that of the sun. If the matching is done for the region between 2200 and 3000 Å a much closer simulation of the solar radiation is obtained. However, if the photochemical reaction of the coating is significantly dependent on wave length; that is, if it gives one product at one wave length and another kind of product at another wave length, or if synergistic effects occur through combination of wave lengths, it is very unlikely that satisfactory simulation with any lamp source of this kind is possible.

Experimental Polyvinyl Chloride Films for Developing Simulation Techniques

Thin films of pure polyvinyl chloride were cast from dilute solutions in methyl ethyl ketone. After being dried in air these were water-white transparent films. After further drying, at 60° C under vacuum, to remove traces of the ketone solvent the films were used in photodegradation studies. Similar films were prepared from a vinyl-chloride, vinyl-acetate, maleic-acid (86:13:1) terpolymer ("VMCH"). These films were cast from solutions containing toluene and methyl Cellosolve, and were dried in a similar manner. The VMCH terpolymer was also studied in combination with a metal substrate. Thin films were cast and affixed to aluminum disks by completing the removal of solvent at 80° C under vacuum. Film thicknesses were calculated to be 7 to 8×10^{-4} cm from the weight of film, density of polymer, and surface area. These films were used in the exposure tests to be described below.

Environmental Simulation Exposure Conditions

The films were irradiated for periods of time up to 72 hours with the total output of a G.E. UA-2 lamp (fig. 5) at a distance of 10-1/2 inches from the film surface. Under these conditions, the output of this lamp amounted to an average of one solar constant in the same wave-length region. The power output of the lamp was maintained constant during the entire exposure by monitoring the output with a photo cell and adjusting the input power as the lamp output degraded. During the radiations the vacuum chamber pressure was between 30 and 40 microns. The films were transferred to a vacuum desiccator where they were kept until spectroscopic measurements were made. The ultraviolet spectra were measured for the films before and after irradiation with a Cary 14 spectrophotometer. The infrared spectra of the films were obtained with a Perkin-Elmer 21 spectrophotometer. The change in reflectance of the terpolymer on the aluminum substrate was determined with a Gier Dunkel integrating sphere spectrophotometer.

The solar absorptance and emittance were determined by Lockheed Missiles and Space Company in a manner described in reference 1.

Discussion of Results

It was found convenient to present and consider the spectroscopic changes in films in terms of the optical density defined by the equation

$$O.D. = \ln I_0/I$$

where I_0 is the incident intensity and I is the transmitted intensity, a change in optical density (Δ(O.D.)) of, say, 1.4, implies that the transmission, T ($=I/I_0$), is essentially reduced to a level which is $10^{-1.4}$ or about 4 percent of the original transmission value. The method of representing the spectroscopic changes in the films by optical density rather than transmission or other quantities, was selected so that the changes in absorption could be related directly to the increased concentration of the color-producing groups. The changes in optical density of the free films of pure polyvinyl chloride with time of exposure to radiation in the wave-length region 2200 to 6000 Å are given in figure 6. The change in optical density, as plotted, is the difference in optical density (or absorption) of the polymer film at a given wave length before and after irradiation. The increase in the optical density and the shift of over-all absorption into the visible region is evident. After a total exposure of 6 hours, the polymer is nearly completely opaque to radiation at 2800 Å.

The basic chemistry underlying this photochemical change in PVC, based on references 3 and 5, is outlined in figure 7. The first step in this process is assumed to involve absorption of energy by trace impurities in the system in the form of unsaturated end groups, catalyst residue, residual solvent, etc. This energy absorption, followed by energy transfer to the basic polymer, is sufficient to initiate the reaction through the removal of an energetic chlorine atom, leaving a residual radical on the chain as shown. Propagation of the reaction involves the removal of the hydrogen atom immediately adjacent to the radical site to form a molecule of hydrogen chloride, termination occurs by formation of a π bond from the available pair of electrons. It has been shown by Boyer (ref. 6) that the continued introduction of double bonds by this mechanism is a nonrandom process, indicating that the removal of chlorine next to the double bond site proceeds more easily than the removal of chlorine from an ordinary carbon in the polymer chain. As the process proceeds, a conjugated linear polyene system is developed which absorbs strongly in the ultraviolet and visible region of the spectrum. To date, the exact concentration and extent of the conjugated system is unknown. Photochemical investigations are under way to determine the nature of this structure.

The change in optical density for pure PVC for a number of wave lengths from 2800 to 6000 Å as a function of time of ultraviolet radiation is shown in figure 8. This figure shows that there is increased opacity at all wave lengths over the ultraviolet and visible regions, and that the region of almost complete opacity (change in optical

density in excess of about 2.0), progressively advances to longer wave lengths with increased dose. No difference has been observed in the rate of color formation between the polyvinyl chloride and polyvinyl chloride terpolymers. In the cases of both polymers, no change in the infrared spectrum of the free films has been observed up to as much as 72 hours of ultraviolet radiation in vacuum.

As mentioned before, for the proposed flight tests, it is necessary to have a polymer which adheres well to an aluminum metal substrate, and is sufficiently flexible as well, so as to not crack during the expected temperature cycle (similar to fig. 1). The vinyl acetate component of the VMCH terpolymer provides internal plasticization and the maleic acid provides the necessary polar groups for adhesion to the substrate. It is interesting to note that the ultraviolet-induced changes in optical density of this terpolymer are similar to those obtained for pure polyvinyl chloride.

In addition to ultraviolet radiation, the flight tested surfaces experience collisions with higher energy photons in space. For this reason, the effects of gamma radiation from 10 to 16 mev were also examined on the polyvinyl chloride films. Figure 9 shows the changes in optical density produced by γ radiation. An essentially analogous situation is obtained here in the way in which the opacity at each wave length steadily increases with increased gamma radiation. An increase in optical density with increasing dose similar to that for ultraviolet radiation is observed. The near equivalence of the effects of ultraviolet radiation and gamma radiation is shown in figure 10. It is clear that a dose of 9 hours of solar ultraviolet energy produces a change equivalent to a dose of gamma radiation of 10 megarads. It would probably take a period of at least 3 to 4 years to obtain a dose of this magnitude from the higher energy photons available in the environment of the OSO satellite, whereas, a similar effect would be produced in a few hours of ultraviolet radiation. These results indicate that the effects of higher energy photons in space can be ignored in this ultraviolet degradation comparison.

The temperature rise which occurred during exposure of the VMCH film on aluminum substrate to ultraviolet radiation in vacuum is given in figure 11. It can be seen that there is a rise in temperature from 27° C to about 46° C in 1200 minutes. Since no change in the rate of formation of chromophore was observed in these tests it appears that the activation energy for the dehydrogenization of polyvinyl chloride is very small under these conditions. No precautions were taken to control or to correct for the energy emitted from the back face of these composites or to shield this surface, therefore, this temperature rise does not quantitatively indicate the expected temperature rise on the satellite experiment.

The decrease in the percent of energy reflected due to 16.5 hours of irradiation with the UA-2 lamp of the VMCH terpolymer cast on an aluminum substrate is given in figure 12. The percent reflectance an

a function of wave length from 3000 to 28,000 Å was determined by the Gier Dunkel hemispherical reflectance spectrophotometer. The shaded area indicates the wave-length region of change in reflectance due to alteration in the film properties. It can be seen that the largest change in reflectance occurs in the visible and ultraviolet region below 7000 Å. This corresponds to the region of change in optical density for the free films of this polymer, and suggests that on the aluminum substrate, the production of chromophores in the polymer is still the principal cause of change in optical properties. It can be seen that above 9000 Å, there is little change in the absorption with ultraviolet exposure, a result also anticipated from infrared absorption spectra of the free films. This behavior of the reflectance spectra indicates that a relatively constant value of emittance and a rapid change of the solar absorptance of this system with time of ultraviolet irradiation can be expected. The initial value of solar absorptance of 0.21 changes to 0.43 with 16 hours of irradiation while the emittance remains constant at a value of 0.80.

The change in the ratio of solar absorptance to emittance for the VMCH terpolymer on aluminum substrate after irradiation at one solar constant between 2000 and 2700 Å for exposure times up to 1900 minutes is given in figure 13. It can be seen that after an initial relatively rapid rise, the change in the ratio of solar absorptance to emittance continues to rise linearly. The change in α/ϵ over the test period is significantly large. The temperature changes calculated for these increases in ratio of solar absorptance to emittance as a function of exposure time are given in figure 14. These results indicate that a temperature increase of 35° C over a test period of 1500 minutes can be expected.

CONCLUDING REMARKS

These results indicate that polymers of vinyl chloride may be satisfactory comparators for correlating the changes in solar absorptance produced by exposure to ultraviolet radiation in flight and ground-based tests. These polymeric films meet the criteria for a well-behaved system, in that they undergo a regular change in optical density with time of exposure, and the change in solar absorptance can be measured easily as a change in temperature. Furthermore, the photochemistry occurring in vacuum is free from complicating side effects such as surface erosion and depolymerization characteristic of many polymers.

Because of the extreme sensitivity of the ultraviolet and visible absorption spectra to the chromophore concentration, these films may find application as accurate ultraviolet dosimeters if it can be shown that the quantum efficiency for the production of these color-forming groups is independent of the wave length of absorbed photons in the photochemically productive region.

These films will be flown on the S-57 OSO satellite sometime in 1964, at which time it will be possible to compare the temperature changes predicted by laboratory tests with in-flight measurements directly.

Future plans include improvements in matching the photochemically productive region of the solar spectrum in the laboratory tests and a critical analysis of the kinetics of the chromophore reaction.

REFERENCES

1. McKellar, L. A.: Effects of Spacecraft Environments on Thermal Control Materials Characteristics. Spacecraft Thermodynamics Symposium, G. S. E. Stemand Holden Day, Inc., ed., 1962.

2. Johnson, F. S.: Solar Radiation: Space Materials Handbook. C. G. Goetzel and J. B. Singletary, eds., Lockheed Missiles and Space Co., 1962, pp. 31-37.

3. Winkler, D. E.: J. Polymer Sci., 35 3, 1959.

4. Neel, C. B.: The Stability of Thermal Coatings for Spacecraft. Paper presented at Fifth International Symposium on Space Technology, Sept. 1963.

5. Ohnishi, Nakajima and Hitta: Mechanism of Discoloration of Irradiated Polyvinyl Chloride. J. of Appl. Polymer Sci., 8 629 1963.

6. Boyer, R. F.: J. Phys. Chem., 51, 1947, p. 80.

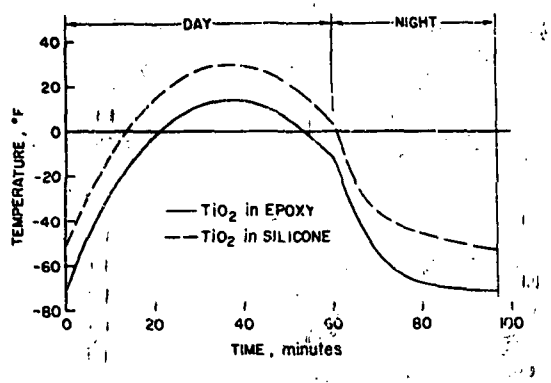

Figure 1.- Observed variation in surface temperatures of TiO_2 epoxy and TiO_2 silicone in a single orbit of S-16 OSO satellite.

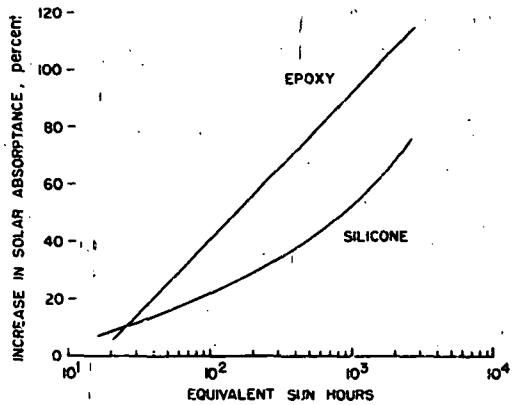

Figure 2.- Changes in solar absorptance of TiO_2-epoxy and TiO_2-silicone coatings due to environmental aging.

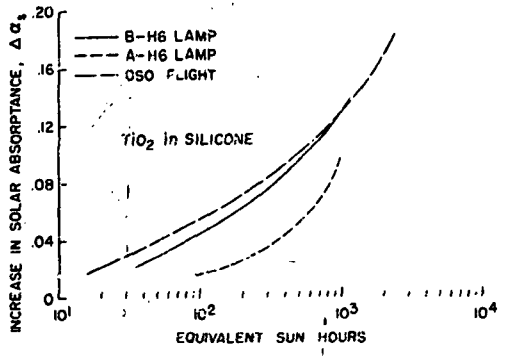

Figure 3.- A comparison of predicted increase in solar absorptance of TiO_2-epoxy coating with in-flight results on S-16.

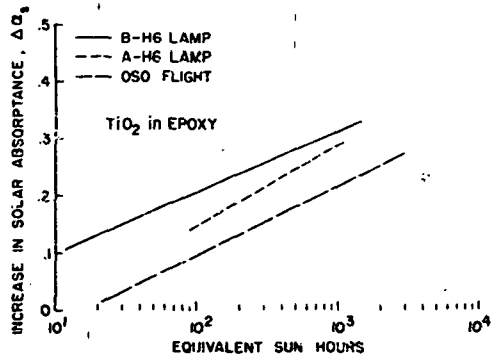

Figure 4.- A comparison of predicted increase in solar absorptance of TiO_2-silicone coating with in-flight results on S-16.

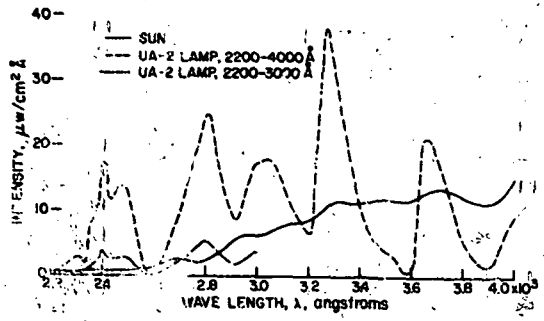

Figure 5.- Comparison of the spectral distribution of G.E. UA-2 lamp and solar spectrum in ultraviolet and near infrared regions.

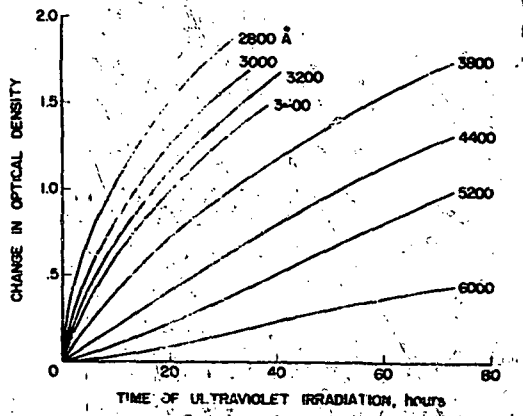

Figure 6.- Change in optical density of polyvinyl chloride in the ultraviolet and visible region with time of exposure to G.E. UA-2 lamp in vacuum.

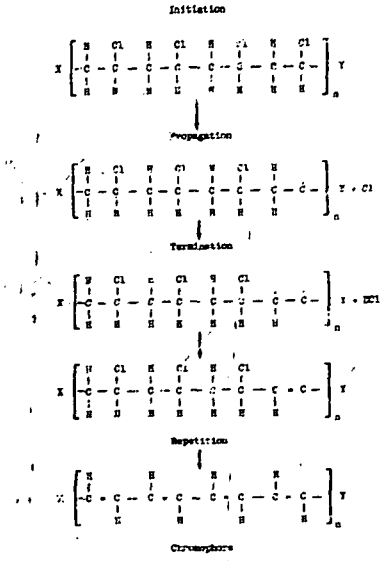

Figure 7.- Radiation production of chromophores in polyvinyl chloride.

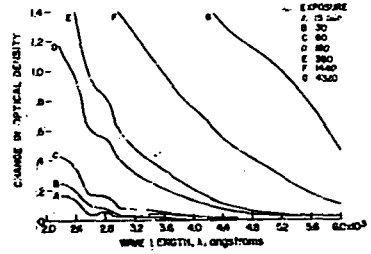

Figure 8.- Change in optical density at various wave lengths of polyvinyl chloride from 2800 to 6000 Å as a function of time of exposure to a G.E. UA-2 lamp.

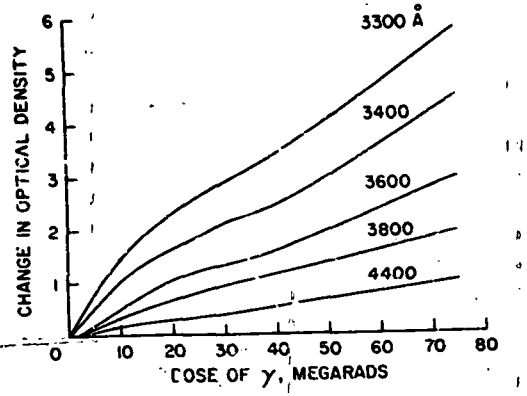

Figure 9.- Change in optical density of polyvinyl chloride at various wave lengths as a function of γ irradiation dose.

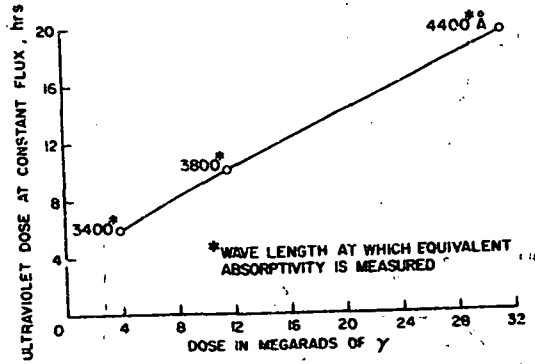

Figure 10.- Equivalency of ultraviolet irradiation dose to gamma dose for polyvinyl chloride.

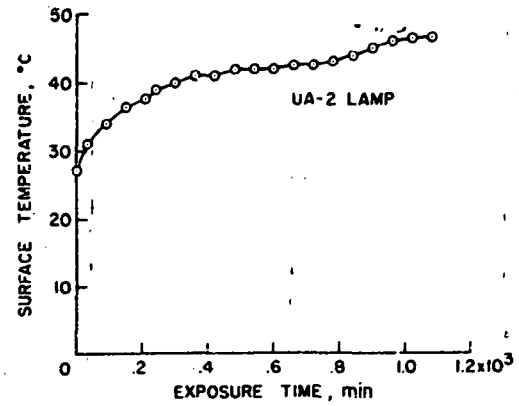

Figure 11.- Change in surface temperature of polyvinyl chloride (VMCH) copolymer on aluminum substrate during irradiation in vacuum at a constant flux with G.E. UA-2 lamp.

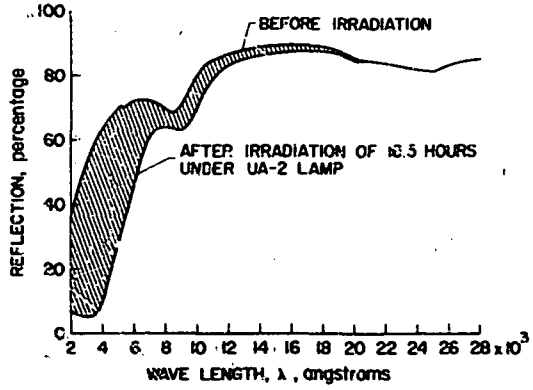

Figure 12.- Change in reflectance of polyvinyl chloride copolymer (VMCH) on aluminum substrate due to irradiation in vacuum with G.E. UA-2 lamp.

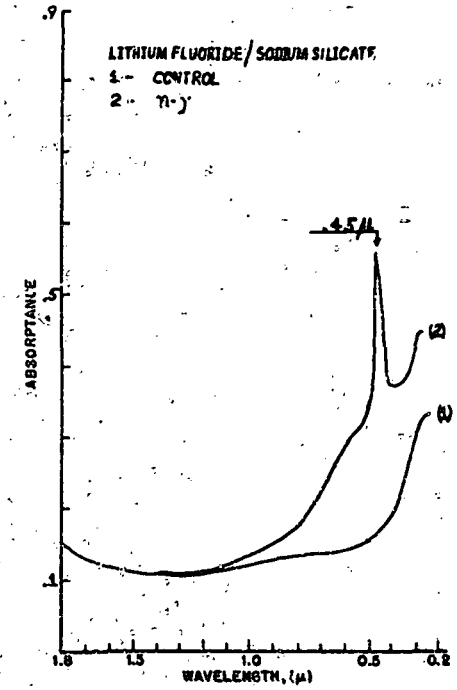

Figure 3

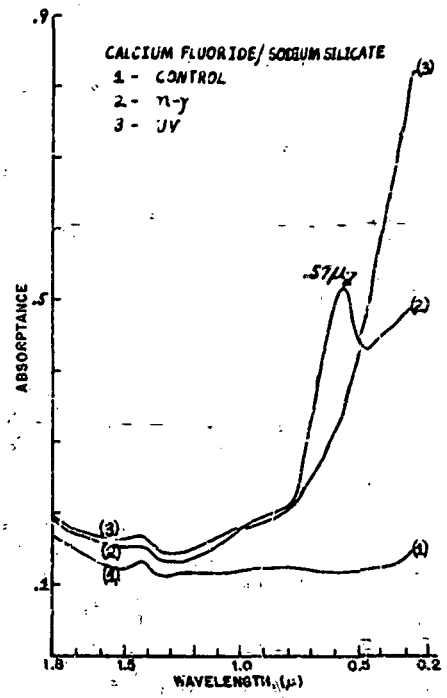

Figure 4

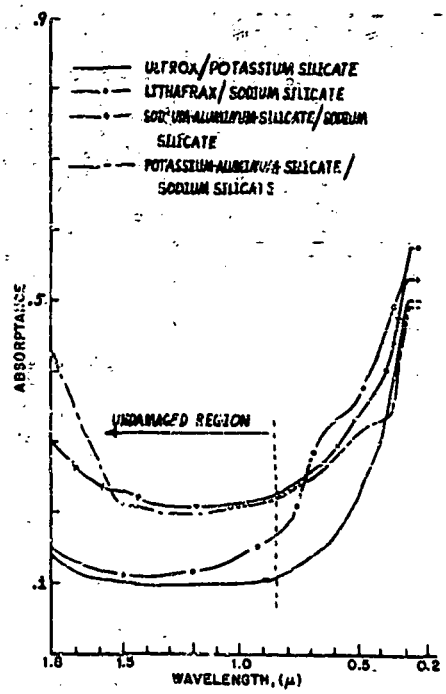

Figure 5

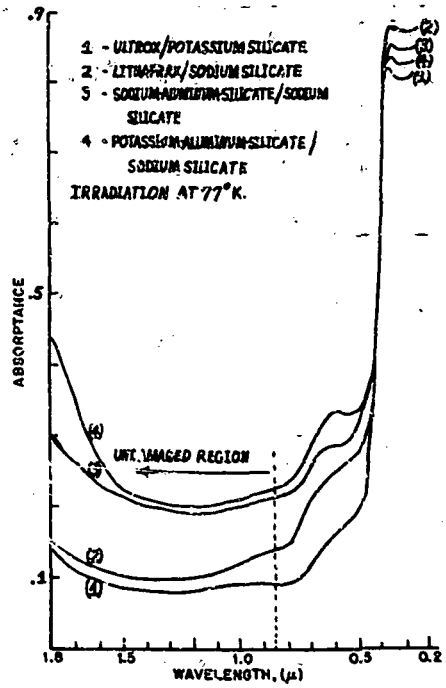

Figure 6

N65
17322

N65 17322

ULTRAVIOLET IRRADIATION IN VACUUM OF WHITE SPACECRAFT COATINGS

By G. A. Zerlaut, Y. Harada, and E. H. Tompkins
IIT Research Institute Chicago, Ill.

SUMMARY

Investigations of stability of materials to simulated space conditions were conducted in conjunction with a developmental program of spacecraft thermal control coatings. Determination of spectral reflectance and solar absorptance before and after exposure showed that none of the materials studied is completely unaffected by ultraviolet irradiation in vacuum. However, zinc oxide and, to a lesser extent, zinc sulfide were found to be unusually stable white pigments, and formed relatively stable coatings when dispersed in pure potassium silicate or in experimental methyl silicone polymers. Exposure to 4200 equivalent sun-hours ultraviolet radiation in vacuum resulted in solar absorptance increases of less than 0.02 for both an experimental silicone and a potassium silicate paint pigmented with zinc oxide.

INTRODUCTION

The principal objective of this research was the development of a white spacecraft-thermal-control coating with exceptional stability to extraterrestrial solar radiation. Emphasis was directed more to the change in value than to the absolute value of solar absorptance. Accordingly, the measurement of spectral reflectance within the solar region was directed more toward precision than toward absolute accuracy.

Conventional or commercial coatings were not studied because they deteriorate rapidly under ultraviolet irradiation in vacuum. Instead, experimental laboratory formulations with known ingredients, purities, and weight ratios were investigated. The work was divided broadly into organic and inorganic coatings. In order to reduce the complexity of the problems involved, pigments and paint vehicles were exposed individually to ultraviolet radiation in vacuum. These screening experiments were the basis for the subsequent choice of potentially stable paint formulations. Determination of spectral reflectance and solar absorptance before and after exposure showed that no material studied was completely unaffected by ultraviolet irradiation in vacuum. Zinc oxide was found to be an unusually stable white pigment and formed relatively stable coatings when dispersed in pure potassium silicate or in methyl silicone polymers.

The bulk of the research effort was devoted to the development of still more stable pigmented potassium silicate and methyl silicone paints. The effects of soiling and cleaning candidate coatings were studied in an attempt to define the problems anticipated during spacecraft fabrication and during checkout just prior to launch.

27 28

The requirement for high stability to the space environment includes not only the solar ultraviolet as a consequence of the sun's temperature, but also other radiations in space, primarily galactic (cosmic) proton radiation and trapped charged particles in the Van Allen belt. Adequate simulation of solar ultraviolet below 2000 A, including Lyman alpha as well as the high-energy particulate radiations, is both difficult and expensive. Furthermore, of a total of 135 watts per square foot at earth-distance, less than 0.25 watts per square foot of electromagnetic radiation is radiated below 2000 A, whereas about 12 watts per square foot is radiated between 2000 and 4000 A in the near-ultraviolet. Since the development of stability to high-energy radiations is useless unless stability to the more prevalent near-ultraviolet is assured, space-simulation efforts were confined to the near-ultraviolet region from 2000 to 4000 A at a vacuum in the range of 10^{-7} torr.

SOLAR ABSORPTANCE MEASUREMENT

Solar absorptance was determined indirectly by measurement of spectral reflectance in the wavelength range of 0.3 to 2.7 mμ (300 to 2700 mμ). The reflectance data were integrated with solar spectral energy data[1] for the upper atmosphere, to yield solar reflectance. Subtraction of the solar reflectance from unity yielded solar absorptance. Comparison of these solar spectral energy data with the data of Nicolet[2] showed that solar absorptance agreed within 0.005.

A General Electric recording spectrophotometer, which employs approximately normal illumination and diffuse viewing of a sample surface, was used for the visible spectrum, 380 to 770 mμ; and an integrating-sphere reflectometer of our own design was used for both the ultraviolet and infrared regions. The latter incorporates a Perkin-Elmer quartz monochromator as a dispersing system along with appropriate sources and detectors.

Both reflectometers measure reflectance relative to a standard. These are comparison instruments, since the sample and the standard are both in place at all times. Magnesium oxide was used as the standard, and the relative reflectance data obtained were converted to the absolute basis by using the absolute reflectance data of magnesium oxide published by Middleton.[3,4] Reflectance data which are presented in the tables are limited to values at 440- and 600-mμ wavelength.

Since it was not economical to provide solar absorptance values during the extensive screening operations, for many materials the effect of space simulation was evaluated in terms of reflectance losses in the visible region. This method is considered satisfactory, since the predominant losses occur in the 400- to 600-mμ wavelength region for most white and transparent materials.

In many cases solar absorptance values are reported as α_1 and α_2, where

$$\alpha = \alpha_1 + \alpha_2$$

α_1 corresponds to that half of the sun's energy spectrum which lies below 700-mμ wavelength, and α_2 corresponds to that half which lies above 700 mμ. By splitting α into two components, that region of the spectrum undergoing the most significant change in absorptance is more readily described. For example, some formulations show little change in solar absorptance on irradiation, but their reflectance decreases in the visible region (increase in α_1) and is counterbalanced by a corresponding increase at longer wavelengths (decrease in α_2).

SPACE SIMULATION

Vacuum Simulation

Oil-Diffusion Pump. - The vacuum of the space environment is variously quoted at 10^{-9} to 10^{-15} torr, but the attainment of such pressures in the laboratory is time-consuming and probably unnecessary for the purposes of this work. At much higher pressures, 10^{-6} torr, there is no evidence of oxidative degradation. Also, the mean free path of evolved molecules is large compared to the dimensions of the chamber, so that further reduction in pressure would not be expected to change the results of space-simulation tests.

These principles guided the design of the space-simulation chamber shown in Figure 1, which was used in the early screening operations. It consists of a cylindrical chamber 24 inches in diameter and 24 inches high, cooled by refrigerant coils on its outer surface and capped with a torispherical head in which three General Electric mercury-arc AH-6 lamps are mounted. The distance from the lamps to the samples, which are mounted on a turntable beneath the lamps, can be adjusted to achieve variation of radiation intensity. The radiation intensity varies at different distances from the center of the turntable, so various acceleration factors are possible. The constancy of the radiation is monitored by reflecting a portion from a first-surface mirror, mounted over the center of the turntable, through a quartz window on the head. The absolute intensity is measured before and after each run by using a wide-angle, temperature-compensated thermopile.

Several types of sample turntables are available. The simplest is a 16-inch flat plate, suitable for use when no measurements are to be made in the chamber. Typically, this was used when the reflectivity of a number of materials was to be measured before and after irradiation. The turntable assures that all samples receive equivalent exposures at a given radial distance. It is rotated by a 12-point Geneva drive and a 2-rpm fractional horsepower motor in a welded housing which is open to the atmosphere through ventpipes in order to eliminate the problems associated with operating motors in a vacuum.

The chamber is mounted on a 10-inch oil-diffusion pump, National Research Corporation model H-10-SP, with an approximate pumping speed of 4000 cfm at 10^{-4} torr. In practice, the pump reaches 10^{-6} torr routinely, and all ultraviolet testing was performed at this level or below.

The samples were of many forms: pigmented and clear films, free and on a substrate, compacted and loose powders. For uncooled samples, as used in this equipment, the nominal specimen temperatures were 150°F at an intensity of about 3 solar equivalents.

Ion Pump. - An ion-pumped space-simulation chamber was constructed and was used for longer-term tests. The system provides a convenient means of obtaining a clean ultrahigh vacuum. The chamber is provided with a quartz window and a liquid-cooled sample table. The table, shown in Figure 2, can be cooled with liquid nitrogen, ice water, or tap water and can accommodate six 1 x 1 inch specimens. The system, shown in Figure 3, consists of a 400-liter/sec Varian VacIon pump,[1] which is prepumped with both a molecular-sieve sorption pump and a mechanical pump. An AH-6 lamp is mounted over the quartz window, which is shown in place in Figure 3. Reproducible equivalent solar factors, as determined with a temperature-compensated thermopile, were achieved from 4 to 18 intensities (2000 to 4000 A). A plot of $1/D^2$ (D = distance from the lamp to the sample table) resulted in a straight-line relation.

Solar Simulation

The solar ultraviolet spectrum is given in Figure 4. Also shown in this figure is the energy spectrum of a typical AH-6 lamp at comparable total intensity. The wavelengths below 2000 A contribute less than 0.1% of the total energy and so can be disregarded without significant error.

The total lamp intensity was measured with a wide-angle temperature-compensated thermopile obtained from the Eppley Laboratories, Inc. From the thermopile output, the solar factor was calculated as follows:

$$\frac{\text{thermopile output (millivolts)}}{2 \times \text{thermopile constant}} = \text{cal/cm}^2\text{/min}$$

The thermopile output was divided by 2, since half of the total energy of the lamp is assumed to be below 4000 A. The solar intensity at wavelengths below 4000 A has been determined to be 13 milliwatts/cm^2. Cal/cm^2/min was converted to milliwatts/cm^2 by applying several conversion factors. By dividing this value by "one" solar factor, 13 milliwatts/cm^2, the number of "suns," or the equivalent solar factor, for a given thermopile output was obtained. Solar factors were determined at various lamp-to-sample distances in the ion-pumped chamber.

Solar Factor	Distance from Lamp to Sample, inches
5.2	9.00
6.1	6.40
10.3	5.40
12.2	4.75
13.2	4.33
15.9	4.00

The AH-6 lamp is positioned over the samples at a distance corresponding to the solar factor desired. A small recording thermopile is positioned over the lamp and is used to monitor changes in the lamp intensity over periods of time. This information is valuable in assigning an equivalent sun-hour radiation value to a given space-simulation experiment.

Assessment of the damage caused by space-simulation tests could be in error if the spectral output of the ultraviolet source were reduced disproportionately, i.e., if the radiation below about 2800 A decreased with lamp age at a higher rate than the longer-wavelength ultraviolet. Therefore, attempts were made to measure the spectral output of several AH-6 lamps before and after operation. A Seya-Namioka vacuum-ultraviolet monochromator manufactured by Jarrell-Ash was used.

The results were inconclusive. There appeared to be a disproportionate decrease in peak intensity at 2285 and 2535A after 100 hours. The decrease, if interpreted properly, amounted to 20%. No such trend was discerned for the lower-wavelength continuum. It was therefore concluded that calculations of equivalent sun-hours of exposure (ESH) on the basis of the overall drop in lamp intensity during a given test were reasonably accurate and meaningful.

The criteria for changing lamps were either a 30% decrease in the overall lamp intensity, as measured with the recording thermopile, or the incipient erratic behavior of a lamp, whichever occurred first.

PIGMENT SCREENING

The prerequisites for selection of pigments were that they be white and of high refractive index and purity. The most important factor in the choice of materials, i.e., stability to the space environment, was determined by screening tests and from limited information in the literature. The search for pigment materials was a continuous activity during this research.

For preliminary screening tests, the samples were prepared as compacted powders that were suitable for both solar-simulation exposure and optical measurements. Powders which were not compactable into a cohesive body were placed in aluminum dishes for solar exposure. This procedure precluded optical measurements and permitted only visual observation of color change.

Considerable coloration occurred in most of the pigments, as shown in Table I. Representative reflectance values are given for two wavelengths in the visible spectrum, 440 and 600 mμ. For most of the early screening work, reflectance curves in the visible spectrum were sufficient to suggest or preclude additional study.

In general, natural, mined minerals were less affected by ultraviolet irradiation in vacuum than synthetic laboratory chemicals. Exceptions were zinc compounds and tin oxide. For example, natural wollastonite was superior to synthetic calcium silicate. Calcination of hydrated materials to their anhydrous forms enhanced stability, as evidenced by the kaolins and talc. Calci-

nation at 1000°C for 16 hours of alumina, zirconia, and zircon, however, had little effect on their stability. Apparently any loss of adsorbed or absorbed water and the possible strain relief gained by thermal treatment did not change the degradation characteristics of these materials. A marked difference in stability was apparent among different crystal forms of the same material. Metastable gamma alumina and cubic (unstabilized) zirconia degraded much more severely than their stable counterparts, alpha alumina and monoclinic zirconia. Materials other than zinc oxide which were fairly stable were zinc sulfide, stannic oxide, diatomaceous earth (amorphous silica), and fired kaolin (mullite plus amorphous silica). Although AlSiMag 243 (forsterite) also exhibited good stability, its low initial reflectance precluded further study.

The following materials, which are not listed in Table 1, were moderately to severely degraded in short exposures to ultraviolet radiation in vacuum: boron nitride, calcium carbonate, calcium fluoride, lanthanum oxide, basic white lead, basic silicate of white lead, hydrated magnesium silicate (talc), titanates of aluminum, lithium, strontium, and zinc, and phosphates of aluminum, calcium, and potassium.

The data in Table 2 show that zinc oxide was clearly the most stable pigment studied, rivaled only by zinc sulfide, tin oxide, and possibly diatomaceous earth (Table 1). Long-term tests at 1720 ESH revealed a surprisingly high absorptance change in SP 500 zinc oxide. Good stability was exhibited in the same tests by calcined SP 500 (Figure 5) and also by the unfired and fired forms of AZO-55LO zinc oxide.

Improvement of stability, observed in SP 500 and AZO-55LO, may be due to both the smaller surface area of the larger calcined particles and the elimination of defects and may also be due in part to volatilization of contaminants. Lowering of the initial absorptance results mainly from reflectance increases in the infrared region; these increases may be due to enhanced scattering at the longer wavelengths by the larger particles.

MISCELLANEOUS INORGANIC PAINTS

Water-based inorganic binders which were investigated were: monoaluminum dihydrogen phosphate, colloidal silica, and alkali silicates. Stability of the binders was studied by their incorporation into paints which were subjected to a simulated space environment. The results revealed the inferior stability of colloidal silica-bonded coatings. Phosphate-bonded paints generally exhibited optical property changes similar to those of silicate-bonded samples.

As a group, the alkali silicates were preferable to aluminum phosphate from the standpoint of both stability and physical properties.

All paint formulations contained three ingredients: pigment, binder, and enough water to achieve a sprayable consistency. Mixing was accomplished by ball milling with porcelain balls. Spray-painting was done with a Paasche type AUTF airbrush; limited brush-painting was done with conventional camel-hair brushes. Aluminum pieces were roughened prior to paint application to promote adhesion. The majority of the non-zinc oxide paints were irradiated in

the oil-diffusion-pumped system with the internally mounted lamps.

Test results for a variety of paints appear in Table 3. In this group, tin oxide- and zinc sulfide-pigmented coatings were the only materials which exhibited stability approaching that of zinc oxide paints. However, both compositions had a higher solar absorptance than zinc oxide paints.

Diatomaceous earth and fired kaolin were relatively stable in the pigment screening studies. Poor stability was exhibited by the paints incorporating this form of silica, in contrast to the favorable data for the pigment alone. Molochite is a highly calcined aluminum silicate produced from a kaolin low in iron and alkali. It is essentially crystalline mullite plus a small amount of amorphous silica. Fairly low reflectance changes due to ultraviolet irradiation in vacuum were observed for the various grades of Molochite.

Although the reflectance changes for paints pigmented with zirconia in the short test (75 ESH) indicated fair stability, later experiments revealed that zirconia-pigmented paints were unsatisfactory. Limited tests showed that coatings incorporating zircon were relatively unstable.

Of the non-zinc oxide paints, only three compositions were relatively stable: those containing zinc sulfide, stannic oxide, or Molochite #6.

ZINC OXIDE INORGANIC PAINTS

Zinc oxide-potassium silicate paints were formulated and applied in the same manner as described for the other inorganic compositions.

Effect of Coating Thickness on Optical Properties

Studies were conducted to determine the effect of coating thickness on solar absorptance and emittance. Figure 6 graphically illustrates the solar absorptances of SP 500 zinc oxide-PS7 potassium silicate coatings which had a pigment-binder ratio (PBR) of 4.30 and a solids content of 46.3%. The data reveal that minimum solar absorptance was obtained with a coating thickness of about 5 mils. Approximately the same thickness was necessary for minimum solar absorptance of coatings pigmented with calcined SP 500. Minimal solar absorptance is approached at a thickness of 4 mils. The predictability of the solar absorptance of a coating thicker than 4 mils is ± 0.01. Total normal emittance is relatively insensitive to coating thickness. Ten samples which range from 1 to 5 mils exhibited emittance values of 0.94 to 0.98.

Stability to a Simulated Space Environment

Preliminary Studies. - In all the early studies zinc oxide paints were clearly more stable than other inorganic coatings. Representative results of the early tests in the oil-diffusion-pumped system are tabulated in Table 4. Very small reflectance losses, mainly in the 440-mμ region of the visible spectrum were experienced by all the coatings.

Total normal emittance values were determined for some of the coatings before and after space simulation. The high values, all in excess of 0.90, were virtually unaffected.

A number of silicate-bonded zinc oxide coatings were deliberately soiled by immersion in Duo Seal vacuum-pump oil. This simulates one of the soiling problems which can be expected to occur in satellite evaluation tests. After removal from the oil, the samples were exposed to ambient conditions for 5 hours. The excess oil was then removed with paper towelling. Two cleaning operations followed, the first consisting of wiping with acetone-soaked paper towels and the second consisting of washing with Alconox-tap water and scouring with a nylon brush. Final rinsing with distilled water preceded drying under an airblast and complete drying at 130°C. Moderate care in all the operations prevented any apparent damage to the coatings. The samples were exposed to ultraviolet irradiation in the oil-diffusion-pump vacuum system.

As shown in Table 4, a slight decrease in reflectance resulted for most of the soiled and cleaned (S-W) samples. Exceptions to this were some samples of initial reflectance lower than 80% at 440 mμ; these coatings exhibited a slight increase in reflectance. Upon exposure to the simulated space environment the samples which suffered losses on washing bleached slightly. On the other hand, coatings which showed an increased reflectance on washing revealed slight losses after exposure to the simulated space environment. In all cases, the washing appeared to have adequately removed any degradable residual oil.

Long-Term Tests. - The longer-term tests were conducted in the ion-pumped vacuum system with an externally mounted ultraviolet lamp. Exposures of 450 to 4170 ESH at solar factors ranging from 8 to 18 suns were used. The limited capacity of the water-cooled shelf in the chamber dictated simple geometries of 1 inch square for maximum use.

More significant optical changes in the zinc oxide compositions became apparent in the longer tests. Several treatments were found to have little or no effect on stability. Ball-milling of the paint formulations for 6 to 8 hours did not introduce enough impurities to change the degradation characteristics. Physical stresses such as fatigue and thermal shock also had negligible effect on the paint. The lack of heat-curing was not detrimental to stability.

Certain factors were shown to be conducive to solar absorptance changes. Foremost was contamination of the coating, *e.g.*, with sebum or acetone residue. Application of a topcoat over a soiled area was not sufficient to retain stability. It is possible that cleaning might remove any soluble degradable material which may be dissolving in the second coat during respraying. Lowering of the PBR was detrimental to initial solar absorptance and also to stability.

The randomness of some test results suggested the possibility of an effect due to an aging factor. Samples investigated for curing and storage effects appear in Table 5. A sample which had been stored for four months was cut into three pieces, each of which received different treatments. The data for these

samples, Z79, Z80, and Z81, reveal the beneficial effect of washing and maximization of stability by heating the paint at 500°C. In view of these results, contamination of the paints appears to be possible. Washing extracted some of the degradable components. It is possible that additional washing may have removed even more. The heat treatment was not at a high enough temperature to decompose such materials as potassium carbonate, potassium sulfate, or zinc orthosilicate had they been present as a contributory factor in degradation. It appears that, on storing, the coating collected impurities which had not actually reacted chemically with the paint but instead were held physically in the porous coatings.

Sample Z83 was cured in a carbon dioxide atmosphere by placing it in a closed box with dry ice. The deleterious effect on stability was obvious from the change in absorptance. Poor stability was also exhibited by Z84; a zinc oxide-potassium silicate formulation has a limited, if any, shelf life. Difficulties in remixing and spraying also resulted after storage.

A group of samples (Z87 through Z92) prepared at the same time from the same formulation was irradiated in the same test. As shown in Table 5, the coatings received various types of cure and storage. Surprisingly, the most stable coating (Z87) was air-cured and stored. Its change in solar absorptance was the smallest noted in any of the extended (>1000 ESH) tests. The desiccator cure appeared to be deleterious to stability, and no difference due to storage in air (Z89), under Saran Wrap (Z90), or in the desiccator (Z88) was observed. The undesirable effect of the desiccator cure was partially eliminated by heat treatment (Z91 and Z92). The slightly detrimental effect of curing in a water-free and carbon dioxide-free atmosphere seems paradoxical. However, good stability was exhibited by all coatings in this group.

4170 ESH Test. - The most severe space-simulation test in the program was for 4170 ESH at a solar factor of 10.6 suns, corresponding to nearly 6 months of direct extraterrestrial ultraviolet irradiation. The optical changes plus short histories of the samples appear in Table 6. Good stability was exhibited by Z93 (Figure 7) and Z94. The comparatively superior behavior of the coating with the high PBR, Z94, indicates the feasibility of increasing pigment concentration. The beneficial effect of a 500°C heat treatment is evidenced by the results for Z96. A limited deleterious effect was imparted by washing.

SCREENING OF ORGANIC AND ORGANOMETALLIC PAINTS

The organic coating vehicles which were considered can be divided into the following chemical categories: organometallic vehicles with organic "framing" groups, fluorine-containing aliphatic resins, organic polyesters, epoxy resins, and miscellaneous vehicles including commercial resins with undisclosed composition. In this discussion, however, these binders are divided into three categories: commercially available silicones, fluorine-containing aliphatic resins, and a modified silicone-epoxy composition. More than 45 resin films were considered for screening. Nearly 300 pigment-binder combinations were prepared, although only about 50 paints were irradiated in vacuum.

The study of experimental methyl silicone resins comprised a major portion of the non-inorganic phase of the research. For this reason, the methyl silicone resins which were synthesized during the course of the program are discussed separately.

Four silicones were evaluated: General Electric Company's RTV-11 silicone paste, their LTV-602 silicone potting compound, their SE551-N silicone gum, and Dow Corning Corporation's 806A silicone resin. The first two materials are polydimethylsiloxane polymers. RTV-11 contains silica, calcium oxide, and calcium carbonate as fillers. It is cured with Thermolite 12, a proprietary catalyst obtained from General Electric. LTV-602 is a transparent liquid containing no fillers and is cured by addition of SRC-05 catalyst. SE551-N is a low-shrink, methyl-phenyl silicone gum stock which is cured with benzoyl peroxide. Dow Corning 806A resin is also a methyl-phenyl silicone, and requires heating to 480° F to cure. However, addition of tetrabutoxy titanium accelerates the cure at a lower temperature.

Nine fluorine-containing polymers were evaluated. Those which were obtained from E. I. DuPont de Nemours and Company were: Teflon TFE Dispersion No. 30, Teflon TFE High Build Clear Finish No. 852-202, Teflon FEP Dispersion No. 120, Viton A, and Viton B. Teflon TFE is polytetrafluoroethylene. Teflon FEP is a copolymer of tetrafluoroethylene and hexafluoropropylene, and Viton is a copolymer of vinylidene fluoride and hexafluoropropylene. The raw polymer of Viton B gum was dissolved in acetone or methyl ethyl ketone. It required about 10 days before the suspended impurities settled and a clear solution was formed.

Kel-F resin No. 800 and Kel-F latex No. KF 8213 were obtained from the Minnesota Mining and Manufacturing Company. The resin and latex are each copolymers of vinylidene fluoride and trifluorochloroethylene. Kel-F No. 8213 was received as an aqueous dispersion. A ketone dispersion was made from it by quenching the aqueous dispersion of the latex with liquid nitrogen, covering the solidified material with acetone, allowing the solid to warm, and decanting the supernatant solution. The process of water extraction was repeated without further freezing. The acetone dispersion was then dried over nonreactive drying agents.

The only epoxy resin evaluated was a silicone-epoxy modified acrylic resin known as Leonite 201-S obtained from the Leon Chemical Industries.

Only two clear organic polymer films were irradiated: one specimen of Teflon TFE No. 30 and one of RTV-11 silicone. The data for these two coatings appear first in Table 7, which also contains data for other representative organic paints. Comparison of the reflectance changes in P-1 and P-3 illustrates the difference between a phenyl and a methyl silicone binder; although some of the degradation in P-1 at 440 mμ was due to the low PBR. Subsequent silicone paints were formulated at a PBR of about 2.5.

Coating P-4 showed exceptional resistance to degradation; the loss in reflectance at 440 mμ was only 1.0%. The PBR of 5 is much higher than is practical, however. This value is in excess of the critical pigment volume concentration for this pigment-binder combination.

Coatings P-10, P-12, and P-14 were also pigmented at a very high PBR and their respective critical pigment volume concentrations were probably exceeded, although fairly good adhesion was observed in these paints. Of all the nonsilicone paints, P-14 showed the best resistance to yellowing. This paint was the acetone dispersion of Kel-F 8213 pigmented with SP 500 zinc oxide.

ZINC OXIDE-PIGMENTED METHYL SILICONE PAINTS

Materials

As a result of the pigment and inorganic screening investigations, the pigmentation of silicone-based paints was confined essentially to the use of SP 500 zinc oxide. Rutile titanium dioxide and zinc sulfide were used in several instances for the purpose of comparison.

Except for two phenyl-methyl silicone paints, efforts were devoted primarily to methyl silicone, or polydimethylsiloxane, polymers. The studies were divided into two phases: (1) evaluation of commercially available methyl silicone polymers, and (2) synthesis and evaluation of experimental methyl silicone resins.

Paint Formulation

All paints were ground in a porcelain jar mill for about 16 hours at approximately two-thirds critical speed.

The formulation data for the silicone paints are given in Table 8. Pigment/binder ratios are shown as both weight and volume ratios. Weight ratios are designated PBR (pigment/binder ratio). Volume ratios are designated PVC (pigment volume concentration).

Synthesis of Experimental Methyl Silicone Resins

The general reaction scheme for methyl silicone resins is given by Rochow and Gilliam.[5] A mixture of mono- and disubstituted silicon halides (or ethoxy esters) is hydrolysed, and the resultant silanetriols and silanediols are condensed to the resinous product. The composition of the resin is controlled by *Me/Si*, the molar ratio of methyl groups to silicon atoms. *Me/Si* is essentially the same for both the reactant mixture and the product.

Molecular weights were obtained on a Mechrolab vapor pressure osmometer, model 301A. The instrument is known as a "thermoelectric" type of osmometer.[6]

The experimental resins were synthesized typically as follows:

Experimental Resin R-4:

Four-tenths moles (59.2 g) of dimethyldiethoxysilane (90%) and 0.48 moles (85.5 g) of methyltriethoxysilane (90%) were mixed with 150 g of 95% ethyl alcohol and added to 400 g of distilled water. To this mixture was added 22 ml of 37% hydrochloric acid, and the mixture was refluxed vigorously for 19 hours. A syrupy, viscous, colorless fluid of density greater than water resulted. The polymer was washed by decantation until a neutral test to litmus was obtained. Then 70 g of xylene was added, effecting separation of a water/organic phase. The organic layer was washed with distilled water twice and was dried over Drierite after weighing. The resultant solution contained 40% resin by volume (47% by weight), and the Me/Si of the polymer was calculated to be 1.46. The specific gravity of the resin solution was 0.965.

Experimental Resin R-5:

Three-tenths moles (38.7 g) of dimethyldichlorosilane (99.4%) and 0.48 moles (72.0 g) of methyltrichlorosilane (95.0%) were mixed in 300 g of anhydrous diethyl ether. The resultant mixture was added dropwise with agitation, over a period of 40 minutes, to 1000 g of ice. The ether layer was separated and washed once with distilled water. It was then washed with 5% solution of sodium bicarbonate, followed by three washings with distilled water. The ether solution was dried over Drierite and evaporated at reduced pressure, leaving a viscous, colorless resin. A resin solution in toluene was made at 67.4% solids by volume. The specific gravity of the resin solution was 1.040. Me/Si was calculated to be 1.38.

Experimental Resin R-9:

The basic R-5 methyl silicone resin was prepared according to the procedure outlined above. The resultant stock resin (containing no solvent) was distilled at an average temperature of 100°C and 0.004 mm Hg pressure in an ASCO '50' Rota-Film molecular still. The upper-molecular-weight fraction was collected as R-9. Its molecular weight was found to be 2000, and its specific gravity was 1.180. The resin was decolorized with Atlas Powder's Darco Activated Carbon G60.

Nine experimental resins were synthesized during the program. The procedure for those not included here were identical in all respects except for ratios of trifunctional to difunctional reactants.

Determination of Optical Properties

The effect of film thickness and PVC on the optical properties of several elastomeric paints is presented in Figure 8. The total normal emittance

values (at 200°F) of S-12 are presented in close proximity to the points on the graph. The data confirm that thick coatings of approximately 10 mils are required to optimize reflectance and to avoid the necessity for thickness control. The effect of PVC on solar absorptance was pronounced only at lower film thickness, except for paint S-26, which was pigmented at 40% PVC. Little difference in solar absorptance was observed when paints S-12, S-13, and S-27 were applied at a film thickness of about 10 mils. On the other hand, considerably thinner coatings appear to optimize emittance.

Paint S-26 was pigmented at 40% PVC and possessed an exceptionally low solar absorptance of 0.16 at a thickness of only 7.5 mils. The low absorptance may be attributable to the fact that 40% represents a concentration equal to or greater than the critical PVC. Thus the coating possessed many pigment particles with an air interface and consequently had a higher average refractive index ratio, which resulted in greater scattering due to enhanced porosity throughout the coating. As a consequence of the excessive pigment concentration, the film was powdery and fragile and lacked cohesive strength sufficient to ensure its utility.

The effect of the film thickness of S-33 on its solar absorptance, total normal emittance, and the ratio of the two is presented in Figure 9. This paint was based on the molecularly distilled experimental resin R-9 with an Me/Si of 1.38. It was pigmented with SP 500 zinc oxide at 40% PVC.

Stability to a Simulated Space Environment

Preliminary Studies. - The results of the initial space-simulation tests on several silicone coatings are given in Table 9. Coatings S-1, S-3, S-4, and S-5 were irradiated in the oil-diffusion-pumped system; S-7 and S-10 were irradiated in the ion-pumped system. The methyl-phenyl silicone paint S-1 exhibited severe degradation, as evidenced by the loss in reflectance at 440-mμ wavelength. Four methyl silicone paints, S-3, S-4, S-5, and S-10, exhibited reflectance changes of 1% or less, with several of the changes representing increases. The increases are considered to be a result of experimental errors such as viewing different measuring positions on the sample before and after exposure.

Although coatings S-3 and S-5 possessed exceptional stability to ultraviolet irradiation in vacuum, their poor physical properties, in comparison with those of S-7 and S-10, precluded their further consideration. They were more difficult to apply, they were brittle, and they checked at moderate temperatures. Subsequent work was therefore confined to the LTV-602 and experimental methyl silicone resins.

Effect of Me/Si. - The effect of varying the Me/Si of methyl silicone resins from 1.29 to 1.46 is presented in Table 10. Examination of the reflectance and solar absorptance changes at various exposures shows that the paints based on resins with lower Me/Si were superior.

The small change in solar absorptance of S-4, however, is belied by the severe decrease in reflectance at 440-mμ wavelength. This decrease in the

visible was counterbalanced by an anomalous increase in reflectance in the near-infrared solar region. While the anomaly cannot be explained at this time, it is interesting to compare coating S-4 with the inorganic paint Z93 (see Figure 7). Resin R-1, the vehicle in S-4, has the lowest Me/Si, and possesses a structure which is more like that of the alkali silicates than any of the other experimental resins. Furthermore, S-4, like Z93, showed an increase in near-infrared reflectance on exposure to ultraviolet radiation in vacuum. R-1 was eliminated from further consideration, however, because of its inherent brittleness and failure when torsionally stressed to 90°.

The selection of resin R-5 rather than R-7 for further evaluation and for use as a stock polymer for molecular distillation studies was somewhat arbitrary. The decision was based on the supposition that an increase in cross-linking and molecular weight probably accompanies molecular distillation. Such an increase, coupled with the fact that the R-7 stock resin was polymerized from a higher ratio of methyl trichlorosilane to dimethyl dichlorosilane, would produce still more brittle, glassy resins.

LTV-602 Paints and Effect of PVC. - Paints were formulated from General Electric's LTV-602 polymer at 20, 25, 30, 35, and 40% PVC in order to determine the effect of pigment concentration on stability to a simulated space environment. Experimental resin R-5 was also pigmented at different PVCs. The results of exposure to a simulated space environment are presented in Table 11. The data for the LTV-602 paints show the dependence of stability on PVC. Coating S-7 at 20% PVC showed an increase in solar absorptance of 0.040 compared with 0.030-0.038 for S-13 at 30% PVC and only 0.012 for S-26 at 40% PVC. Similarly, coating S-19 at 35% PVC exhibited a comparatively smaller increase in solar absorptance than either S-11 or S-15 at 25 and 30% PVC, respectively.

The data on LTV-602 in Table 11 are plotted in Figure 10 to show the inverse relation of solarization to PVC. The dependence of stability on PVC is more easily discerned in less stable systems, such as those based on zinc sulfide- or rutile-pigmented methyl-phenyl silicones. The zinc oxide-methyl silicone and the zinc oxide-silicate systems are, by virtue of their stability, more susceptible to differences caused by soiling, measurement errors, etc.

Paints Based on Distilled Resins. - Zinc oxide paints based on undistilled methyl resins (e.g., R-5) undergo optical flattening and an increase in porosity upon curing. Even though this process may involve thermal erosion on the surface of the organic portion of the resin, the cured films are very stable to the simulated space environment (see Table 11), but their porosity and their 300°F curing requirement provide no advantages over the porous potassium silicate paints. It was this porosity and the resultant susceptibility to soiling which prompted molecular distillation experiments with resin R-5. These experiments were aimed at the production of higher-molecular-weight resins in the hope that paints based on them would produce glossy, more soil-resistant, and easily cleanable coatings.

The effects of ultraviolet irradiation in vacuum on the paints based on molecularly distilled resins are presented in the table below.

EFFECT OF UV IRRADIATION IN VACUUM ON OPTICAL PROPERTIES OF ZINC OXIDE-PIGMENTED PAINTS BASED ON MOLECULARLY DISTILLED EXPERIMENTAL METHYL SILICONE RESIN R-8

Paint No.	PVC, %	Exposure ESH	Exposure Solar Factor	Solar Absorptance α_1	Solar Absorptance α_2	Solar Absorptance α	Solar Absorptance $\Delta\alpha$
S-29	35	0		.128	.125	.253	
		1000	10.5	.136	.130	.266	.013
		0		.125	.117	.241	
		1600	10.2	.130	.126	.257	.016
S-31	40	0		.132	.129	.261	
		1600	9	.139	.138	.277	.016
		0		.134	.131	.265	
		1780	9.4	.146	.139	.285	.020
	Heated 1 hr at 500°F	0		.134	.126	.260	
		1780	9.4	.136	.130	.266	.006

Miscellaneous Silicone Paints. - The results of exposure of several miscellaneous silicone paints are presented in Table 12. Paint S-17 was formulated from Dow Corning's 808 methyl-phenyl resin pigmented with Titanox RA-NC, a nonchalking rutile titanium dioxide. This paint was formulated for the Round Robin Testing Program and is included here for purposes of comparison.

S-18 was based on General Electric's SR-80 resin. SR-80 was reported to be a purely methyl silicone resin containing zinc octoate catalyst. Unlike the other methyl silicone resins studied, however, the zinc oxide paint (S-18) made from SR-80 degraded severely after exposure to only 1600 ESH. It increased 40% in solar absorptance. Therefore, we concluded that the resin was not purely methyl silicone. Infrared transmission analysis of the resin did not show typical methyl-phenyl structure nor did the absorption spectra match polydimethylsiloxane spectra.

S-32 was pigmented with Du Pont's new TiPure R-900-1. The exceptional reflectance properties of this paint are manifested in the α_1 and α_2 of only 0.099 and 0.080, respectively. Unfortunately, paints prepared from R-900-1 do not offer any other advantage over those pigmented with a standard rutile, since S-32 increased 67% in solar absorptance after only 1650 ESH.

Coating Q-9-0106 was formulated by Dow Corning Corporation at our request. Dow Corning's Q-9-0106, Q-9-0107, and Q-9-0108 are all based on a proprietary methyl silicone RTV elastomer and are pigmented with SP 500 zinc oxide, rutile titanium dioxide, and zinc sulfide, respectively. All three coatings air-dried overnight to adherent, soft, resilient films. The large increase

in the solar absorptance of Q-9-0108 was attributed in part to the low PVC. Q-9-0106 compared favorably with S-13 in resistance to degradation, although S-13 was tougher and less easily scratched or gouged. However, Q-9-0106 appeared to possess less affinity for dirt than S-13.

4170-ESH Test. - The results of exposure of four zinc oxide-pigmented methyl silicone paints to 4170 ESH of ultraviolet radiation in vacuum are presented in Table 13.

Paint S-13 increased 0.058 (18%) in solar absorptance. Coating S-31 increased 12% in solar absorptance, from 0.282 to 0.316, due to degradation. This specimen was applied in a thinner coat than usual, which probably accounts for the unusually high initial solar absorptance.

Paint S-33 was formulated from experimental resin R-9, which was synthesized just prior to the test. The 4170-ESH exposure is the only test to which coating S-33 was subjected. The principal difference between R-9 and the other upgraded resins was the pressure at which it was distilled: 0.004 mm Hg for R-9 and 0.04 mm Hg for the other resins. S-33 increased only 9% in solar absorptance.

The S-33 specimen which was heated to 500° F for 1 hour showed the greatest stability to ultraviolet irradiation in vacuum of all the organic and semi-organic paints studied. The increase in solar absorptance of only 0.011, or 4.6%, compares favorably with the best zinc oxide-pigmented potassium silicate paint, which increased 0.008 in solar absorptance in the same 4170-ESH exposure.

DISCUSSION OF SPACE-SIMULATION EFFECTS

Radiation Intensity

The time-intensity reciprocity of the thermal-control coatings of interest was studied. The effect of ultraviolet intensity on the degradation of three potassiumsilicate paints pigmented with zinc oxide is presented in Table 14. Corresponding samples were: Z69 and Z70, Z73 and Z74, and Z75 and Z76. The uncalcined SP 500 pair was formulated and prepared from the same batch. One-inch-square samples of the calcined pairs were obtained by cutting a 1 x 3 inch painted panel. A significant increase in degradation was apparent at the higher solar factor, indicating that 17 suns was an unrealistically harsh treatment. The effect of ultraviolet intensity on the degradation of three methyl silicone coatings pigmented with zinc oxide and prepared and cured alike is tabulated in Table 15.

The data in Tables 14 and 15 indicate that time-intensity reciprocity is not valid between solar factors of 10.7 and 17.4 intensities for the coatings examined. The question of the validity of photochemical reciprocity, however, was not answered, because the observed increase in degradation may be due in whole or in part to thermal effects or to a discrepancy in the measurement of the solar factors at the two intensities. The choice of 10 suns as the factor for

later experiments may not be valid either, since no experiments were conducted at 1 solar intensity. Nevertheless, accelerated tests are imperative for obtaining data in a reasonable amount of time.

Exposure Time

Solar absorptance changes of three paints are plotted against the logarithm of exposure (in ESH) in Figure 11. The linear relationship between the absorptance change and the logarithm of exposure obeys the classical Hurter-Driffield equation for photographic materials:[7]

$$A = \gamma (\log E - \log i)$$

where A is the optical density; γ is the slope (the "contrast" in photography); E is the exposure, or product of intensity and time (in joules); and i is the inertia (in joules). Hirt, Schmitt, and Dutton[8] and Schmitt and Hirt[9] have discussed this relation for unpigmented and ultraviolet-absorber-containing films.

The usefulness of the Hurter-Driffield relation is that it may permit extrapolation of the curves in order to determine the most extensive damage at long exposures. More work needs to be done on such extrapolation of data. As shown in Figure 11, the long-term behavior of the less stable LTV-602-based paint, S-13, is more easily predicted by extrapolation than the behavior of more stable paints--especially S-19, which is one of the most stable coatings studied. The scatter in the data for S-19 precluded the drawing of a line through the points. As discussed earlier, the effects of contamination are more readily apparent in stable systems and are obscured in degradable systems, where their effects are less important.

Photolysis Mechanisms

Pigment. - Much has been learned about zinc oxide and other oxides through studies of catalysis and photoconductivity, but rates of separation of photolyzed metal and oxygen are not known. It is conceivable that solar radiation might product negligible photolysis, even in the high vacuum of space.

To prevent undesired photolysis, the problem is essentially the opposite of trying to make a good photoconductor or semiconductor. Light produces an excited state or nonequilibrium condition which persists for a relatively long time in a photoconductor. During this time atoms in the lattice may diffuse to more stable sites. For example, silver in silver bromide diffuses toward segregated silver metal particles, which grow as photolysis proceeds. If the diffusion of the silver were more restricted, the photolysis would be less efficient. A zinc oxide of high solar stability should therefore be a poor photoconductor, and the diffusion rate of excess zinc (actually interstitial Zn^{++}) should be low.

In the following discussion zinc oxide is used as the prime example because it has been studied more than any other metal oxide, but the principles involved apply to magnesium oxide, zirconium dioxide, titanium dioxide, and other oxides suitable for pigments. A consistent picture of zinc oxide behavior has

been worked out only in the past few years.

Collins and Thomas[10] have analyzed the behavior of zinc oxide. It is normally an n-type conductor. When its surface absorbs oxygen, a negative surface layer composed of oxygen ions forms and an electron depletion layer or space charge develops below the surface. Diffusion of photolysis products proceeds in this depleted layer. On the other hand, when the surface is reduced with hydrogen or absorbs zinc atoms, a conductive "enrichment" layer with a high concentration of donors forms near the surface. An enrichment layer having the same characteristics can be produced by photolysis. The light produces hole-electron pairs which break up and diffuse in the surface field. The holes discharge surface oxygen ions and generate oxygen molecules which then evaporate. Further photolysis releases oxygen from the lattice and leaves excess zinc. This zinc remains dissolved in the lattice, at least in the early stages of photolysis, as interstitial Zn^+ ions. These ions are not stable in the presence of oxygen, and they are concentrated in the centers of the crystals. The high free-electron concentrations that are generated by light tend to discharge Zn^+ ions and precipitate zinc metal, but other factors may hinder this reaction. The rate of diffusion of the Zn^+ is particularly important.

There is some evidence that the stability of oxide pigments may depend almost entirely on the binding energy and reaction rate of peroxide-type ions on the surfaces of the pigments. Peroxide is readily detectable on ZnO (after exposure to light) by the starch-iodide test.

Since O_2 is observed to be evolved in a vacuum system when ZnO is irradiated with UV the following steps may be postulated for photolysis:

$$O^{--}\text{ (lattice)} + h\nu \rightarrow O^- + e^-$$

$$2O^- \rightarrow O_2^- + e^-$$

$$O_2^- \rightarrow O_2\text{ (adsorbed)} + e^-$$

$$O_2\text{ (adsorbed)} \rightarrow O_2\uparrow$$

On TiO_2 we have not been able to detect peroxide, but Ag^+ reacts (in light) to form Ag_2O. The silver ion probably combines directly with O^-. In order to make TiO_2 more stable, the O_2^- state should be made more stable, or the O_2^- concentration might be increased by adding peroxide additives.

If O_2^- is strongly bonded to the surface of the oxide, photolysis would be inhibited. Perhaps it is significant that zinc does form a peroxide by non-photolytic reactions. Since hydrogen peroxide is notoriously sensitive to surface catalytic decomposition we suspect that much about the stability of O_2^- (and HO_2) on surfaces can be learned from the observed stabilities of H_2O_2 in the presence of various surfaces.

Past work on the photolysis of silver bromide is helpful in analyzing possible mechanisms in pigments. Large single crystals of oxides show less photolysis than powders subjected to the same exposure. In silver halides the silver ions near imperfections or surfaces are more vulnerable to reduction by free electrons generated by light than silver ions at normal lattice sites. These surface or imperfection effects could be important in the photolysis mechanisms of oxides. At one surface, free oxygen may be generated; at another surface less exposed to the light or more favorable for metal separation, the free metal may separate. In other words, light generates electric field and concentration gradients which are equalized by the separation of the elements in the oxide. In fact, an analogous argument can be advanced for the reason why quartz windows are virtually unaffected by ultraviolet irradiation in vacuum but powdered quarts (silica) is severely degraded. A similar argument can be advanced for magnesium oxide windows versus magnesium oxide powder.

In silver bromide the photolysis is sensitized by small islands of silver sulfide, gold, or silver itself. These islands trap electrons, which later reduce silver ions. Trapping is important because it increases the lifetime of chemically active excess carriers. When zinc oxide is made so that small islands of zinc metal remain in the oxide crystals, these crystals might be unusually sensitive to photolysis. This sensitivity could mean that once photolysis produces metal, further photolysis of the satellite coating might be rapid and catastrophic.

When zinc oxide crystals are exposed to zinc vapor at elevated temperatures and cooled rapidly to room temperature, they acquire a red or yellow color due to "dissolved" excess zinc. From conductivity data, Thomas[11] determined the concentration of excess zinc in equilibrium with zinc metal at temperatures of 450° to 700°C. Data from his plot of solubility (in atoms of excess zinc per cubic centimeter of the crystal) are recorded in Table 16 .

Photolysis by light in a vacuum can produce the same excess zinc concentrations. When crystals which have been exposed to zinc vapor are quenched, why does the zinc not segregate? The diffusion coefficient for interstitial excess zinc in the temperature range from 180° to 350°C is given by Thomas as:

$$D = 2.7 \times 10^{-4} \exp(-0.55/kT)$$

where kT is in electron volts.

At 300°K, $D = 7.3 \times 10^{-14}$. For a sphere of radius 10^{-5} cm around a zinc metal particle, the concentration gradient might be about 10^{22} atoms of interstitial zinc per cubic centimeter per centimeter in photolysed material. Such a gradient could exist over a distance of 10^{-5} cm between yellow zinc oxide and the surface of a segregated zinc particle. This condition corresponds to a transfer rate of about 0.62 atom of excess zinc per second to the zinc particle. A zinc particle of 100-A radius would require about 1.2×10^7 seconds, or 140 days, to build up these conditions. In other words, if nucleation started, darkening due to metal separation could develop over a period of months at 300°K. This slow diffusion rate of interstitial zinc may be responsible for the apparent stability of quenched zinc oxide crystals that contain excess zinc.

Particularly significant is the effect of interstitial zinc produced by photolysis on the lifetime of excess carriers generated by light. Although a hole has the same positive charge as interstitial Zn^+, high polarization effects around an interstitial Zn^+ may favor hole capture and recombination. If this is the case, the stability of zinc oxide in light may stem from this increased recombination after a certain concentration of interstitial Zn^+ is produced by the light. In magnesium oxide, aluminum oxide, and zirconium oxide, which are more easily photolysed by light, interstitial cations are not readily formed, either because of the compact lattices or because of the large size of the Zr cations. This means that magnesium, aluminum, and zirconium are not as soluble in their oxides as zinc is in zinc oxide. Since there are ways of reducing excess carrier lifetime by adding impurities different from the host cation, the addition of impurities is of interest. Such methods have been tried, but much work remains to be done on correlation with the types and quantities of impurities added.

Binder. - Since the predominant photochemical reactions in a high vacuum are cross-linking and color center formation, large changes in the physical properties of plastic structural members will not occur in a vacuum, particularly in the absence of any accompanying thermal effects. Thus, for polymeric materials which do not undergo catastrophic main-chain cleavage, the predominant physical changes will be discoloration and surface embrittlement as a result of cross-linking. The cross-linking can be considered as self-limiting, since the polymer material acts as a filter which possesses a high extinction coefficient for ultraviolet, particularly for the more damaging, shorter wavelengths.

Thus, the primary concern in the utilization of pigmented organic, semi-organic, and inorganic coatings for the purposes of spacecraft thermal control is the prevention of color center formation (i.e., coloration which increases the solar absorptance). The secondary concern is the prevention of erosion of the surface due to main-chain cleavage, side-chain cleavage, or both.

The aim of photochemical investigation is to determine the mechanisms associated with the chemical change which occurs when a substance absorbs ultraviolet light. The reactions are complex, and the actual change measured is seldom that produced by the primary process of light absorption. Therefore it is necessary to distinguish between the "primary" effect of ultraviolet and the "secondary" thermal reactions which follow. The frequent production of atoms or radicals in photochemical processes leads to extremely complex secondary reactions.

The basic difficulty in studying the formation of radicals in solids was pointed out by Franck and Rabinowitch,[12] who discussed the cage effect. This effect, often described as the Rabinowitch cage effect, is associated with the framing of a free radical by its surrounding molecules in such a way that free-radical recombination prevails. Such an effect may account for the fact that the gamma irradiation of higher hydrocarbons at 77°K results in the cleavage of C-H rather than the weaker C-C bonds.[13,14] That is, the cage effect may permit the diffusion of hydrogen and simultaneous trapping of the larger carbon radicals, which subsequently recombine.

The predominant reaction in the photoinduced decomposition of polymers in the presence of oxygen is oxidative, unless the polymer unzips to yield monomer. The quantum yields in the absence of oxygen are much lower than in its presence, due to the cage effect. When C-C bonds are part of the polymer backbone, they cannot diffuse away rapidly enough and, as a general rule, recombination and cross-linking occur. By contrast, when a C-H bond is broken, the hydrogen atom formed is highly mobile and the statistical probability of recombination is reduced. Thus, the eventual reaction is the production of a molecule of hydrogen and the formation of a new cross-link, representing the combination of two volatile (hydrogen) fragments and two residual, nonvolatile fragments, respectively. This does not preclude the existence of various chain transfer steps as intermediate reactions, but these do not contribute to the net reaction.

$$R\dot{C}\text{-}\dot{C}R + h\nu \longrightarrow R\dot{C} + \cdot\dot{C}R \longrightarrow R\dot{C}\text{-}\dot{C}R + \Delta \qquad (1)$$

$$R\dot{C}H + h\nu \longrightarrow R\dot{C} + \cdot H \qquad (2)$$

$$R\dot{C} + H\dot{C}\text{-}CR \longrightarrow RCH + \cdot\dot{C}\text{-}CR \longrightarrow C{=}CR \qquad (3)$$

$$\cdot H + \cdot H \longrightarrow H_2 \qquad (4)$$

Thus, the creation of stable molecular species is encouraged by: (a) back reaction, (b) cross reaction, and (c) molecular rearrangement. Should the higher-molecular-weight radical ($R\dot{C}$ or C-$\dot{C}$R in Eq. 2 and 3) be sufficiently immobilized, or trapped, the possibility of providing a permanent color center in the absence of oxygen or a similar reactive substance is apparent. Lawton et al[15] claim that radical trapping in polymer systems occurs under three conditions: (a) within the crystallites of the polymer, (b) in the amorphous phase below the glass transition temperature, and (c) in heavily cross-linked polymers, because they may be attached to a network structure in a position in which no other radical is accessible.

In the presence of oxygen, the possibility of chain scission is much greater due to the irreversibility of the reaction with oxygen. Moreover, this is a chain reaction and can therefore be expected to have a higher quantum yield.

$$R\dot{C}\text{-}CR + h\nu \longrightarrow R\dot{C} + \dot{C}R \qquad (5)$$

$$R\dot{C} + O_2 \longrightarrow R\dot{C}OO\cdot \qquad (6)$$

$$R\dot{C}OO\cdot + HCR' \longrightarrow R\dot{C}OOH + R'\dot{C} \qquad (7)$$

$$R'\dot{C} + O_2 \longrightarrow R'\dot{C}OO\cdot, \text{ etc.} \qquad (8)$$

Miller[16] has shown by electron spin resonance that irradiated polyvinyl chloride which has been exposed to air loses radicals at a far greater rate than samples treated similarly in a vacuum. Chapiro[17] reports a lack of coloration of the material when it is exposed to air and attributes it to the formation of the peroxy radical. St. Pierre and Dewhurst[18] found it possible to totally in-

hibit the formation of C-C cross-links by the introduction of sufficient oxygen. These same authors, in another paper,[19] describe the oxygen termination of free radicals in irradiated siloxane. They found a carboxylic acid and two types of peroxides were formed during radiolysis of hexamethyldisiloxane:

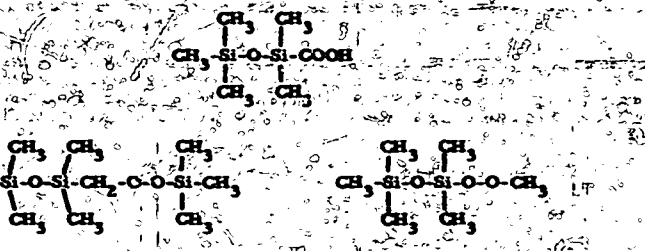

The foregoing analysis provides a general picture of the various possible photochemical reactions and their complexity, against which the results of this program can be evaluated. Upon irradiation with ultraviolet in vacuum, the methyl silicones proved to be among the most resistant materials known. This is not surprising, since short alkyl groups (e.g., methyl) are inherently more transparent to extraterrestrial ultraviolet than both longer-chain alkyl and phenyl groups. Finally, the -Si-O-Si-O- backbone possesses a quartzlike structure which is both relatively transparent to ultraviolet and at the same time is thermally resistant.

Binder-Rich Layers (Gloss)

A protective effect of increasing PVC on ultraviolet stability was demonstrated. Yellowing of zinc oxide pigments was shown to be inversely dependent on PVC. Since ultraviolet damage occurs only in the outermost layers (approximately 5 μ) of these paints and since some pigment probably settles before the vehicle "sets," an unprotected, pigment-deficient (glossy) layer might contribute to the observed degradation.

Accordingly, an experiment was designed to determine the extent of the contribution to degradation of a pigment-poor layer, if present. For the purposes of defining the problem, a moderately degradable paint was chosen rather than one of the more stable coatings. Four 1 x 3 inch aluminum panels were abraded and coated with paint S-1, a zinc sulfide methyl-phenyl silicone with a PVC of 40%. The coatings were applied at thicknesses in excess of 3 mils, allowed to air-dry for 24 hours, and then baked at 300° F for 16 hours and at 400° F for 2 hours. Two of the coatings were gently scraped with a razor blade in order to remove the top layers; approximately 0.5 mil was removed.

The results after exposure to simulated space environment are presented below. The data indicate that a pigment-deficient glossy layer was originally present and that it contributed significantly to the degradation of the untreated samples. The higher reflectance of the scraped samples than that of the untreated samples before exposure to space simulation is further indication of the existence of a binder-rich layer. While the existence of a binder-rich layer is not as serious in the more stable zinc oxide-pigmented methyl silicones (e.g., LTV-602), it will be significant when such paints are exposed to 4000 or more ESH.

EFFECT OF REMOVAL OF GLOSSY LAYER ON REFLECTANCE OF PAINT S-1

Glossy Layer	Exposure, ESH	Reflectance, % 400 mμ	440 mμ	500 mμ	600 mμ	700 mμ
Present	0	72.0	93.9	88.0	87.6	59.0
	315	35.5	50.8	68.6	81.5	59.2
Present	0	72.0	82.5	85.0	83.5	58.8
	315	39.0	53.2	68.5	78.2	58.0
Scraped off	0	75.0	86.4	89.3	88.7	60.0
	315	51.2	66.2	78.6	85.4	60.0
Scraped off	0	73.0	84.1	86.3	84.7	59.5
	315	44.5	59.0	73.0	80.5	58.5

ACKNOWLEDGMENTS

This work was performed for the Jet Propulsion Laboratory, California Institute of Technology, sponsored by the National Aeronautics and Space Administration under Contract NAS7-100. The authors wish to acknowledge the valuable assistance of Dr. Caroline D. Miller, Mr. Harold L. Rechter, O. Harry Olson, Richard J. Larson, William C. Stepp, Douglas G. Vance, and Dr. Klaus Guenther. The valuable contributions of Mr. William F. Carroll, JPL Cognizant Engineer, are gratefully acknowledged.

REFERENCES

1. Smithsonian Physical Tables, 9th Ed.
2. Nicolet, M.: Chap. XII in "Solar Physics and the Atmosphere of the Earth," C.S. White and O.O. Benson, Jr., ed.; Univ. New Mexico Press, Albuquerque, 1952.
3. Middleton, W.E.K.: Journal of the Optical Society of America, Vol. 41, No. 6, 1951.
4. Middleton, W.E.K.: Journal of the Optical Society of America, Vol. 43, No. 1, 1953.
5. Rochow, E.G. and Gilliam, W.F.: The Journal of the American Chemical Society, Vol. 63, p. 798, 1941.
6. Brody, A.P. et al: Journal of Physics and Colloid Chemistry, Vol. 55, p. 304, 1951.
7. Mees, C.E.K.: The Theory of Photographic Process, Macmillan, New York, 1946.
8. Hirt, R.C., Schmitt, R.G., and Dutton, W.C.: Journal of Solar Energy, Vol. 3, No. 2, p. 19, 1959.
9. Schmitt, R.G. and Hirt, R.C.: Report WADD-TR-60-704, Feb. 1961.
10. Collins, R.J. and Thomas, D.G.: Physical Review, Vol. 112, p. 338, 1958.
11. Thomas, D.G.: The Journal of Physics and Chemistry of Solids, Vol. 3, p. 229, 1957.
12. Franck, J. and Rabinowitch, E.: Transactions of the Faraday Society, Vol. 30, p. 120, 1934.
13. Norman, I. and Porter, G.: Nature, London, Vol. 174, p. 508, 1954.
14. Smaller, B. and Matheson, M.S.: The Journal of Chemistry and Physics, Vol 28, p. 1169, 1958.
15. Lawton, E.J., Balwit, J.S., and Powell, R.S.: Journal of Polymer Science, Vol. 32, pp. 257 and 277, 1958.
16. Miller, A.A.: Journal of Physical Chemistry, Vol. 62, p. 1755, 1959.
17. Chapiro, A.: The Journal of Chemistry and Physics, Vol. 53, p. 895, 1956.

REFERENCES (cont.)

18. St. Pierre, L.E. and Dewhurst, H.A.: The Journal of Chemical Physics, Vol. 29, p. 241, 1958.
19. St. Pierre, L.E. and Dewhurst, H.A.: Journal of Physical Chemistry, Vol. 64, p. 1060, 1960.

Table 1

EFFECT OF UV IRRADIATION IN VACUUM
ON OPTICAL PROPERTIES OF MISCELLANEOUS INORGANIC PIGMENTS

Material	Manufacturer's Designation	Exposure ESH	Exposure Solar Factor	Reflectance, % 440 mμ	Reflectance, % 600 mμ
Al_2O_3	Alucer MC (alpha),	0		100.0	100.0
	Gulton Industries	180	3	74.0	91.5
Al_2O_3	Alucer MA (gamma),	0		93.5	90.0
	Gulton Industries	75	1.5	49.5	82.5
$Al_2O_3 \cdot 2SiO_2 \cdot 2H_2O$	Ajax P kaolin,	0		73.0	84.5
	Georgia Kaolin	180	3	46.5	60.0
$Al_2O_3 \cdot 2SiO_2$	Ajax SC kaolin,	0		78.0	87.0
	Georgia Kaolin	200	3	65.0	81.0
$3Al_2O_3 \cdot 2SiO_2 + SiO_2$	Molochite, Paper Makers Importing Co.	0		84.5	86.5
		180	3	75.5	84.5
Sb_2O_3	National Lead Co.	0		92.5	96.5
		75	1.5	36.5	50.0
$CaSiO_3$	Synthetic,	0		86.0	90.0
	Johns-Manville	75	1.5	58.0	81.0
$CaSiO_3$	Wollastonite C-1,	0		92.5	94.5
	Cabot	75	1.5	81.0	91.5
$MgAl_2O_4$	Spinel,	0		97.5	97.0
	Linde	75	1.5	70.0	92.5
MgO	Reagent-grade powder,	0		97.5	98.5
	Mallinckrodt	75	1.5	71.0	92.5
$MgSiO_3 \cdot nH_2O$	No. 140 Alabama talc,	0		89.0	94.0
	Whittaker, Clark and Daniels	180	3	62.0	73.5
$2MgO \cdot SiO_2$	AlSiMag 243,	0		33.0	59.0
	American Lava	1036	15	35.5	60.0
Magnesium trisilicate	USP,	0		97.5	99.0
	Mallinckrodt	200	3	18.5	44.5
SiO_2	Ottawa Special,	0		88.5	92.5
	Ottawa Silica	75	1.5	77.5	90.0
SiO_2	Diatomaceous earth,	0		92.0	93.5
	Dicalite WB-5, Great Lakes Carbon	180	3	87.5	93.0
SnO_2	CP,	0		88.0	90.0
	Fisher	300	3	78.5	88.0

Table 1 (cont.)

EFFECT OF UV IRRADIATION IN VACUUM
ON OPTICAL PROPERTIES OF MISCELLANEOUS INORGANIC PIGMENTS

Material	Manufacturer's Designation	Exposure ESH	Exposure Solar Factor	Reflectance, % 440 mμ	Reflectance, % 600 mμ
ZrO_2	CP,	0		92.5	97.0
	Titanium Alloy Mfg	75	1.5	65.5	90.5
ZrO_2	Cubic,	0		88.0	95.5
	Titanium Alloy Mfg.	180	3	33.0	73.5
$ZrSiO_4$	Superpax	0		86.5	92.5
	Titanium Alloy Mfg.	180	3	65.0	84.5
ZnS	Reagent grade,	0		91.0	94.5
	Matheson, Coleman and Bell	75	1.5	89.0	94.0

Table 2

EFFECT OF UV IRRADIATION IN VACUUM
ON OPTICAL PROPERTIES OF ZINC OXIDE PIGMENTS

Manufacturer's Designation	Particle Size, μ	Purity %	Exposure ESH	Exposure Solar Factor	Reflectance, % 440 mμ	Reflectance, % 600 mμ	Solar Absorptance α	Solar Absorptance Δα
SP 500	0.30	>99.90	0		95.0	99.0		
			75	1.5	95.0	99.0		
AZO-66	0.20	99.80	0		93.0	99.0		
			200	3	91.0	98.0		
USP 12	0.30	99.80	0		93.5	98.0		
			300	3	92.0	97.5		
AZO-33	0.20	99.20	0		88.0	95.0		
			300	3	86.5	93.5		
SP 500			0		95.0	99.0		
			3100	10	91.0	98.0		
SP 500			0		93.5	98.0	.138	
			1720	10.2	90.5	96.0	.164	.026
SP 500	(Calcined at 700°C)		0		92.5	97.5	.133	
			1720	10.2	91.5	97.5	.140	.007
AZO-55LO	0.40	99.20	0		86.5	93.5	.198	
			1720	10.2	83.5	92.0	.213	.015
AZO-55LO	(Calcined at 700°C)		0		90.0	95.5	.156	
			1720	10.2	88.5	95.0	.164	.008

Table 3

EFFECT OF UV IRRADIATION IN VACUUM
ON OPTICAL PROPERTIES OF MISCELLANEOUS INORGANIC COATINGS
All samples cured at 140°C for 18 hr.

Sample	Composition* Pigment	Solids Content, %	Exposure ESH	Exposure Solar Factor	Reflectance, % 440 mμ	Reflectance, % 600 mμ	Solar Absorptance α	Solar Absorptance Δα
C2	$Al_2O_3 \cdot 3H_2O$ C-35, Alcoa	63.9	0		75.5	75.5	.345	
			200	3	64.5	72.5	.371	.026
C3	$CaSiO_3$, Wollastonite	62.8	0		78.5	83.5		
			180	3	52.5	71.5		
C4	La_2O_3	56.9	0		92.5	95.0		
			180	3	54.0	77.5		
C5	$LiAlSi_4O_{10}$, Foote Mineral	64.4	0		59.0	64.5		
			250	2.5	52.0	62.5		
C7	$LiAlF_4$, Lithafrax, Carborundum	64.4	0		85.0	86.0		
			2100	10	43.5	60.5		
C8	$MgAl_2O_4$	37.9	0		93.5	98.0		
			75	1.5	76.0	94.5		
C9	$MgSiO_3$	56.9	0		92.5	94.5	.130	
			200	3	66.5	84.0	.219	.089
C11	SiO_2 fused quartz powder, GE	62.8	0		87.0	87.5	.177	
			300	3	76.0	85.0	.221	.044
C13	SnO_2	61.7	0		77.0	82.5	.264	
			300	3	76.5	82.0	.278	.014
C17	SnO_2	61.7	0		76.5	83.0		
			2100	10	67.0	78.5		
C18	ZnS	59.0	0		85.0	90.5	.220	
			260	4	81.0	88.5	.231	.011
C19	ZnS, XXXN, Chas. Osborne	56.9	0		88.5	88.0		
			250	2.5	86.5	87.5		
C23	SiO_2, Dicalite WB-5	30.4	0		90.0	91.5	.136	
			300	3	77.0	88.5	.173	.037
C25	SiO_2, Dicalite WB-5	26.5	0		89.0	91.5	.128	
			300	3	73.5	88.0	.186	.058

Table 3 (cont.)

EFFECT OF UV IRRADIATION IN VACUUM
ON OPTICAL PROPERTIES OF MISCELLANEOUS INORGANIC COATINGS
All samples cured at 140°C for 18 hr.

Sample	Composition* Pigment	Solids Content, %	Exposure ESH	Exposure Solar Factor	Reflectance, % 440 mμ	Reflectance, % 600 mμ	Solar Absorptance α	Solar Absorptance Δα
C34	Molochite	56.9	0		77.5	81.0	.251	
	SF		300	3	71.0	73.0	.281	.030
C36	Molochite	56.9	0		76.5	82.5	.243	
	#6		300	3	73.5	81.5	.260	.017
C39	Molochite	61.7	0		74.5	83.5		
	#6 (HCl leached)		250	2.5	74.5	83.5		
C42	Molochite	61.7	0		75.0	84.5		
	#6 (HCl leached)		2100	10	63.5	76.5		
C45	ZrO_2, CP	73.0	0		89.0	92.0		
			75	1.5	83.5	90.5		
C46	ZrO_2, CP	72.0	0		76.0	86.0		
			75	1.5	71.5	85.0		
C47	ZrO_2, CP	74.8	0		88.0	95.5		
			75	1.5	61.5	88.0		
C52	ZrO_2, CP	64.4	0		90.5	93.0	.140	
			200	3	73.5	87.0	.205	.065
C57	$ZrSiO_4$, Superpax	56.9	0		79.0	88.5	.180	
			200	3	63.0	81.5	.249	.069

* The binder for all paints was PS7 potassium silicate (Sylvania) except for C46 and C47 which were bonded with aluminum acid phosphate and colloidal silica respectively.

The pigment-to-binder ratio (PBR) was 4.30 for all paints with the following exceptions: C8, 1.50; C18, 3.19; C23, 2.13; C46, 2.80; C47, 5.33.

Table 4

EFFECT OF UV IRRADIATION IN VACUUM
ON OPTICAL PROPERTIES OF INORGANIC ZINC OXIDE COATINGS
All samples cured at 140°C for 18 hr.

Sample	Composition* Pigment	Solids Content, %	PBR	Exposure ESH	Exposure Solar Factor	Reflectance, % 440 mμ	Reflectance, % 600 mμ	Solar Absorptance α	Solar Absorptance Δα
Z5	SP 500	46.3	4.30	0		96.0	98.5	.132	
				200	3	93.5	97.5	.138	.006
Z8	SP 500	56.9	4.30	0		94.5	96.0	.146	
				200	3	90.5	96.0	.150	.004
Z9	SP 500	51.9	2.13	0		88.5	89.5	.258	
				200	3	86.5	86.5	.269	.011
Z10	SP 500	46.3	4.30	0		94.0	97.0	.139	
				300	3	93.0	98.0	.142	.003
Z27	SP 500	46.3	4.30	0		91.0	94.5		
				S-W**		90.5	92.5		
				225	2.5	90.5	94.0		
Z28	SP 500	49.3	3.58	0		89.0	92.5		
				S-W		88.5	90.5		
				270	3	87.0	92.0		
Z29	SP 500	51.3	3.22	0		89.5	92.5		
				S-W		86.0	88.5		
				225	2.5	86.5	91.0		
Z35	SP 500	64.4	4.30	0		54.0	75.0		
				S-W		57.5	77.0		
				225	2.5	56.0	76.5		
Z39	E-P 730	73.0	4.30	0		52.5	75.0		
				S-W		56.5	76.5		
				270	3	55.0	76.5		
Z42	XX 254	73.0	4.30	0		75.5	89.0		
				S-W		78.0	88.5		
				270	3	75.0	87.0		

* The binder for all coatings was PS7. The pigment for Z35 was calcined at 800°C/12 hr.

** S-W: After soiling and washing.

Table 5

COMBINED EFFECTS OF VARYING THE CURING AND STORAGE TIMES AND OF UV IRRADIATION IN VACUUM ON OPTICAL PROPERTIES OF INORGANIC ZINC OXIDE COATINGS

Sample	Cure	Treatment	Exposure ESH	Exposure Solar Factor	Solar Absorptance α_1	α_2	α	$\Delta\alpha$
Z79	140°C/18 hr.	A 1 x 3 in. sample stored as described above was cut into three 1 in. squares. Z79 was not treated, Z80 was washed with detergent and water, and Z81 was heated at 500°C/2 hr.	0		.116	.079	.195	
			1600	10.2	.152	.079	.231	.036
Z80	140°C/18 hr.		0		.112	.077	.189	
			1600	10.2	.135	.075	.209	.020
Z81	140°C/18 hr.		0		.111	.077	.188	
			1600	10.2	.116	.077	.193	.005
Z83	Air-dried	Cured in CO_2 atmosphere	0		.102	.073	.175	
			1780	9.5	.178	.084	.262	.088
Z84	140°C/18 hr.	Shelf-life sample. The formulation was originally prepared and milled 4 months previously. Vigorous shaking was required to resuspend the pigment.	0		.096	.050	.146	
			1780	9.5	.159	.059	.219	.073
Z87	Air-dried	Stored between sheets of vellum open to the laboratory environment. for 27 days.	0		.099	.059	.157	
			1650	9	.103	.056	.159	.002
Z88	Air-dried	Cured and stored in a desiccator containing Drierite (a desiccant) and Ascarite (a carbon dioxide absorbant) for 27 days.	0		.099	.062	.161	
			1650	9	.115	.063	.179	.018
Z89	Air-dried	Cured in a desiccator for 22 hr. and stored in air for 26 days.	0		.100	.060	.161	
			1650	9	.115	.060	.175	.014

Table 5 (cont.)

COMBINED EFFECTS OF VARYING THE CURING AND STORAGE TIMES AND OF UV IRRADIATION IN VACUUM ON OPTICAL PROPERTIES OF INORGANIC ZINC OXIDE COATINGS

Sample	Cure	Treatment	Exposure ESH	Exposure Solar Factor	Solar Absorptance α_1	α_2	α	$\Delta\alpha$
Z90	Air-dried	Cured in a desiccator for 22 hr. and stored under Saran Wrap for 26 days.	0		.102	.063	.165	
			1650	9	.115	.064	.179	.014
Z91	140°C/18 hr.	Cured in a desiccator for 22 hr, heated in air at 500°C for 2 hr, and stored in a desiccator for 25 days.	0		.101	.060	.161	
			1650	9	.104	.061	.165	.004
Z92	140°C/18 hr.	Cured in a desiccator for 22 hr, heated in air at 500°C for 2 hr, and stored in air for 25 days.	0		.103	.067	.171	
			1650	9	.109	.070	.179	.008

Composition: The pigment was SP 500 calcined at 700°C/16 hr., and the binder was PS7 for all samples. PBR was maintained at 4.30. Solids content was 56.9% for all samples except Z84 (46.3%).

Table 6

EFFECT OF 4170 ESH OF UV IRRADIATION IN VACUUM ON OPTICAL PROPERTIES OF INORGANIC ZINC OXIDE COATINGS
All samples cured by air drying.

Sample	Composition* PBR	Solids Content, %	Treatment	Exposure ESH	Solar Absorptance α_1	α_2	α	$\Delta\alpha$
Z93	4.30	56.9	Stored in air, between sheets of vellum, for 37 days.	0	.102	.063	.165	
				4170	.120	.059	.179	.014
Z94	5.31	58.5	Stored in air, between sheets of vellum, for 21 days.	0	.096	.051	.147	
				4170	.106	.049	.155	.008
Z95	4.30	56.9	Stored in air, between sheets of vellum, for 36 days; washed with detergent and water; air-dried for 1 day.	0	.100	.061	.161	
				0-washed	.098	.049	.147	-.014
				4170	.122	.050	.172	.025
Z96	4.30	56.9	Stored in air, between sheets of vellum, for 24 days; heated at 500°C for 2 hr; stored in air for 13 days	0	.102	.064	.166	
				0-heated	.101	.058	.159	-.007
				4170	.109	.057	.166	.007

*The pigment was SP 500 calcined at 700°C/16 hr., and the binder was PS7 for all samples.

Table 7

EFFECT OF UV IRRADIATION IN VACUUM ON OPTICAL PROPERTIES OF SEVERAL ORGANIC PAINTS

Paint No.	Composition Pigment	Binder	PBR	Exposure ESH	Solar Factor	Reflectance, % 440 mμ	600 mμ
-	-	RTV-11	-	0		73.5	77.5
				108	4	60.5	76.5
-	-	Teflon TFE 30	-	0		84.7	80.6
				74	4	69.2	74.7
P-1	SP 500 ZnO	906A	0.7	0		89.0	87.5
				108	4	56.0	83.5
P-2	SP 500 ZnO	SE551-N	3.4	0		88.5	94.5
				500	4	84.0	93.5
P-3	SP 500 ZnO	RTV-11	1.0	0		91.0	92.0
				500	4	88.0	91.5
P-4	SP 500 ZnO	LTV-602	5.0	0		91.0	93.5
				500	4	90.0	93.5
P-5	ZrO_2	Teflon TFE 30	0.66	0		87.8	70.0
				74	4	42.0	59.6
P-7	SP 500 ZnO	Teflon TFE 852-202	0.67	0		84.0	91.5
				108	4	46.0	74.5
F-8	SP 500 ZnO	Teflon FEP 120	0.4	0		84.2	77.3
				314	4	52.4	67.5
P-10	SP 500 ZnO	Viton B	4.0	0		88.5	92.0
				500	4	76.5	89.0
P-11	SP 500 ZnO	Kel-F 800	0.5	0		84.0	77.6
				108	4	64.8	72.7
P-12	ZnS	Kel-F 800	5.0	0		89.5	92.0
				108	4	49.5	78.0
P-13	SP 500 ZnO	Kel-F 8213	1.5	0		87.0	87.5
				108	4	52.0	72.5
P-14	SP 500 ZnO	Kel-F 8213 (acetone dispersion)	5.0	0		97.0	98.0
				500	4	80.5	95.0
P-19	SP 500 ZrO	Leonite 201-S	0.67	0		85.0	85.0
				108	4	71.0	83.0
P-20	MgO	Leonite 201-S	0.44	0		93.5	92.5
				108	4	35.0	78.5

Table 8

FORMULATION DATA FOR SILICONE PAINTS

Paint No.	Ingredients, parts by wt.		PVC, %	PBR	Solids % by vol.
S-1	Superlith XXXN zinc sulfide	107.5	40	2.15	40
	806A resin	100.0			
	Toluene	37.0			
S-3	SP 500 zinc oxide	141.0	20	1.19	40
	XR-6-1057 resin	173.0			
	Tetrabutoxy titanium (TBT)	3.0			
	Toluene	108.0			
S-4	SP 500 zinc oxide	45.0	25	1.35	26
	R-1 exptl. resin soln.	111.0			
S-5	SP 500 zinc oxide	93.4	25	1.80	40
	XR-6-0049 resin	100.0			
	Xylene	38.0			
S-7	SP 500 zinc oxide	140.1	20	1.40	40
	LTV-602 polymer	100.0			
	SRC-05 catalyst	0.5			
	Toluene	160.0			
S-8	SP 500 zinc oxide	112.0	25	1.70	40
	R-2 exptl. resin soln.	100.0			
	Toluene	67.0			
S-10	SP 500 zinc oxide	77.5	25	1.78	40
	R-4 exptl. resin soln.	100.0			
	Xylene	17.7			
S-11	SP 500 zinc oxide	123.6	25	1.63	40
	R-5 exptl. resin soln.	104.0			
	Toluene	86.0			
S-13	SP 500 zinc oxide	240.0	30	2.40	40
	LTV-602 polymer	100.0			
	SRC-05 catalyst	0.5			
	Toluene	183.8			
S-15	SP 500 zinc oxide	212.0	30	2.12	40
	R-5 exptl. resin	100.0			
	Toluene	157.0			
S-16	SP 500 zinc oxide	163.0	25	1.64	40
	R-7 exptl. resin	100.0			
	Toluene	150.0			

Table 8 (cont.)

FORMULATION DATA FOR SILICONE PAINTS

Paint No.	Ingredients, parts by wt.		PVC, %	PBR	Solids % by vol.
S-17	RA-NC rutile	140.0	45	2.80	40
	808 resin	100.0			
	Tetrabutoxy titanium (TBT)	1.0			
	n-Butanol	47.0			
	Toluene	24.0			
S-18	SP 500 zinc oxide	48.0	25	1.45	31
	SR-80 resin	100.0			
S-19	SP 500 zinc oxide	268.0	35	2.68	40
	R-5 exptl. resin	100.0			
	Toluene	176.0			
S-26	SP 500 zinc oxide	373.0	40	3.73	40
	LTV-602 polymer	100.0			
	SRC-05 catalyst	0.5			
	Toluene	214.0			
S-27	SP 500 zinc oxide	304.0	35	3.04	40
	LTV-602 polymer	100.0			
	SRC-05 catalyst	0.5			
	Toluene	197.0			
S-29	SP 500 zinc oxide	264.0	35	2.64	40
	R-8 exptl. resin	100.0			
	Tetrabutoxy titanium (TBT)	1.0			
	Toluene	176.0			
S-31	SP 500 zinc oxide	316.0	40	3.16	40
	R-8 exptl. resin	100.0			
	Tetrabutoxy titanium (TBT)	1.0			
	Toluene	179.0			
S-32	TiPure R-900-1 rutile	237.0	35	2.2[illegible]	40
	LTV-602 polymer	100.0			
	SRC-05 catalyst	0.5			
	Toluene	198.5			

Table 8 (cont.)

FORMULATION DATA FOR SILICONE PAINTS

Paint No.	Ingredients, parts by wt.		PVC, %	PBR	Solids % by vol.
S-33	SP 500 zinc oxide	316.0	40	3.16	40
	R-9 exptl. resin	100.0			
	Tetrabutoxy titanium (TBT)	1.0			
	Toluene	225.0			

Dow Corning: 806A resin, XR-6-1057 resin, XR-6-0049 resin, and 808 resin.
Du Pont: Tetrabutoxy titanium (TBT) and TiPure R-900-1 rutile.
General Electric: LTV-602 polymer, SRC-04 catalyst, SRC-05 catalyst, SR-80 resin, and 81932 resin.
National Lead: Titanox KA-NC rutile.
New Jersey Zinc: SP 500 zinc oxide
Nuodex Products: Silicure Z-775
C. J. Osburn Co.: Superlith XXXN zinc sulfide

Table 9

EFFECT OF UV IRRADIATION IN VACUUM ON OPTICAL PROPERTIES OF SEVERAL SILICONE PAINTS

Paint No.	Composition		PVC, %	Exposure ESH	Exposure Solar Factor	Reflectance, % 440 mμ	Reflectance, % 600 mμ
S-1	ZnS	806A	40	0		84.4	89.0
				300	3	63.0	87.3
S-4	SP 500 ZnO	R-1	25	0		79.0	81.5
				300	3	79.5	80.5
S-5	SP 500 ZnO	XR-6-0049	25	0		80.5	83.5
				300	3	81.0	84.5
S-7	SP 500 ZnO	LTV-602	20	0		87.5	92.5
				450	10	82.5	90.5
S-10	SP 500 ZnO	R-4	25	0		77.0	87.5
				450	10	77.0	87.0

Table 10

EFFECT OF UV IRRADIATION IN VACUUM ON OPTICAL PROPERTIES OF SILICONE PAINTS AS A FUNCTION OF Me/Si (PVC = 25%)

Paint No.	Composition Binder	Me/Si	Exposure ESH	Exposure Solar Factor	Reflectance 440 mμ	Reflectance 600 mμ	Solar Absorptance, α
S-4	R-1	1.29	0		79.0	81.5	
			300	3	79.5	80.5	
			0		83.0	85.5	.26
			1460	9	71.0	81.5	.27
S-16	R-7	1.33	0		80.5	88.5	.26
			615	9	78.0	87.0	.27
			0		81.5	88.5	.27
			1600	11	78.5	86.0	.27
S-11	R-5	1.38	0		86.5	91.0	.23
			1460	9	82.5	88.5	.25
S-8	R-2	1.46	0		80.5	92.0	
			450	10	76.0	91.5	
			0		85.5	94.0	.20
			1460	9	82.0	91.0	.23

Table 11

EFFECT OF UV IRRADIATION IN VACUUM ON OPTICAL PROPERTIES OF SILICONE PAINTS AS A FUNCTION OF PVC

Paint No.	Composition Binder	PVC, %	Exposure ESH	Exposure Solar Factor	Solar Absorptance α_1	α_2	α	$\Delta\alpha$
S-7	LTV-602	20	0				.220	
			1460	9			.260	.040
			0				.240	
			3350	17.6			.300	.060
S-12	LTV-602	25	0				.230	
			1460	9			.260	.030
S-13	LTV-602	30	0				.230	
			1460	9			.260	.030
			0		.115	.087	.202	
			1200	8.7	.141	.099	.240	.038
			0				.230	
			3350	17.6			.280	.050
S-27	LTV-602	35	0		.107	.068	.175	
			1600	10.2	.117	.075	.192	.017
			0		.106	.071	.176	
			1850	10.1	.120	.081	.201	.025
S-26	LTV-602	40	0		.105	.056	.161	
			1200	8.7	.111	.062	.173	.012
S-11	R-5	25	0				.230	
			1460	9			.250	.020
S-15	R-5	30	0				.230	
			1700	10.7			.240	.010
S-19	R-5	35	0		.125	.099	.224	
			1200	8.7	.126	.100	.226	.002
			0		.124	.099	.223	
			1850	10.1	.132	.105	.237	.014

Table 12

EFFECT OF UV IRRADIATION IN VACUUM
ON OPTICAL PROPERTIES OF MISCELLANEOUS SILICONE PAINTS

Paint No.	Composition Binder	Pigment	PVC, %	Exposure ESH	Solar Factor	Solar Absorptance α_1	α_2	α	$\Delta\alpha$
S-17	808 TBT	Titanox RA-NC	45	0				.296	
				1600	11			.406	.110
S-18	SR-80	SP 500 ZnO	25	0				.279	
				1600	11			.390	.111
S-32	LTV-602	TiPure R-900-1	35	0		.099	.080	.179	
				1650	9	.158	.140	.298	.119
Q-9-0107*	Proprietary	r-TiO_2	25	0		.103	.111	.214	
				1480	10.7	.165	.206	.371	.157
Q-9-C108*	Proprietary	ZnS	15	0		.100	.120	.220	
				1530	11.1	.193	.131	.324	.104
Q-9-0106*	Proprietary	SP 500 ZnO	25	0		.120	.108	.228	
				1850	10.1	.144	.117	.261	.033

* Furnished by Dow Corning Corp.

Table 13

EFFECT OF 4170 ESH OF UV IRRADIATION
IN VACUUM ON OPTICAL PROPERTIES OF SILICONE PAINTS

Paint No.	Composition Binder	PVC, %	Cure	Exposure ESH	Solar Factor	Solar Absorptance α_1	α_2	α	$\Delta\alpha$
S-13	LTV-602	30	16 hr at room temperature	0		.124	.087	.211	
				4170	10.6	.160	.109	.269	.058
S-31	R-8	40	1 hr at 300° F	0		.145	.137	.282	
				4170	10.6	.165	.151	.316	.034
S-33	R-9	40	1 hr at 300° F	0		.119	.097	.216	
				4170	10.6	.128	.108	.236	.020
			1 hr at 300° F + 1 hr at 500° F	0		.128	.109	.237	
				4170	10.6	.134	.114	.248	.011

Table 14

COMBINED EFFECTS OF VARYING THE SOLAR FACTOR OF UV IRRADIATION IN VACUUM ON OPTICAL PROPERTIES OF INORGANIC ZINC OXIDE COATINGS
All samples cured by air drying

Sample	Composition* Pigment	Pigment Calcination	Solids Content, %	Exposure ESH	Exposure Solar Factor	Solar Absorptance α_1	α_2	α	$\Delta\alpha$
Z69	SP 500		46.3	0		.090	.067	.156	
				3180	10.7	.119	.069	.188	.032
Z70	SP 500		46.3	0		.093	.063	.156	
				3300	17.4	.129	.074	.202	.046
Z73	SP 500	16 hr at 700°C	56.9	0		.105	.067	.172	
				3180	10.7	.136	.064	.200	.028
Z74	SP 500	16 hr at 700°C	56.9	0		.104	.067	.171	
				3300	17.4	.157	.074	.231	.060
Z75	AZO-55LO	16 hr at 700°C	56.9	0		.113	.067	.180	
				3180	10.7	.136	.072	.209	.029
Z76	AZO-55LO	16 hr at 700°C	56.9	0		.115	.070	.185	
				3300	17.4	.154	.074	.228	.043

* The binder was PS7 and the PBR 4.30 for all samples.

Table 15

COMBINED EFFECTS OF VARYING THE SOLAR FACTOR AND OF UV IRRADIATION IN VACUUM ON OPTICAL PROPERTIES OF METHYL SILICONE ZINC OXIDE PAINTS

Paint No.	Composition* Binder	PVC, %	Exposure ESH	Exposure Solar Factor	Solar Absorptance α_1	α_2	α	$\Delta\alpha$
S-18	SR-80	25	0		.130	.123	.253	
			3180	10.7	.243	.185	.428	.175
			0		.125	.119	.244	
			3300	17.4	.284	.187	.471	.227
S-13	LTV-602	30	0		.113	.086	.199	
			3180	10.7	.153	.110	.263	.064
			0		.107	.073	.180	
			3300	17.4	.164	.108	.272	.092
S-19	R-5	35	0		.123	.103	.226	
			3180	10.7	.131	.108	.239	.013
			0		.123	.102	.225	
			3300	17.4	.144	.109	.253	.028

* S-13 was air-cured, all others were cured 1 hr at 300°F.

Table 16

SOLUBILITY OF ZINC IN ZINC OXIDE FROM SATURATED VAPOR

Temperature, °C	Concentration of Zinc Atoms
800	3×10^{17}
600	6×10^{16}
500	2×10^{16}
400	5×10^{15}
300	8×10^{14}
162	10^{13}
72	10^{11}

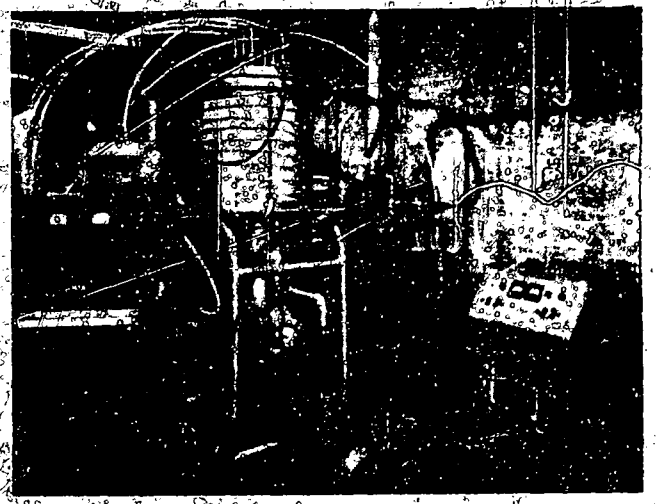

Figure 1.- Diffusion-pumped space-simulation chamber and associated equipment.

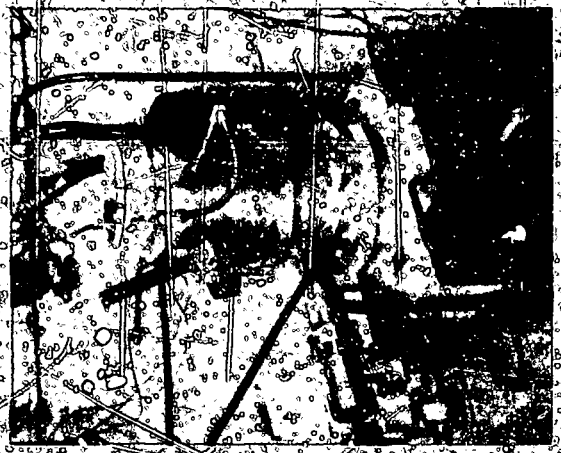

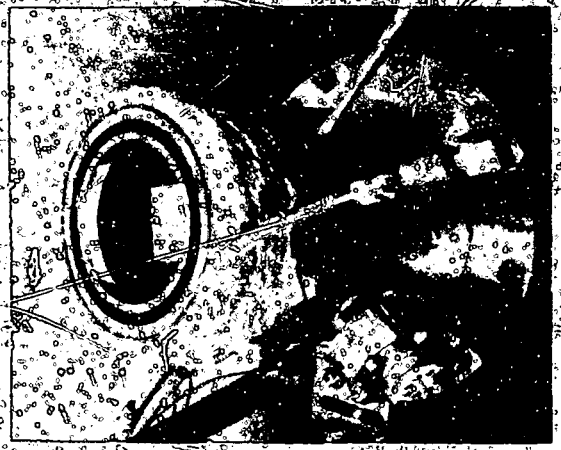

Figure 2.- Ion-pumped space-simulation chamber with equipment in place.

Figure 3.- Ion-pumped space-simulation chamber.

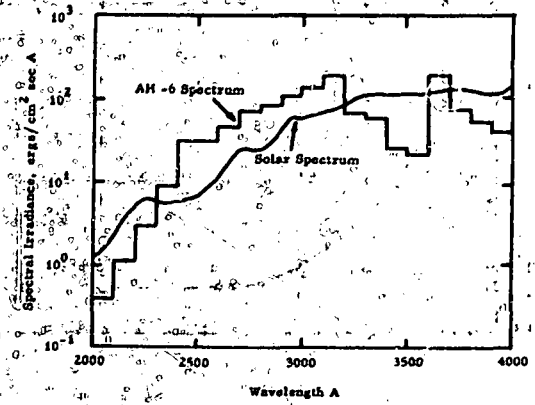

Figure 4.- Comparison of the solar spectrum with the spectrum of an AH-6 lamp.

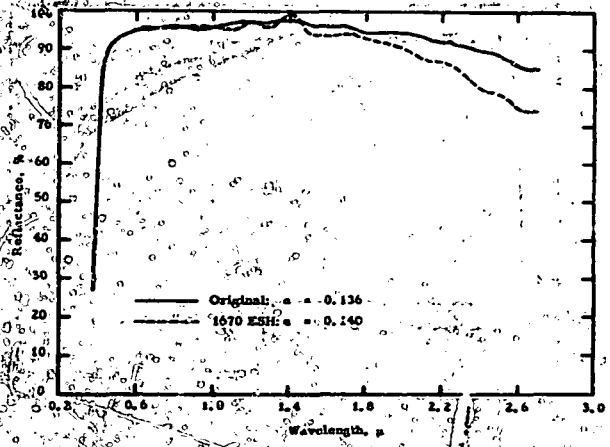

Figure 5.- Effect of 1670 ESH in vacuum on solar spectral reflectance of ZnO 500 zinc oxide calcined at 700° C for 5 hours.

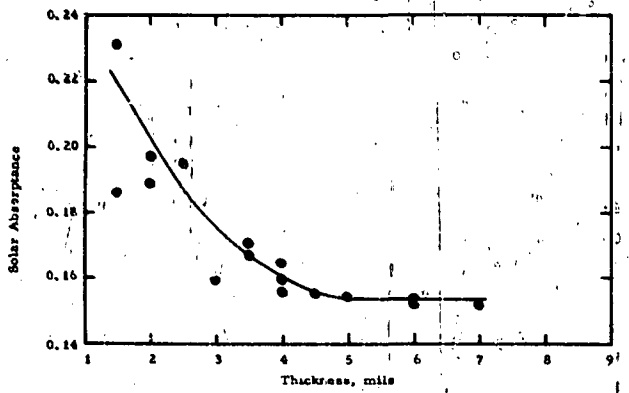

Figure 6.- Solar absorptance versus thickness in zinc oxide-potassium silicate coatings.

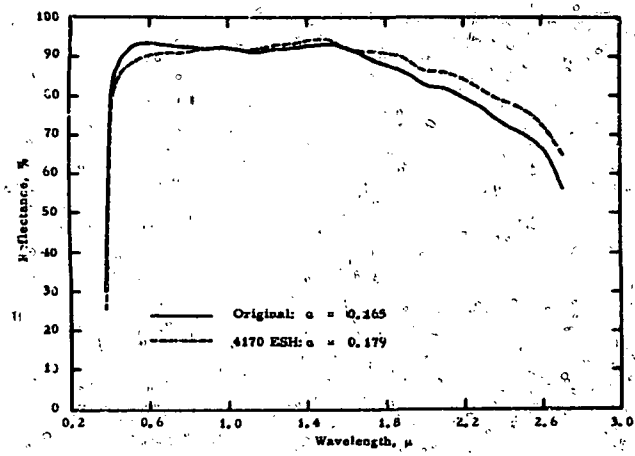

Figure 7.- Effect of 4170 ESH in vacuum on solar spectral reflectance of zinc oxide (calined)-potassium silicate coating (sample 293).

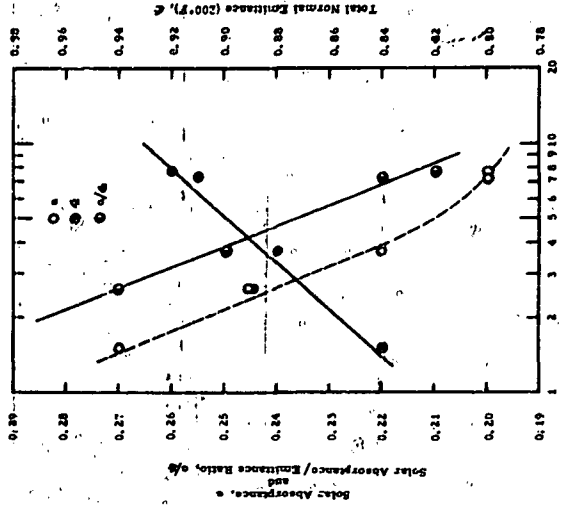

Figure 9.- Solar absorptance, solar absorptance/emittance ratio, and total normal emittance versus thickness in zinc oxide-K9 experimental methyl silicone coating (paint S-33).

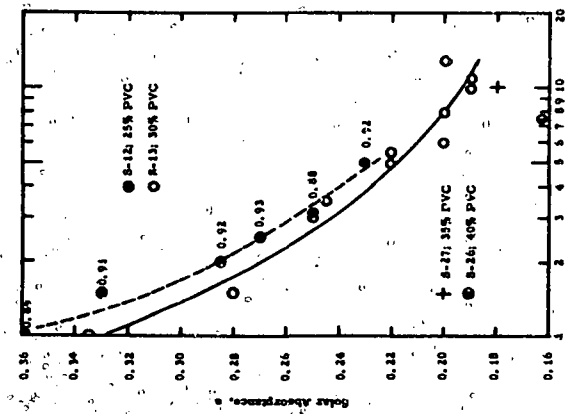

Figure 8.- Solar absorptance versus thickness in zinc oxide-LMV 602 methyl silicone coatings (paints S-12, S-13, S-26, and S-27).

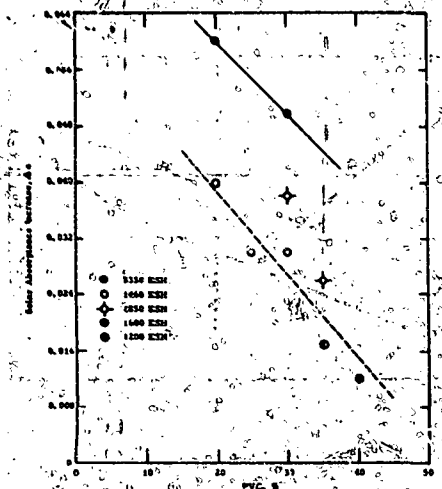

Figure 10.- Solar absorptance versus PVC in zinc oxide-UV 602 methyl silicone coatings.

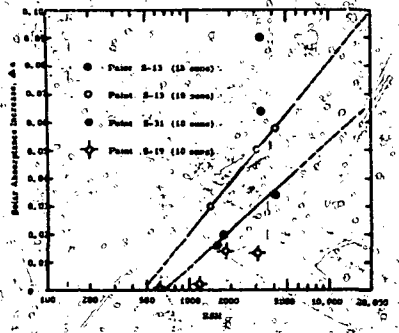

Figure 11.- Effect of UV irradiation in vacuum on solar absorptance of several zinc oxide-methyl silicone paints.

THE EFFECTS OF ULTRAVIOLET RADIATION ON LOW α_s/ϵ SURFACES

By R. L. Olson, L. A. McKellar, and J. V. Stewart

Lockheed Missiles and Space Company, Sunnyvale, Calif.

SUMMARY

The predominant source of natural environmental damage to spacecraft thermal control surfaces is solar ultraviolet energy. An experimental investigation of this damage is described. The primary purposes in this work are (1) the evaluation of candidate materials, and (2) the prediction of operational behavior for selected materials. Candidate surfaces are exposed in vacuum to near-ultraviolet energy; the effect of these exposures on the materials' normal spectral reflectance is determined. The primary energy source is the A-H6 mercury-argon high-pressure lamp, this is used bare and with filters. Incident fluxes are determined with calibrated phototubes and with thermopiles. Sample ambient pressures are maintained at 10^{-6} to 10^{-7} Torr; sample temperatures are varied from 70°F to 500°F. Incident flux densities are varied tenfold. Both initial damage and damage reversibility (bleaching) are investigated. Efforts are concentrated on white pigment-vehicle binary systems; these are candidate low α_s/ϵ spacecraft surfaces. Results demonstrate the dependence of damage upon wavelength of irradiation and upon sample temperature. Materials studied include silicate, silicone, acrylic, and epoxy vehicles, and TiO_2, ZnO, $ZrSiO_4$, and $Li/Al/SiO_3$ pigments. Possible damage mechanisms are reviewed.

Author

INTRODUCTION

Ultraviolet radiation from the sun is the primary cause of damage to thermal control surfaces in an orbital environment. This damage is most severe for surfaces selected to provide a low ratio of solar absorptance (α_s) to emittance (ϵ). An experimental program has been in progress to investigate this damage. This program has as its primary goals (1) the evaluation of candidate materials, and (2) the prediction of operational behavior for selected materials. To aid in the achievement of both goals, insight into damage processes is also sought.

Samples of surfaces to be studied are exposed in high vacuum to near-ultraviolet radiation. Primary criteria for damage are spectral reflectance data. The exposure parameters of irradiation flux density and wavelength, and sample temperature are varied. In addition, exploratory post-exposure bleaching studies have been performed.

To provide engineering design data, the results of ultraviolet studies are generally interpreted as if simulation of pertinent constituents of the orbital environment were achieved. It must be noted, however, that precise environmental simulation is never achieved in the laboratory. The most notable discrepancy is the spectral dissimilarity between extraterrestrial solar radiation and the output of sources suitable for material screening and development studies. Even if one assumes that all significant sources of orbital damage to thermal control surfaces are found in the laboratory test chamber, a straightforward prediction of behavior in space from laboratory data is not possible. There is evidence that (1) the observed changes in radiative properties may result from several reactions, and (2) the dependence of the reactions on irradiance wavelength is likely to be different for each reaction and each material. Large uncertainties in predictions of orbital stability result. Both to reduce these uncertainties, and to guide material development programs, information on the energetics and mechanisms of ultraviolet damage is desired. The work reported herein, therefore, seeks to investigate the damage processes as well as provide engineering design data.

EXPERIMENTAL EQUIPMENT

Ultraviolet Source

The source of ultraviolet radiation is a 1 KW A-H6 (PEK Labs Type C) mercury-argon arc high-pressure, high-intensity lamp. Approximately 30% of this lamp's radiant energy is in the 2000Å to 4000Å range. The lamp is water-cooled and has a quartz water jacket and velocity tube. This assembly is lowered into a quartz envelope extending into the exposure chamber from the top. The lamp assembly can be withdrawn to change lamps without disturbing the vacuum in the system.

Detector and Monitor

The ultraviolet intensity is monitored with calibrated phototubes (RCA 935) that are filtered to monitor radiation in the 2000Å to 4000Å interval. Corning 7-54 filters are used to pass only the near ultraviolet radiation. Neutral-density filters are used to reduce the flux density incident on the detector, in order to avoid saturation of the phototube. The phototubes have been calibrated by actinometry and with a thermopile. The output of the phototubes is automatically measured and recorded for a few minutes every hour with a recording microammeter. When desired, a Corning 0-54 filter is used to compare the intensity in the 2000-3000Å region to that in the 3000-4000Å region. This is of interest since the A-H6 lamp output reduces with time more in the short than in the long wavelength region.

Chamber and Vacuum System

The exposure chambers are metal bell jars 14 inches high by 14 inches in diameter mounted on 18 inch base plates. The sample holders are water-cooled copper blocks mounted at different distances from the ultraviolet radiation source. Three exposure chambers are used. In two of these chambers pairs of sample holders are permanently installed at 3.0, 4.6, 7.5, and 11.2 inches from the source. These distances give nominal irradiances of 10, 5, 2 and 1 "suns" of ultraviolet energy. A flux density of one "sun" of near ultraviolet radiation is herein defined as the flux density of extraterrestrial radiation at one astronomical unit from the sun, in the wavelength interval from 2000Å to 4000Å. In the other chamber 2 sample holders are located 3.9 inches from the source for a nominal flux density of 6 "suns."

Normally water is passed through copper tubes soldered to the sample holders. This maintains the specimen temperatures between 65°F and 95°F, depending on the tap water temperature and the ultraviolet irradiance at the sample holders. At the 10 "sun" position, with no cooling except by radiation to the chamber walls and by conduction through the sample holder to the base plate, the steady-state sample temperature is about 500°F. Through controlled use of cooling water and additional conduction paths from the sample holders, specimen temperatures between 90°F and 500°F can be achieved. For cryogenic temperatures liquid nitrogen can be passed through the cooling tubes.

High vacuums in the range of 10^{-6} to 10^{-7} Torr are maintained with electronic high vacuum pumps using standard vacuum techniques.

Spectral Reflectance Measurements

Normal spectral reflectance measurements are performed with a Cary Model 14 Spectrophotometer with integrating sphere attachment. The solar irradiance data of F. S. Johnson (Ref. 1) is used as the basis for calculations of solar absorptance and of one "sun" of ultraviolet energy.

EXPERIMENTAL RESULTS

Exposure Dependency of Damage

Ultraviolet radiation exposure is herein defined as the product of ultraviolet radiation intensity multiplied by the exposure time. The unit of exposure is "sun-hours." Degradation increases with increasing intensity and with increasing exposure time.

The usual working assumption is that a reciprocal relationship exists between the effects of time and ultraviolet irradiance, with regard to the damage produced; i.e., exposure to one "sun" for ten hours will produce the same effect as exposure to 10 "suns" for one hour. This assumption serves as a useful first approximation; it has not been verified for the

materials under discussion. At least part of the difficulty in attempting to prove or disprove reciprocal behavior of a given material lies in lamp-to-lamp spectral output variations and temporal spectral shifts of a given lamp output.

Plots of solar absorptance (α_s) vs. exposure ("sun-hours") for 6 materials are given in Fig. 1. The exposure times were 50 to 275 hours with nominal intensities of 1, 2, 5 and 10 "suns." The assumption is made that reciprocity holds. Even if reciprocity did not hold exactly, the comparison of degradation of materials at the same high intensity should reflect their relative stability for screening purposes.

In general, the solar absorptance increases with exposure but at a decreasing rate and appears to approach a saturation value that is less than unity (usually between 0.6 and 0.2). The materials are described more completely in Table 1. It should be noted that the three commercial paints are off-the-shelf-materials which were not originally developed for space use. Their immediate availability, ease of application, and low cost are major reasons for their selection. More importantly, for short-lived vehicles (less than one month's orbital lifetime) or in locations where a certain amount of environmental damage is permissible, these materials have provided successful thermal control.

The data demonstrates the general superiority of silicate and silicone systems to organic paints. This data is representative of that employed for engineering design use. (Ref. 2)

Temperature Dependency of Damage

Five samples of white surface coatings were exposed simultaneously to ultraviolet radiation at the same distance from the source. With different cooling paths for each sample holder the samples were maintained at five different temperatures in the range from about 90°F to 500°F during exposure. Spectral reflectance measurements were made after an exposure of 50 hours at a nominal intensity of 10 "suns" of near ultraviolet radiation. An unexposed sample was used as a control coating. Solar absorptances (α_s) were determined from the reflectance data. These together with the increase in solar absorptance ($\Delta\alpha_s$) are given in Table 2. Plots of the spectral absorptance data for two of the five materials are shown in Figs. 2 and 3.

The increase in solar absorptance ($\Delta\alpha_s$) has been correlated graphically to within ± 10% as a function of temperature according to the relationship:

$$\Delta\alpha_s = A e^{-\frac{W}{kT}}$$

The term W is an approximation of the energy of activation for the increase in solar absorptance due to the temperature effects during exposure. The values of A and W are tabulated below:

Parameters Correlating Results of Temperature-Dependancy Studies

Pigment/Binder	A	W(ev)
Syn. Li-Al-SiO_2/K_2SiO_3	0.78	0.053
Li-Al-SiO_2/K_2SiO_3	0.50	0.049
ZrO_2-SiO_2/K_2SiO_3	0.33	0.032
TiO_2/epoxy	1.00	0.031
TiO_2/silicone	0.93	0.053

While the increase in solar absorptance is of practical importance, the spectral changes in absorptance are of interest in the study of the processes involved in degredation. The spectral absorptance curve for the TiO_2/epoxy surface coating are shown in Fig. 2. An initial large change in absorptance due to exposure to ultraviolet radiation at 92°F is observed. At increasing temperatures the same exposure causes a general increase in absorptance with a fairly regular pattern. A slight decrease in absorptance in the infrared region is noted. The shape of the curve at 505°F appears to deviate from the pattern as if a different process or a different rate of degradation has begun.

The spectral absorptance curves for the ZrO_2-SiO_2/K_2SiO_3 surface coating in Fig 3 show a large initial change in absorptance due to exposure to ultraviolet radiation at 90°F. As the exposure temperature increases, the absorptance increases in the visible and infrared regions of the spectrum but decreases in the ultraviolet region. The net result is an increase in the solar absorptance with increasing temperature.

Irradiation Wave-Length Dependency of Damage

Filters have been used with the A-H6 lamp to study the energetics of degradation of white surfaces. Identical specimens were placed side by side, at the same distance from the A-H6 lamp; one specimen would have a filter over it and the other would be bare. Transmission spectra were obtained for all filters employed. Spectral reflectance data for samples before and after exposure were examined.

Often, but not always, exposure of materials to ultraviolet radiation in a vacuum caused the absorption edge to shift to longer wavelengths as seen in Figs. 4, 5, 6, 7 and 8; subsequent exposure to visible light in air caused the absorption edge to shift to shorter wavelengths. The first process results in degradation or an increase in solar absorptance for the material. The reverse process is a bleaching or decrease in the solar absorptance. The energetics for these processes can be illustrated schematically as below:

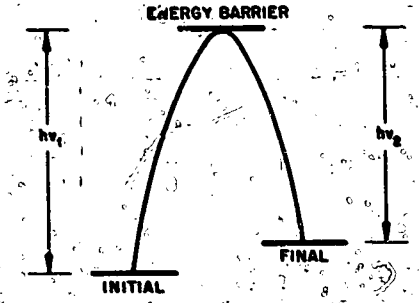

ENERGETICS OF DEGRADING AND BLEACHING

The initial state is a white surface of low α_s. If this surface is exposed to photon energies greater than the threshold energy ($h\nu_1$) the energy barrier is surpassed and the process can proceed to the final state. This state is indicated by a shift in the absorption edge to longer wavelengths and an increase in α_s. Since $h\nu_2$, the threshold energy for the reverse process, is less than $h\nu_1$, the threshold energy for the forward process, this process is also possible. However, the rate is not only dependent on sufficient energy but on the probability that the radiation is absorbed and that all of the reactants are present. Before degradation has occurred no bleaching is possible. As the degradation process proceeds the rate of bleaching will increase. When the rates of the two processes are equal an equilibrium will be reached.

The degradation experiments were done in vacuum and the bleaching experiments in air. This fact may be significant, depending on the processes involved. Optical damage could result from the breaking of oxygen bonds and subsequent removal of oxygen. In such cases the reverse reaction might be slow in a vacuum environment. Even if the photon energy $h\nu_2$ were available, significant bleaching might not occur. However, upon exposure of the degraded surface in air to photon energies greater than $h\nu_2$ and less than $h\nu_1$, the reverse process could proceed with no competition. The initial state would then again be achieved.

From the experiments described, limits and ranges of threshold energies for the photo degrading and bleaching process for some materials have been found. These are tabulated below:

Threshold Energies For Degrading and Bleaching

Pigment/Binder	$h\nu_1$	$h\nu_2$
Syn. Li-Al-SiO_2/K_2SiO_4	4.3-5.4 ev	<3.9 ev
Li-Al-SiO_2/K_2SiO_4	4.3-4.7	<3.9
ZrO_2-SiO_2/K_2SiO_4	4.3-4.7	<3.9
TiO_2/epoxy	4.2-4.4	<3.9

The exact processes of degradation and bleaching are not known at this time. As suggested, removal of oxygen may be involved. The process of breaking one chemical bond and making another may be occurring, especially in polymeric materials. The production of electron-hole pairs in dielectrics like the pigments can happen. Subsequent trapping of freed electrons at imperfection sites can result in coloration.

The changes in the spectral absorptance curve for the ZrO_2-SiO_2/K_2SiO_4 system (Fig. 6) suggests a single reversible process. With photon energies greater than $h\nu_1$ in vacuum there is a marked increase in absorptance in the ultraviolet region. Photon energies less than $h\nu_1$ did not cause this increase. In air, photons of energies between $h\nu_1$ and $h\nu_2$ caused the original changes in the spectral reflectance curve to be almost completely reversed.

In the TiO_2/epoxy system photon energies greater than $h\nu_1$ caused the absorption edge to shift to longer wavelengths (Fig. 4). Photons with energy less than $h\nu_1$ did not, (Fig. 5) but the absorptance increased in the visible and infrared regions of the spectrum more than when energy of greater than $h\nu_1$ was present. Both changes were partially reversed upon exposure in air to photons with energy between $h\nu_1$ and $h\nu_2$. This more complicated behavior of the TiO_2/epoxy system indicates more than a single reversible process. The threshold energy $h\nu_1$ tabulated above is for the absorption edge shift. The value for $h\nu_2$ is for both reverse processes.

CONCLUSIONS

Low α_s/ϵ surfaces suffer an increase in α_s upon exposure to ultraviolet radiation in vacuum; this damage is enhanced both by increased ultraviolet flux density and by increased exposure time. The supposition of a reciprocal relationship between flux density and exposure time appears to be a valid working assumption for development of rough engineering data.

It allows the use of accelerated tests in materials development and evaluation programs. Solar absorptances as a function of exposure in "sun-hours" increase at a decreasing rate and appear to approach a saturation value that is less than unity for all materials studied.

Samples of white surface coatings degraded more with increasing temperature over the temperature range 900F to 5000F. The energies of activation for the increase in solar absorptance due to the temperature effects during exposure for the materials studied are estimated to be in the range from 0.03 to 0.05 ev. However, the spectral absorptance did not increase with increasing temperatures over the entire solar spectrum. In fact, in some regions the degraded absorptance decreased.

Threshold energies for the shift to longer wavelength of the ultraviolet absorption edge have been found to be about 4.5 ev for the materials studied. This absorption edge shift is a primary but not the only cause for the increase in solar absorptance. Bleaching in air for the same materials occurs with photon energies of less than 3.5 ev.

Further detailed studies are required to identify the first-order damage mechanisms in practical low α_s/ϵ materials. This information is desired both to guide material development efforts, and to improve predictions of operational performance based on laboratory data.

REFERENCES

1. Johnson, F. S. (editor): Satellite Environment Handbook. Stanford University Press, 1961.

2. Lockheed Missiles and Space Co: Thermophysics Design Handbook. Report No. 8-55-63-3, Lockheed Missiles and Space Co., 1963

APPENDIX

TABLE 1

Materials Investigated

Description	Source	Remarks
TiO_2/Epoxy: White Skyspar Enamel (A423, color SA9185)	Andrew Brown	In LMSC Production use on short lifetime satellites; commercially available.
TiO_2/Acrylic: tinted white Remacryl Enamel (M49 WC17)	Sherwin-Williams	In LMSC Production use; commercially available.
TiO_2/Silicone: Fuller Gloss White Silicone (517-W-1)	W. P. Fuller	In LMSC Production use; commercially available.
ZnO/Silicone (Experimental)	LMSC/Dow-Corning	Under development by Dow-Corning and LMSC
TiO_2/Silicone (Experimental)	LMSC/Dow-Corning	Under development by Dow-Corning and LMSC; In limited use on LMSC/USAF satellites.
Li-Al-SiO_2/Na_2SiO_4	LMSC	Developed by LMSC; in use for special applications on LMSC/USAF satellites
Synthetic Li-Al-SiO_2/K_2SiO_3	LMSC	Experimental LMSC paint.
Li-Al-SiO_2/K_2SiO_3	LMSC	Experimental LMSC paint.
ZrO_2·SiO_2/K_2SiO_3	LMSC	Experimental LMSC paint.

TABLE 2

Temperature Dependency Data

Pigment/Binder	Temp. (°F)	α_s	$\Delta\alpha_s$
Syn. Li-Al-SiO_2/K_2SiO_3 LMSC Experimental Paint	Unexposed	0.14	----
	90	0.26	0.12
	225	0.25	0.09
	330	0.29	0.15
	532	0.32	0.18
		0.39	0.25
Li-Al-SiO_2/K_2SiO_3 LMSC Experimental Paint	Unexposed	0.13	----
	88	0.26	0.07
	97	0.21	0.08
	215	0.13	0.11
	325	0.27	0.14
	500	0.30	0.17
ZrO_2·SiO_2/K_2SiO_3 LMSC Experimental Paint	Unexposed	0.09	----
	90	0.19	0.10
	102	0.19	0.10
	210	0.21	0.11
	315	0.21	0.12
	460	0.26	0.17
TiO_2/Epoxy White Skyspar Enamel (A. Brown A423 Color SA9185)	Unexposed	0.20	----
	92	0.50	0.30
	101	0.53	0.33
	230	0.58	0.38
	350	0.62	0.42
	505	0.72	0.58
TiO_2/Silicone Fuller Gloss White Silicone Paint (517-W-1)	Unexposed	0.21	----
	95	0.34	0.13
	101	0.34	0.13
	227	0.42	0.21
	362	0.41	0.20
	525	0.52	0.31

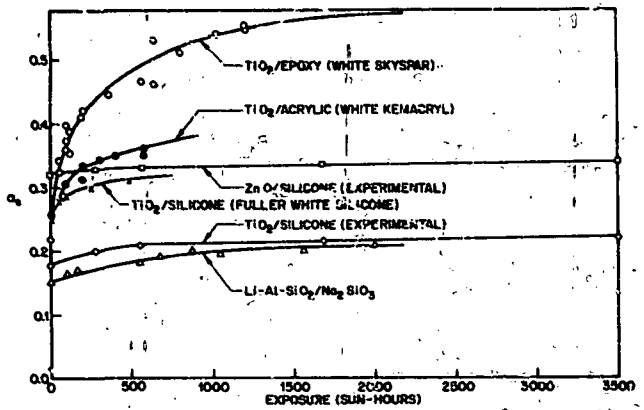

Figure 1.- Solar absorptance vs. exposure.

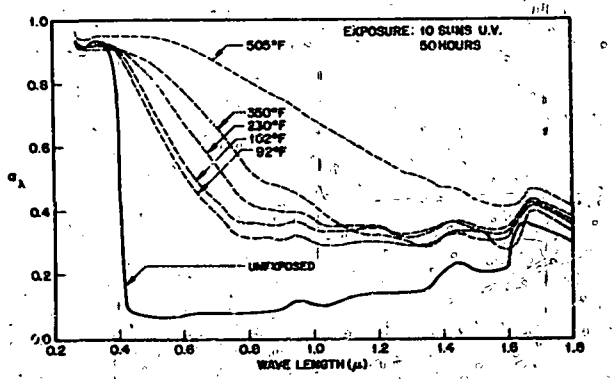

Figure 2.- Spectral absorptance - TiO_2/epoxy.

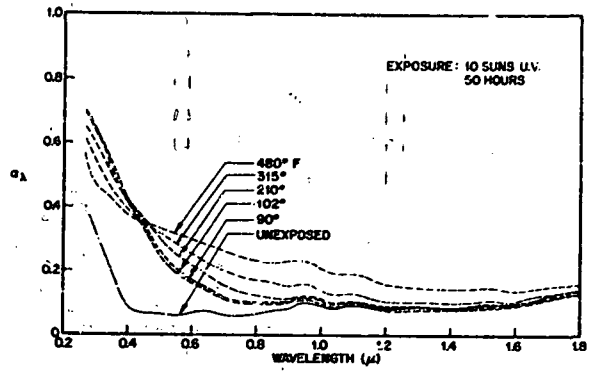

Figure 3.- Spectral absorptance - $ZrO_2.SiO_2/K_2SiO_3$.

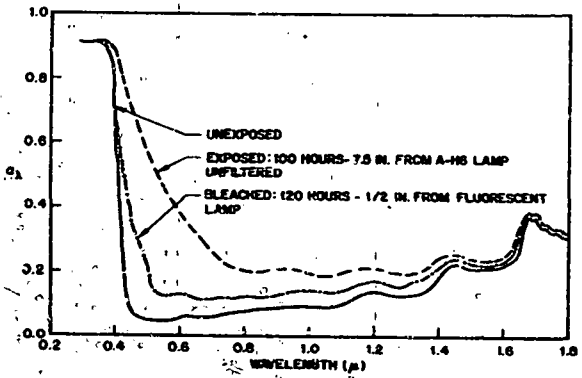

Figure 4.- Spectral absorptance - TiO_2/epoxy.

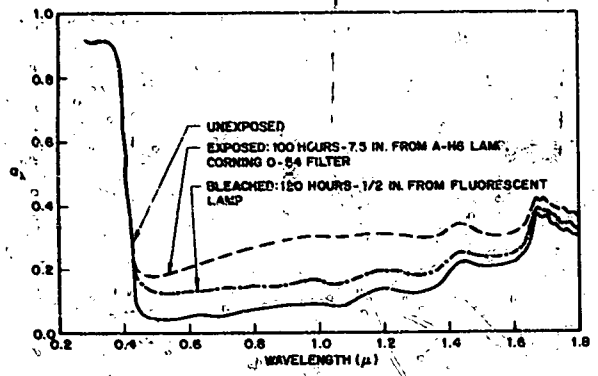

Figure 5.- Spectral absorptance - TiO_2/epoxy.

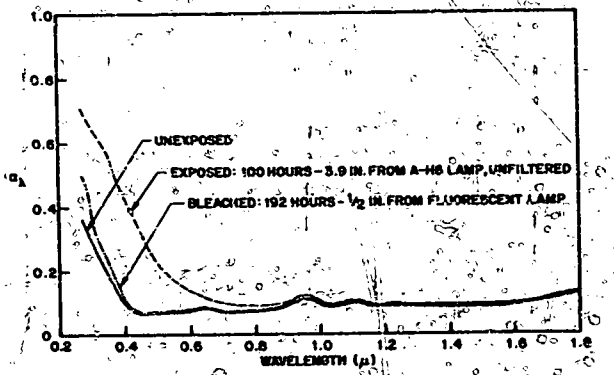

Figure 6.- Spectral absorptance - $ZrO_2.SiO_2/K_2SiO_3$.

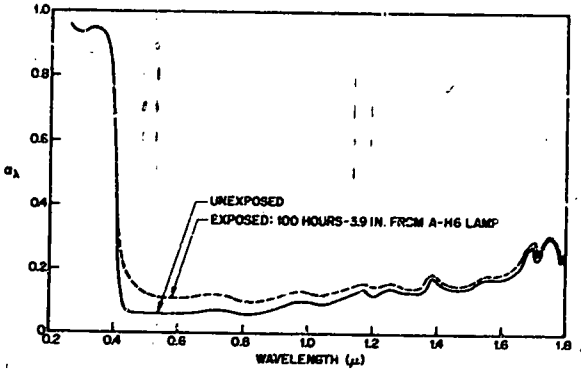

Figure 7.- Spectral absorptance - TiO_2/silicone (experimental).

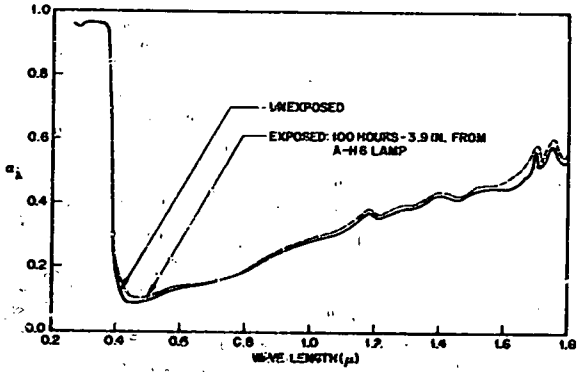

Figure 8.- Spectral absorptance - ZnO/silicone (experimental).

Abstract of proposed report for Symposium on Thermal Radiation Properties of Solids, to be held in San Francisco, March 4-6, 1964

PRELIMINARY RESULTS FROM A ROUND-ROBIN STUDY OF ULTRAVIOLET DEGRADATION OF SPACECRAFT THERMAL-CONTROL COATINGS

By J. C. Arvesen, C. B. Reed, and C. C. Shaw

ABSTRACT

Comparisons of laboratory results of ultraviolet degradation of thermal-control coatings for spacecraft with data obtained during flight in space have shown generally poor agreement in the rate of coating degradation. Consequently, it has become apparent that improvements must be made in laboratory ultraviolet-simulation techniques. In November of 1962, a round-robin testing program was organized in an attempt to advance the technology of ultraviolet testing of thermal-control coatings. In this program, samples of four different temperature-control coatings were distributed among a number of organizations for tests in their ultraviolet simulation facilities. Sixteen organizations are participating in the program. Three of the coatings were known to be unstable when exposed to ultraviolet, whereas the fourth was considered to be relatively stable. The stable coating and two of the unstable samples have been included in the complement of test coatings for the flight emissivity experiment on the S-17 Orbiting Solar Observatory. The satellite will be launched early in 1964, and results from this experiment should provide a basis for evaluating the capability of the various laboratory facilities to simulate the degrading effects of solar ultraviolet radiation.

The information presented is based on a preliminary analysis of the results reported by approximately half of the participants. The rate of increase in solar absorptance of the test coatings varied widely among the different investigators. For example, the rate of degradation of samples of one of the coatings was found to differ by factors exceeding 50. In addition, initial values of solar absorptance for the same coatings were found to differ in some cases by nearly 100 percent.

Preliminary analysis of the results obtained from this program illustrates the need to standardize test techniques for ultraviolet degradation studies, and to obtain correlations of laboratory measurements with data taken during flight in the actual space environment. It is also evident that standardization of measurement techniques for determining thermal-radiation properties is required.

NASA-Langley, 1964

a NASA facsimile reproduction

OF

N63 17331